
[All ETDs from UAB](#)

[UAB Theses & Dissertations](#)

2017

Delivery Of Deoxyribonucleic Acids As Drugs: A Structural Study, Encapsulation, And Controlled Release Of G-Quadruplex Forming Deoxyoligonucleotides Of The Human Telomeric Sequence

Brenna Alyssa Tucker
University of Alabama at Birmingham

Follow this and additional works at: <https://digitalcommons.library.uab.edu/etd-collection>

Recommended Citation

Tucker, Brenna Alyssa, "Delivery Of Deoxyribonucleic Acids As Drugs: A Structural Study, Encapsulation, And Controlled Release Of G-Quadruplex Forming Deoxyoligonucleotides Of The Human Telomeric Sequence" (2017). *All ETDs from UAB*. 3178.
<https://digitalcommons.library.uab.edu/etd-collection/3178>

This content has been accepted for inclusion by an authorized administrator of the UAB Digital Commons, and is provided as a free open access item. All inquiries regarding this item or the UAB Digital Commons should be directed to the [UAB Libraries Office of Scholarly Communication](#).

DELIVERY OF DEOXYRIBONUCLEIC ACIDS AS DRUGS: A STRUCTURAL
STUDY, ENCAPSULATION, AND CONTROLLED RELEASE OF G-QUADRUPLEX
FORMING DEOXYOLIGONUCLEOTIDES OF THE HUMAN TELOMERIC
SEQUENCE

by

BRENNALYSSA TUCKER

DR. EUGENIA KHARLAMPIEVA, CHAIR
DR. MAAIKE EVERTS
DR. DAVID E. GRAVES
DR. AARON LUCIUS
DR. DAVID SCHNEIDER

A DISSERTATION

Submitted to the graduate faculty of The University of Alabama at Birmingham,
in partial fulfillment of the requirements for the degree of
Doctor of Philosophy

BIRMINGHAM, ALABAMA

2017

DELIVERY OF DEOXYRIBONUCLEIC ACIDS AS DRUGS: A STRUCTURAL
STUDY, ENCAPSULATION, AND CONTROLLED RELEASE OF G-QUADRUPLEX
FORMING DEOXYOLIGONUCLEOTIDES OF THE HUMAN TELOMERIC
SEQUENCE

BRENNA ALYSSA TUCKER

CHEMISTRY

ABSTRACT

Nucleic acids are known to play numerous important roles in the cell. Recently, interest in the delivery of DNA to treat disease, also known as gene therapy, has increased with new non-viral encapsulation strategies becoming available. Unfortunately, challenges with sufficient delivery of the DNA still plague these systems causing the need for improved DNA delivery vehicles. To overcome DNA delivery barriers, two-component poly(methacrylic acid) (PMAA)/ poly(N-vinylpyrrolidone) (PVPON) microcapsules were developed using Layer-by-Layer (LbL) technology. G-quadruplex forming deoxyoligonucleotides of the human telomeric sequence were used to model the delivery of the thrombin binding aptamer (TBA), a DNA therapeutic that folds into a G-quadruplex structure. Because the structure of the nucleic acid therapeutic dictates their mechanism of action, the structural stability of G-quadruplex sequences of the human telomere were explored, first, before these structures were encapsulated within PMAA/PVPON microcapsules. Release of the DNA from the microcapsules was achieved using a controlled therapeutic ultrasound technique. A summary of these experiments is described below.

In Chapter 3, a library of G-quadruplex forming deoxyoligonucleotides was built by mutating either one, two, three, or four adenines at a time to a thymine in the loop sequence regions of the structure. The unfolding properties and energetics associated with

each sequence were examined using differential scanning calorimetry (DSC) and circular dichroism spectropolarimetry (CD). The melting profiles for the wild-type human telomeric G-quadruplex sequence were biphasic in nature, indicating the presence of an unfolding intermediate. As the number of modified loops increased, the melting profiles were fit by a single monophasic curve. DSC and circular dichroism (CD) spectra were collected to determine how the mutations influenced the stability and secondary structures of these G-quadruplex forming deoxyoligonucleotides. It was found that all sequences could fold into G-quadruplex structures and varied by the magnitude of their peaks at 245 and 295 nm. CD spectra were also collected as a function of temperature and then analyzed by singular value decomposition to further probe the biphasic melting profiles observed by DSC. Results from deconvolution of CD data are consistent with the presence of intermediates during the unfolding for the wild-type G-quadruplex as well as the loop modified G-quadruplexes.

In Chapter 4, the encapsulation and release of G-quadruplex forming deoxyoligonucleotides of the human telomeric sequence by two-component PMAA/PVPON multilayer hydrogel capsules is described. LbL deposition was used to coat PMAA and PVPON layers onto CaCO₃ inorganic microparticles that were co-precipitated with the G-quadruplex structures. The PMAA molecules within the multilayer were crosslinked with cystamine and dissolution of the CaCO₃ cores with ethylenediaminetetraacetic acid (EDTA) yielded hollow microcapsules loaded with G-quadruplex forming deoxyoligonucleotides. The microcapsules were characterized using a variety of techniques including FTIR, Zeta-potential measurements as a function of pH, and scanning electron microscopy. These studies demonstrate that these capsules are highly efficient at releasing their DNA cargo, unharmed, by treatment with ultrasound to mechanically burst the capsules.

Keywords: G-quadruplex, DNA delivery, Layer-by-Layer, microcapsules, ultrasound release,

DEDICATION

This work is dedicated to the dreamers of this world. May you always know that your dreams are possible through continuous hard work and perseverance.

“Making your mark on the world is hard. If it were easy, everybody would do it. But it’s not. It takes patience, it takes commitment, and it comes with plenty of failure along the way. The real test is not whether you avoid this failure, because you won’t. It’s whether you let it harden or shame you into inaction, or whether you learn from it; whether you choose to persevere.”

-Barack Obama

ACKNOWLEDGEMENTS

This work could not have been possible without the excellent mentoring of Drs. David Graves and Eugenia Kharlampieva. Thank you, Dr. Graves, not only for recruiting me to UAB, but for providing me with a tremendous amount of support while I worked in your lab as well as making sure I was taken care of as I moved between labs. I am grateful to have had you as a mentor and I really enjoyed our project meeting phone calls after your retirement. Your commitment to my success was apparent and I am thankful that you have always believed in me. To Dr. Kharlampieva, thank you for taking a chance on me and inviting me to your lab when I needed a mentor. I have thoroughly enjoyed my time in your lab and I am very grateful for the many opportunities you have provided me to learn while working in your lab. You have always let me know that you believed in me and that has played a direct role in boosting my confidence in my own scientific abilities. Thank you for being so understanding and always knowing just what to say.

I would also like to thank the other member of my committee, Dr. Aaron Lucius, Dr. Maaike Everts, and Dr. David Schneider, for their input, encouragement, and support throughout our time together.

In addition, I would also like to thank my family and friends for your continued support through the years. Matt, I know it hasn't been easy at times, but being surrounded by your love gave me the strength to never give up. Thank you for always being there.

TABLE OF CONTENTS

	<i>Page</i>
ABSTRACT	ii
DEDICATION	v
ACKNOWLEDGMENTS	vi
LIST OF TABLES	ix
LIST OF FIGURES	x
CHAPTER	
1. INTRODUCTION	1
Nucleic Acid Structures	2
The G-Quadruplex	9
Nucleic Acids Used in Gene Therapy.....	15
Drug Delivery Vehicles	17
Layer-by-Layer Self-Assembly of Microcapsules.....	19
Research Summary	22
2. METHODS	24
Preparation of Buffers.....	24
DNA Preparation	25
Preparation of Polymer Solutions	27
Differential Scanning Calorimetry.....	28
Circular Dichroism Spectroscopy	29
Analysis of Data by Singular Value Decomposition	30
Encapsulation of DNA Within Sacrificial Cores	32
LbL Assembly of DNA Loaded Microcapsules	33
Zeta-Potential Studies	36
FTIR Studies	37
Therapeutic Ultrasound Release of DNA	38
3. STABILITY OF THE NA ⁺ FORM OF THE HUMAN TELOMERIC G- QUADRUPLEX: ROLE OF ADENINES IN STABILIZING G-QUADRUPLEX STRUCTURE.	39

4. ENCAPSULATION AND CONTROLLED RELEASE OF NUCLEIC ACIDS THROUGH TWO COMPONENT PMAA/PVPON MICROCAPSULES	88
5. CONCLUSIONS.....	126
GENERAL LIST OF REFERENCES	130

LIST OF TABLES

<i>Table</i>	<i>Page</i>
STABILITY OF THE NA⁺ FORM OF THE HUMAN TELOMERIC G- QUADRUPLEX: ROLE OF ADENINES IN STABILIZING G-QUADRUPLEX STRUCTURE	
1 Sequences Showing the A to T Base Modifications in the Loops of the Human Telomeric G-quadruplex Sequences Used in this Study.....	75
2 Summary of DSC and CD Data for Loop Mutants.....	76
3 Summary of Singular Values and Autocorrelation Data for the Wild-type Human Telomeric G-quadruplex DNA Sequence.....	78
4 Singular Value Decomposition Data for the Wild-type Human Telomeric G- quadruplex DNA sequence	79
ENCAPSULATION AND CONTROLLED RELEASE OF NUCLEIC ACIDS THROUGH TWO COMPONENT PMAA/PVPON MICROCAPSULES	
1 Relationship Between Encapsulation Efficiency and Number of Bilayers	120

LIST OF FIGURES

Figures *Page*

INTRODUCTION

1	Nucleotide Units of RNA and DNA	3
2	Nucleobases Found in RNA and DNA	4
3	Base Pairs of DNA	5
4	Side View of A-, B-, and Z-DNA	6
5	DNA Triplexes and Hairpins	7
6	DNA Cruciform Structures	8
7	Various G-quadruplex Structures	10
8	Structure of the G-tetrad	11
9	Different Molecularities and Strand Orientations of G-quadruplex Structural motifs	13
10	General Strategy for LbL Creation of Hollow Microcapsules.....	21

METHODS

1	Co- and Counter-ion Distribution at the Surface of Charged Particles	36
---	--	----

STABILITY OF THE Na^+ FORM OF THE HUMAN TELOMERIC G- QUADRUPLEX: ROLE OF ADENINES IN STABILIZING G-QUADRUPLEX STRUCTURE

1	Cartoon Representing the Chair and Basket Conformations of the Na^+ Human Telo- meric G-quadruplex	80
2	CD Wavelength Scans for the Human Telomeric G-quadruplex	81

3	Composite CD Melting Curves of the Human Telomeric Sequence and A to T modified Loop Sequences	82
4	A DSC Thermogram of the Wild-type Human Telomeric G-quadruplex	83
5	Representative DSC Thermograms for the Single A to T Base Modifications of the Telomeric G-quadruplex	84
6	Representative DSC Thermograms for the Multiple A to T Base Modifications of the Telomeric G-quadruplex	85
7	Three-dimensional CD Plot for the Thermal Denaturation of Wild-type Human G-quadruplex.....	86
8	SVD Analysis of Wild-type Human Telomeric G-quadruplex.....	87

ENCAPSULATION AND CONTROLLED RELEASE OF NUCLEIC ACIDS THROUGH TWO COMPONENT PMAA/PVPON MICROCAPSULES

1	Schematic of Layer-by-Layer Assembly	112
2	FTIR Confirmation of Two-component (PMAA/PVPON) ₁₃ Hydrogel Capsules....	113
3	Relationship between pH and Surface Charge of the (PMAA/PVPON) ₁₃ Hydrogel Capsules	114
4	Scanning Electron Microscopy of (PMAA/PVPON) ₁₃ Hydrogel Capsules.....	115
5	Schematic of Cargo Release by Ultrasound.....	116
6	Confirmation of G-quadruplex Structure.....	117
7	Glutathione Turbidity Studies.....	118
8	Optimization of Capsule Synthesis.....	119

CHAPTER 1

INTRODUCTION

The importance of deoxyribonucleic acid (DNA) as a chemical (biopolymer) that stores genetic information has long been known (1 – 4). However, interest in using DNA as a drug to treat disease has increased significantly since the early 1990s when using DNA vaccinations were first explored with success (5). The widespread practice of using nucleic acids as drugs has been stalled by many limitations that are associated with trying to deliver DNA within the body, namely the degradation of DNA by exo- and endonucleases before reaching the nucleus of the cell (6 – 8). Various nucleic acid drugs have been designed with different sequences and structures that drive their specificity (8 – 10). One DNA structure of particular interest is the G-quadruplex structure, described in greater detail later in this chapter. Naturally occurring G-quadruplex structures have been shown to be biologically relevant in a number of different processes and its innate resistance to nuclease degradation makes them attractive for use as a nucleic acid drug. The research described in this dissertation seeks to solve these delivery barriers through the creation of polymeric microcapsules that can encapsulate and protect G-quadruplex forming deoxyoligonucleotides of the human telomeric sequences upon transport. Chapter 1 will provide an overview of the background information related to the various themes of this body of work. Specifically discussed are 1) the various structures of nucleic acids, 2) the nucleic acid drugs used in gene therapy, 3) an overview of various drug delivery strategies, and 4) a description of the Layer-by-Layer technology used in the synthesis of microcapsules.

Nucleic Acid Structures

Nucleic acids are polymeric biomolecules that play an important role in numerous cellular functions (11). The discovery of nucleic acids is attributed to Friedrich Miescher (12). In 1868, Miescher isolated a new biomolecule from the nucleus of white blood cells that was neither protein, carbohydrate, nor lipid. Because this new biomolecule was extracted from the nucleus, it was referred to as 'nuclein' (13). The term, nucleic acid, was coined in 1889 when Richard Altmann discovered that the 'nuclein' biomolecule, had acidic properties (12, 14). Watson and Crick published the first structure of deoxyribonucleic acid (DNA) in 1953 (15 – 17) after viewing the X-Ray diffraction pattern of DNA produced by Rosalind Franklin (18 – 21). However, it wasn't until the 1970s that the first structure of ribonucleic acid (RNA) was solved through the refinement of two independent X-ray crystallography studies (22 – 25).

The structures of nucleic acids can generally be described as being composed of nitrogen rich nucleobases linked together by a sugar-phosphate backbone. The monomeric units of these biopolymers are referred to as nucleotides and consist of a single nucleobase with a phosphorylated sugar attached to it at either the 5' or 3' OH. As depicted in Figure 1, the nucleobase is attached to the 5'-carbon (ribose or deoxyribose) sugar at the C1' position and the phosphate is found attached to C5' atom of the same sugar. Nucleic acids are classified as either ribo- or deoxyribo- depending upon the type of sugar attached to the nucleobase. Ribose simple sugar units are found in ribonucleic acids (RNA) whereas deoxyribose sugars, are found in deoxyribonucleic acid (DNA). The difference between ribose and deoxyribose sugars is the removal of the hydroxyl group on the C2' atom of the ribose sugar also illustrated in Figure 1.

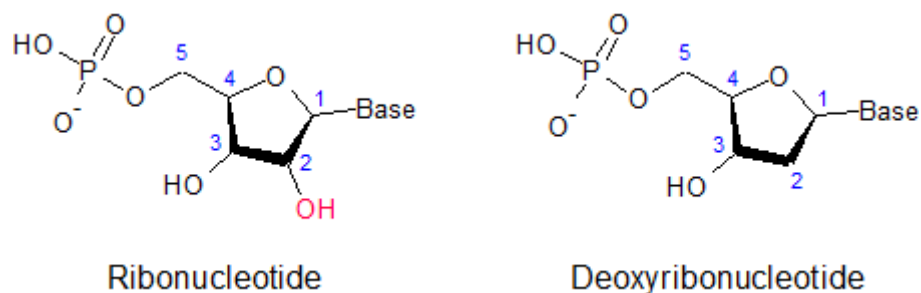


Figure 1. Nucleotide Units of RNA and DNA. Nucleotides are composed of a ribose sugar with a phosphate group attached at the C5 position and a nucleobase attached at the C1 position. Ribonucleotides with a simple ribose sugar are found in RNA and deoxyribonucleotides with a ribose derivative sugar are found in DNA. Figure created with ACD/ChemSketch 2016 2.2.

There are five major nucleobases that make up nucleic acids including adenine, thymine, guanine, cytosine, and uracil. These nucleobases can be seen in Figure 2. Nucleobases are generally separated into two categories, pyrimidines and purines. Purine nucleobases include adenine and guanine which binds to the sugar at the N9 position while pyrimidine nucleobases include cytosine, thymine, and uracil and bind to the sugar through the N1 atom. While three of the five common nucleobases, adenine, cytosine, and guanine, can be found in both RNA and DNA structures, uracil and thymine are specific for either RNA or DNA, respectively.

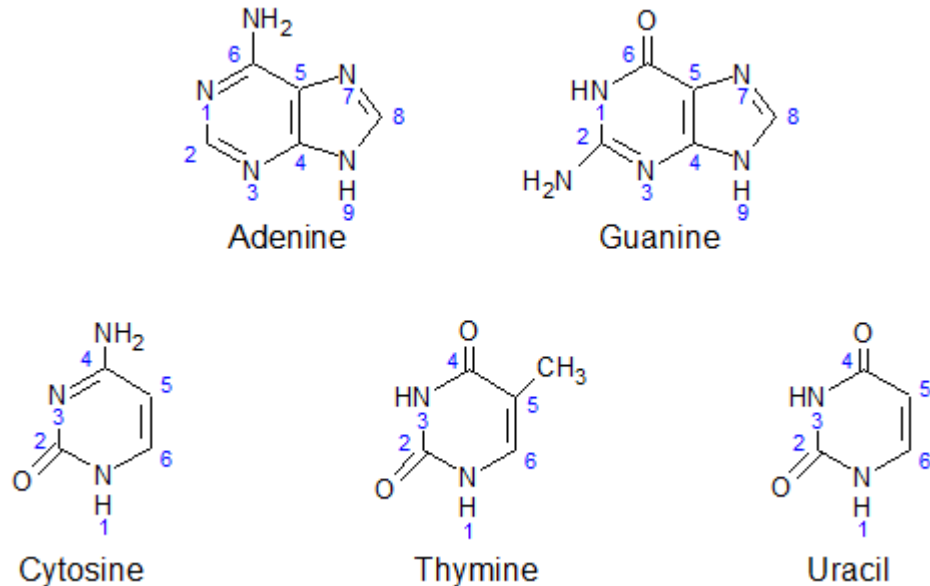


Figure 2. Nucleobases Found in RNA and DNA. Nucleobases are classified as either purines or pyrimidines. The purine nucleobases consist of adenine and guanine. Cytosine, thymine, and uracil are pyrimidine nucleobases. Figure created with ACD/ChemSketch 2016 2.2.

DNA can fold into several different structures with the most commonly recognized being the double-stranded helix, or the double helix, that was first identified in 1953 (15 – 17). The double helix arises from base pairing, adenine with thymine and guanine with cytosine, between two complementary strands of DNA, as shown in Figure 3. Two hydrogen bonds occur between adenine and thymine base pairs and three hydrogen bonds occur between guanine and cytosine base pairs. Due to the increased hydrophobicity of the nucleobases relative to the sugar-phosphate backbone, the two strands orient themselves so that the bases pairs can stack upon one another towards the center of

the molecule. This base stacking allows the DNA to exclude the maximum amount of water from the planar hydrophobic base-pairs of the molecule. To reduce the steric hindrance, the strands twist around one another resulting in the double-helical structure.

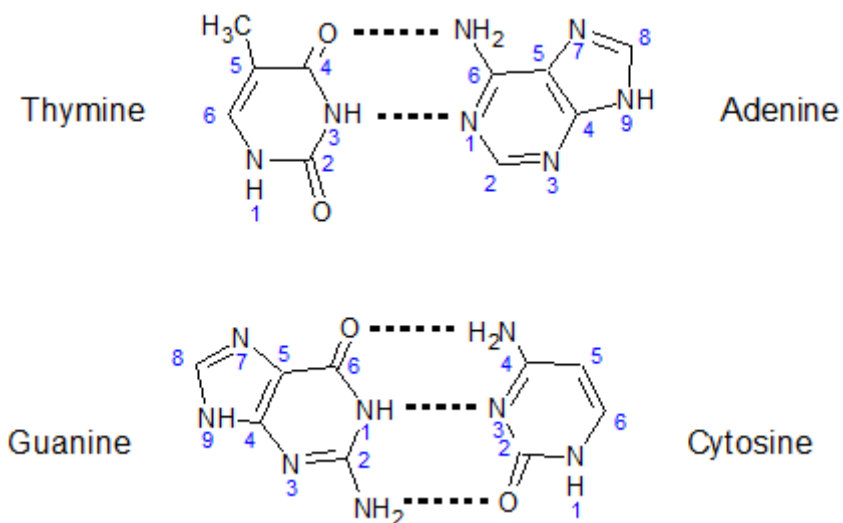


Figure 3. Base Pairs of DNA. In DNA, thymine and adenine bind with two hydrogen bonds while guanine and cytosine bind with three hydrogen bonds. Figure created with ACD/ChemSketch 2016 2.2.

The three types of double helical structural motifs that can be formed by DNA include the A-, B-, and Z forms as shown in Figure 4 (26 – 29). Even though the B-DNA structure (the hydrated form) is the shape taken on by the majority of naturally occurring, double stranded DNA, both the A- and Z- forms can be found within the cell under certain conditions (30).

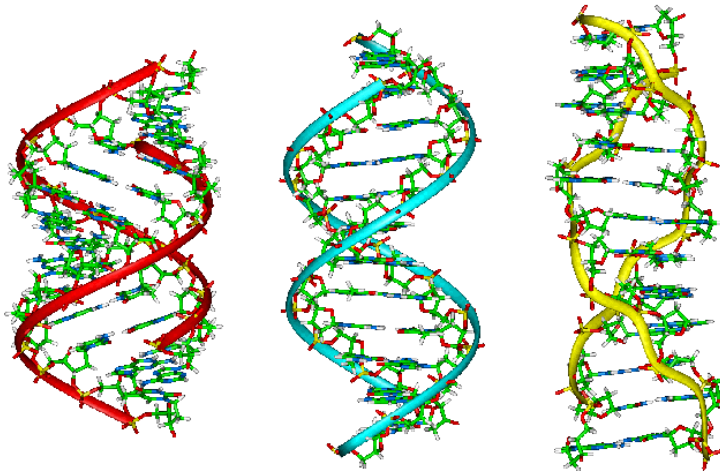


Figure 4. Side View of A-, B-, and Z-DNA. The compaction and extension of A-DNA (red) and Z-DNA (yellow), respectively, compared to B-DNA (blue) as view from the side of these molecules. Figure by Thorwald at *English Wikipedia* [Public domain].

The major difference between these structures lies primarily in the number of base pairs per turn of the helix. As seen in Figure 4, A-DNA (in red) is more compact than B-DNA (in blue) and Z-DNA (in yellow) is more extended than B-DNA. In addition, Z-DNA has a left-handed turn to its helix whereas both the A- and B- form of DNA have a right handed helical twist. The overall stability of DNA structures can be described by a combination of factors including: 1) the hydrogen bonding network found between complementary base pairs (31, 32), 2) the favorable London dispersion forces that arise from π - π stacking of the base-pairs within the helix (31, 33), 3) the hydrogen bonds formed between the complementary bases, the base substituents ($-\text{NH}_2$ and O) with the water cage

that surround the DNA and the solvent exposed polar backbone (34, 35), and 4) the spatial arrangement of the negatively charged phosphate backbone along the outside of the DNA molecule that results in charge minimizing, electrostatic interactions with surrounding cations such as Mg^{2+} or Na^+ (36 – 38).

Along with the double helix, DNA can fold into triple helices, hairpins, and can even exist as a single strand in a random coil (39, 40). DNA triple helices, or triplexes, exist when three strands of DNA are oriented together as shown in Figure 5A.

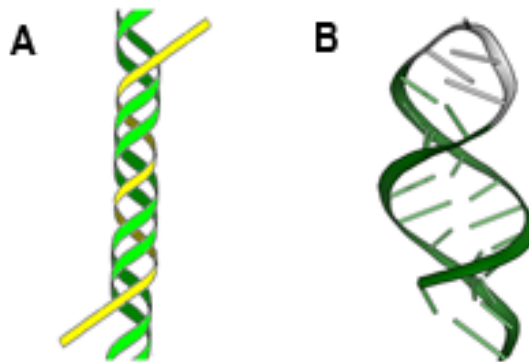


Figure 5. DNA Triplexes and Hairpins. DNA triplexes (A) are formed when a single strand of DNA (yellow) interacts with double stranded DNA (green). DNA hairpins (B) arise when a DNA strand is complementary to itself and form a stem region (green) and a loop region (gray). Figure 5A by InfoCan, Figure 5B by Thomas Shafee, both Figures via *Wikimedia Commons*

In this case, a single strand of DNA, as illustrated in yellow, is likely to combine with a B-DNA double helix, shown in green, to form a triple stranded helical structure. The DNA strands of a triplex are held together through Hoogsteen base pairing, meaning that each nucleotide base pairs to two adjacent nucleotides.

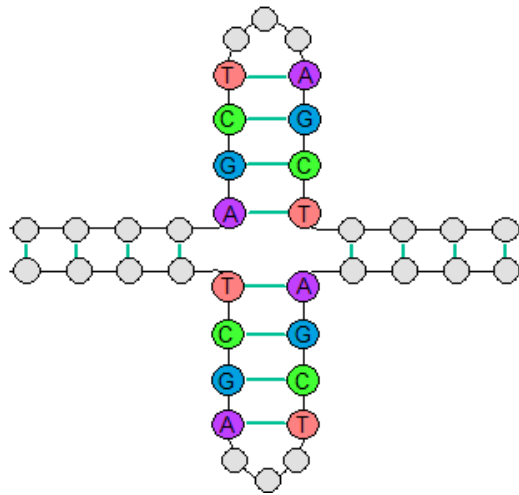


Figure 6. DNA Cruciform Secondary Structure. DNA cruciforms occur within double stranded regions of DNA that are palindromic. Both strands of the duplex form hairpin structures that extend away from the double helix. Figure created with ACD/ChemSketch 2016 2.2.

In the case of DNA hairpins, a single strand of DNA that is complementary to itself folds over in such a way that it can base pair with itself. Two prominent structural features of DNA hairpins include the stem, made up by the base paired region, and the loop, which contains the non-complementary bases found between the two complemen-

tary regions. The structural features of DNA hairpins can be seen in Figure 5B. These hairpin structures are also able to form with double stranded sequences of DNA that are palindromic (41). When this occurs, both strands of the DNA jut out to form a double stem loop structure as seen in Figure 6. These structures are commonly referred to as DNA cruciforms.

The G-Quadruplex

Another interesting structure that can be formed by nucleic acids is known as the G-quadruplex. This structure was first predicted in 1962 from X-ray diffraction patterns of guanylic acid (42). G-quadruplex structures are found within the promoter regions for some oncogenes and at the ends of chromosomes (43 – 45). Because of their location within the chromosome, G-quadruplex structures are thought to regulate the expression of oncogenes as well as to protect the ends of the DNA that contain genetic information. Sequences of nucleic acids that are rich in guanine repeats, specifically those that have contiguous tracts of two to four guanine bases, may fold into G-quadruplex structures. The term G-quadruplex represents a broad class of secondary structures as seen in Figure 7, that all fold through the stacking of guanine tetrads (G-tetrads) (46). The exact shape and stability of a G-quadruplex structure is determined by many factors including the sequences of the bases (i.e. the number of repeating guanines and the number of bases between the repeating guanines) and the buffer environment of the strands (47 – 49). The factors that influence G-quadruplex structure will be discussed in greater detail later in this section.

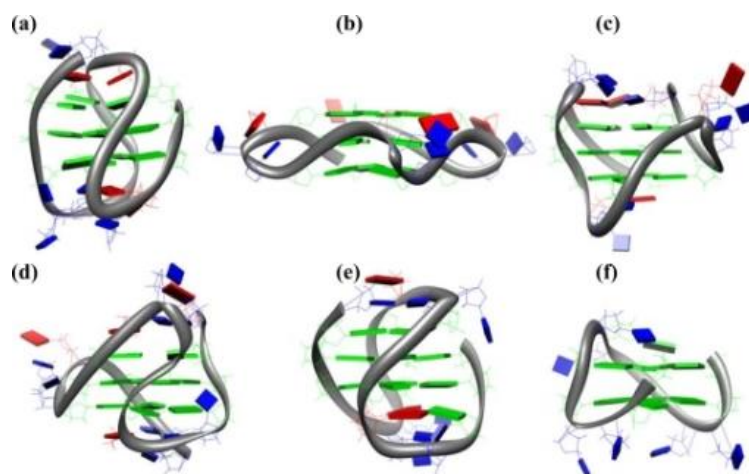


Figure 7. Various G-quadruplex Structures. Each structure displays the characteristic stacking of G-tetrads (shown in green) indicative of a G-quadruplex structure. Figure borrowed from B. Pagano et al., *Int J Mol Sci*, Jul. 2009, Creative Commons

While both DNA and RNA can fold into these stable secondary structures, this work makes use of G-quadruplexes formed by synthetic deoxyoligonucleotides and thus, any subsequent mention of the G-quadruplex refers to those structures formed by DNA or deoxyoligonucleotides.

A characteristic feature of the G-quadruplex structural motif is the formation of G-tetrads that stack upon one another contributing to the increased stability of these structures relative to duplex DNA (50). As shown in Figure 8, the G-tetrad can be described by four guanine bases oriented with a square co-planar geometry (51). Like the triple helix mentioned earlier, the G-tetrad also makes use of Hoogsteen base pairing.

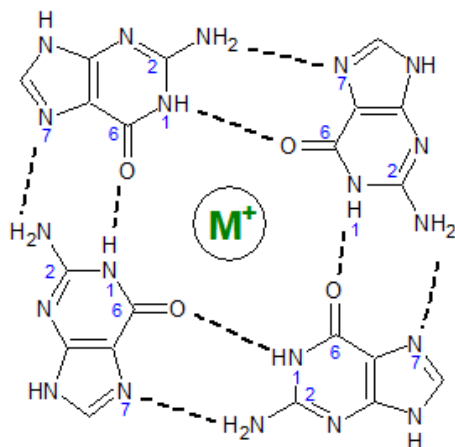


Figure 8. Structure of the G-tetrad. Four guanine bases are arranged in a square coplanar fashion with Hoogsteen base pairing between the neighboring units. A monovalent cation situates itself within the central pore of the tetrad. Figure created with ACD/ChemSketch 2016 2.2.

In these structures, two hydrogen bonds exist between neighboring guanine bases for a total of four hydrogen bonding events per guanine base. As shown in Figure 8, the amide proton at the N1 position and one of the amine protons on the C2 atom of one guanine base make hydrogen bonds with the amide oxygen at the C6 position and the N7 atom, respectively, of the neighboring guanine base. This arrangement allows for a total of eight hydrogen bonds within each tetrad, increasing the stability of these structures (52).

The stacking of G-tetrads to form the G-quadruplex occurs in a right handed, helical fashion creating a central pore throughout the length of the structure (53). As shown

in Figure 8, monovalent metal cations such as potassium or sodium are situated in the central pore in between the G-tetrad layers and help to stabilize the structure (54-56). Folding of the G-quadruplex structure is dependent upon the presence of metal cations and although divalent cations including Mg^{2+} , Ca^{2+} and Sr^{2+} can induce quadruplex formation, they do not stabilize the structure to the extent of the monovalent metal cations (57, 58). Thus, most studies on the G-quadruplex structure have been completed in the presence of either sodium or potassium (59-61). The difference in folding topologies between G-quadruplexes formed in the presence of either sodium or potassium is most likely due to size differences between the ionic radii of the atoms (60).

The length of the sequence and the number of repeating tracts of guanine residues dictates the number of strands needed to form a G-quadruplex structure. Intramolecular quadruplexes are formed from a single strand of DNA whereas intermolecular quadruplexes can exhibit molecularities of either two or four (54, 60, 62, 63). The differences in molecularity of various G-quadruplex structures gives rise to various strand orientations including parallel, anti-parallel, and a combination of both parallel and anti-parallel (64, 65). A summary of the different molecularities and the resulting strand orientations exhibited by G-quadruplex structures is presented in Figure 9.

Tetramolecular species give rise to all parallel strand orientations while both intramolecular and bimolecular species have strand orientations that are anti-parallel. Due to the parallel strand orientation, tetramolecular species are more thermally stable when compared to intramolecular and bimolecular species. This is due to a favorable rotation about the glycosidic bond in parallel species leaving the all guanine bases within the G-tetrads in an anti-conformation relative to the sugar (60, 61). In the anti-parallel species, the guanine bases adopt both the anti- and syn-conformations which contribute to the

polymorphism of the anti-parallel G-quadruplex structures (66). In all structures, the glycosidic bond angles allow for the orientation of the oxygen at the C6 position towards the center of the tetrad, allowing for the coordination of the metal cation (67).

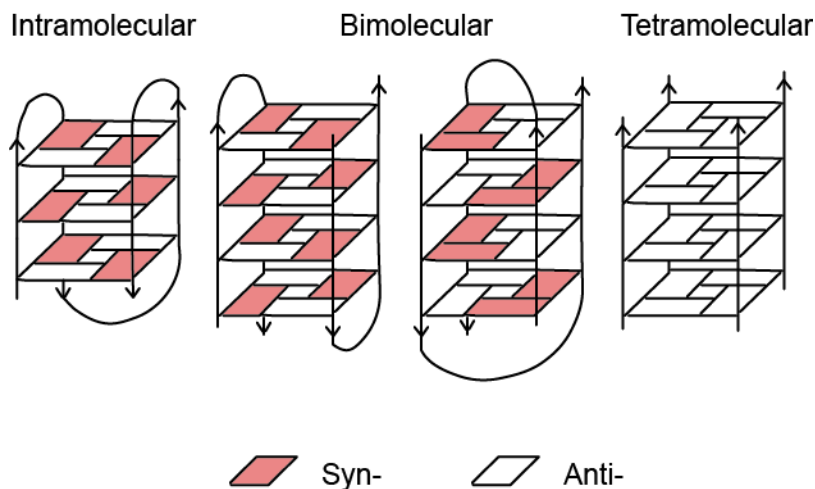


Figure 9. Different Molecularities and Strand Orientations of G-quadruplex Structural Motifs. Intramolecular G-quadruplexes are formed from one strand of DNA whereas bimolecular and tetramolecular G-quadruplexes are formed from two and four strands of DNA, respectively. Figure created in Adobe Illustrator CC.

The human telomere is an important sequence of non-coding DNA located at the end of chromosomes serving to protect the coding regions of the genome from chromosomal degradation (68). Telomeric DNA consists of a repeating sequence of 5'-TTAGGG-3' that ranges between 2 and 50 kilobase pairs in length with the last 100 to 600 bases exist as a single strand. With each round of cell division, the telomere is short-

ened due to the end replication problem. The end replication problem that occurs during DNA replication is a result of the directionality of DNA polymerase. The replication of the 5'- and 3'- strands occurs separately and because DNA polymerase works in the 5- to 3' direction, only the 3' strand of the original DNA duplex is able to be replicated continuously. For replication of the 5' strand, short Okasaki fragments are created and the gaps in between each fragment are filled in and joined through the combined actions of a second DNA polymerase and a DNA ligase. Removal of the RNA primer from the 5'-ends of the parent strands leaves a 3'-overhang on the newly synthesized daughter strand. These 3'-overhangs are removed from DNA in adult cells, thus causing a shortening of the DNA replicated (69).

Once the telomere is shortened to the point that the cell can no longer divide without damaging the coding region of DNA, apoptosis is triggered within the cell. This can occur after 60 to 80 rounds of replication with about 50 bases lost per replication cycle (70). The actual length of the telomere is regulated by a reverse transcriptase enzyme called telomerase which works to extend the length of the 3' end of the telomere (71). Telomerase has been shown to be upregulated in cancer cells (resulting in the extension of the telomeric region) allowing these cells the ability to divide infinitely without signaling apoptosis (72). The single-stranded region of the human telomere can fold into a unique secondary structure known as a G-quadruplex that has been shown to inhibit telomerase activity. Because of this, the quadruplex structure formed by the human telomere is an attractive target for study in relation to cancer inhibition, specifically the stabilization of the G-quadruplex structures in vivo through the binding of small molecules to actively inhibit the actions of telomerase in cancer cells (73, 74).

Nucleic Acid Drugs Used in Gene Therapy

The use of synthetic oligonucleotides as therapeutic drugs became a topic of interest after it was reported that oligodeoxynucleotides complementary to specific regions of RNA or mRNA within the AIDS virus were able to inhibit replication of the virus (75). Since that time, numerous therapeutic oligonucleotides have been developed to make use of a variety of different types of nucleic acids. The section below provides a brief overview of the various types of synthetic oligonucleotides that are used as DNA drugs.

Antisense oligonucleotides have been developed from short sequences of DNA or RNA oligonucleotides that bind to complementary regions of RNA or mRNA. Upon binding, antisense therapeutics signal degradation of the RNA component by Ribonuclease H (RNaseH), which is an endoribonuclease that hydrolyzes the phosphodiester bonds of RNA. Several antisense oligonucleotide drugs have been developed in response to diabetes (76), rheumatoid arthritis (77), and cancer (78, 70). The most successful of which have been modified along the backbone to increase stability and prevent degradation by nucleases (80). For a summary of the various chemical modifications available to therapeutic oligonucleotides, the reader is directed to a recent review (81).

Another type of common nucleic acid therapeutic is interfering RNAs, either small interfering RNAs (siRNAs) or micro RNAs (miRNAs). Both siRNA and miRNA consist of short sequences of RNA, however the major difference between the two is that siRNA is double stranded, whereas miRNA is single-stranded. These types of nucleic acid therapeutics are complementary to a particular gene of interest and when inserted into the cell, interact with that gene to inhibit its transcription. It is because of this down-

regulatory mechanism that siRNAs are thought to be able to be applied to a wide range of diseases including cancer (82), Ebola (83), and glaucoma (84).

Aptamers are a class oligonucleotide therapeutics that works by interacting with specific proteins or small molecules within the cell such as dopamine (85) and human thrombin (86). Aptamers can be composed of DNA or RNA and fold into a complex tertiary structure. These structures have also been shown to be effective in reducing angiogenesis in age-related macular degeneration patients by binding to VEGF165 and inhibiting it from reacting with the VEGF receptor (87). Due to their high specificity, aptamers have also shown promise as a targeting mechanism. In some cases, aptamers have been attached to small molecule drugs to increase their targeting specificity (88) and in other cases, drug-loaded nanoparticles have been coated with aptamers to increase the efficiency of their delivery (89).

Our lab is particularly interested in those DNA aptamers that fold into a G-quadruplex structure such as the thrombin binding aptamer (TBA) (90) and the anti-nucleolin aptamer, designated AS1411 (91). The TBA was first discovered through SELEX (systematic evolution of ligands by exponential enrichment) experiments in 1992 (90) and the G-rich, single-stranded sequence, 15 bases in length, has been shown to fold into a G-quadruplex (92). Binding of TBA to human thrombin occurs in the same binding pocket as fibrinogen, which is needed for the formation of blood clots, and it is this mechanism of action allows TBA to act as an anti-coagulant (93). The AS1411 aptamer is a G-rich phosphodiester oligodeoxynucleotide that is 26 nucleotides in length (91). This aptamer is the truncated form of a 29-mer oligodeoxynucleotide sequence known as GRO29A, originally studied at the University of Alabama in Birmingham (94). Studies on AS1411 have shown it to bind to the nucleolin expressed on the surface of cancer cells

and induce apoptosis of these cells (95). Both G-quadruplex forming aptamers described above have been tested in clinical trials and show promising therapeutic potential (96, 97).

Even with the number of clinical trials for oligonucleotide therapeutics, major limitations still exist concerning the in-vivo delivery efficiency and the number of doses necessary to sustain a therapeutic level of oligonucleotide. In summary, the use of nucleic acids as therapeutics is a promising area of research that is applicable to a wide range of diseases provided that advancements are continuously made to improve the delivery and bioavailability of the oligonucleotide therapeutics.

Drug Delivery Vehicles

Many diseases, including a large number of cancers, sickle-cell anemia, cystic fibrosis, and Huntington's disease, are caused by problems with the expression of genes within specific tissues of the body. Once this was identified, researchers began to look towards the creation of new technologies to correct the undesirable genetic mutations that result in disease. These approaches, also known as gene therapy, are relatively new concepts that were first studied in the 1980's when research began to develop a method to insert functional genes into cells (98). Today, gene therapy exploits the use of nucleic acids to perform a certain cellular function once inserted into the cell.

A major challenge to the success of gene therapy is in the delivery of the gene to the target cell and into its nucleus (79). Encapsulation of the genetic material as a method of delivery is a promising approach to protecting the oligonucleotides from degradation before reaching their target. Viral vectors were first used as a way of transfecting cells but due to increasing concerns over the safety of these methods, non-viral vectors

have been determined to be the more advantageous route for gene therapy (99). Non-viral vectors have been designed from mixtures of cationic lipids and co-lipids to form lipoplexes (100), small molecules (101), and polymers such as polyethylenimine (PEI) or poly(DL-lactide-co-glycolide) (PLGA) (102, 103). Non-viral vectors offer not only a safety advantage, but also a controllable vehicle for delivery that can be modified to target specific tissues. Even with these advantages, poor delivery efficiency is still a major barrier for non-viral vectors.

A second challenge that limits the functionality of gene therapy is the ability to express the transgene in a sufficient amount that results in a therapeutic effect (79). To overcome this limitation, the therapeutics must be delivered in a larger quantity or the DNAs delivered must be modified with an expression system to ensure the proper expression levels of proteins. We therefore suggest that one method to overcome current limitations in the amount of transgene expression in gene therapy is by fabricating a hydrogel capsule capable of synthesizing nucleic acids, as these capsules can provide a larger amount of nucleic acid fragments than can be delivered through current techniques.

Ideal drug delivery vehicle will (1) be composed of biocompatible materials that do not elicit an immune response, (2) have high encapsulation efficiencies of the desired drug without leaking of the cargo, (3) have the ability to be modified with targeting ligands, and (4) have a mechanism for the controlled release of cargo.

Thus far, several methods have been used to accomplish this delivery and can broadly be characterized by either viral or non-viral transport vesicles. While viral vectors provide an efficient *in vivo* delivery system, it is non-viral delivery mechanisms that have been a major focus of research over the past decade due to their increased biosafety. Besides their lessened immunotoxicity and decreased pathogenicity when compared to

their viral counterparts, nonviral vectors also have the advantage of selective targeting. Even with advantages, the need for increased delivery efficiency of its cargo still poses major challenges and drives the research towards the development of a novel non-viral vector that maintains its biosafety while increasing its delivery efficiency. Recent research from our laboratory has demonstrated that hydrogel capsules offer a unique ability to encapsulate small molecules and to be internalized by cells to deliver its cargo without causing cytotoxicity.

Encapsulation of nucleic acids as a form of gene therapy is a well addressed field that has not been able to overcome the challenges associated with delivering target oligonucleotides to the nucleus of a cell with enough specificity to reach a therapeutic level of transgene expression over the desired time. Using polymeric nanoparticles as a delivery vehicle provides the advantage of being able to create bio-compatible capsules that are highly tunable. That is, the synthesis of capsules can be modified to produce capsules with controlled sizes, capacities, targeting, environments for diverse cargo loading, and release mechanisms. Several types of nucleic acids have been shown to be able to be encapsulated by polymeric capsules including DNA (104) and siRNA (105), both encapsulated through the layer-by-layer synthesis of poly(methacrylic acid) hydrogel capsules, and plasmid DNA (pDNA) which has been encapsulated through a double emulsion technique using poly(DL-lactide-co-glycolide) (PLGA) and polyvinyl alcohol (106).

Layer-by-Layer Self-Assembly of Microcapsules

Layer-by-Layer (LbL) technology originated in the mid-1960s, and was pioneered by the work of Drs. Iler, Kirkland, and Nicolau (107-110). However, it wasn't until the early 1990s, when the Decher group incorporated the use of synthetic polyelectrolytes,

that this technique began to be more widely utilized (111). The LbL technique can be broadly defined as a process to build up materials on a templated surface, one layer at a time, through the non-covalent interactions between natural or synthetic polyelectrolyte substances (111). LbL self-assembly of films and capsules has been used in a broad number of biomedical applications including biomimicry (112-114), sensing (115, 116), and drug delivery (117, 118). While LbL techniques can be applied to the creation of films (119, 120), microcapsules (121, 122), and microparticles (123, 124), the following section will discuss LbL technology as it applies to hollow microcapsules.

The synthesis of hollow microcapsules utilizing LbL technology offers the user a controlled method to impart specific functionalities into the resulting material (125, 126). In this process, polymers are first adsorbed to a sacrificial template such as porous silica spheres (117, 127, 128), manganese carbonate (129, 130), or calcium carbonate (129, 131, 132). Polymers are then layered atop of one another, alternating between different polymers until the desired number of layers is reached. The cyclic nature of this process is illustrated in Figure 10. Hollow microcapsules are obtained once the sacrificial template is removed. It should be noted that the hollow microcapsule presented in Figure 10 is not drawn to scale relative to the sacrificial template; the microcapsule has been enlarged for easier viewing of the multilayer assembly. Microcapsules formed via LbL assembly possess a unique characteristic of having a nano-sized multilayer shell while taking up space at a microlevel (133, 134). It is for this reason that the synthesis of microcapsules using LbL technology are said to be controllable at a nanoscale level.

The buildup of multilayers is achieved by taking advantage of non-covalent interactions such as hydrogen bonding, electrostatic interactions, van der Waals forces, and the exclusion of water from hydrophobic portions of the polymers (135, 136). The inter-

actions that drive the self-assembly of the multilayer can influence various properties of the resulting material including the thickness of the multilayer shell and the morphology (i.e. rough or smooth) and permeation properties of the microcapsule (137). The non-covalent forces such as these are dependent upon environmental factors like pH and salt concentration and thus, the stability of microcapsules is often reinforced through chemical crosslinking of the polymer multilayers (138, 139). LbL self-assembly is a versatile technique that offers several advantages in comparison to traditional coating methods. One important benefit to using LbL techniques is that they are not limited to the type of substrate or its size. This means that the size of the resulting microcapsule is directly influenced by the size of the sacrificial template.

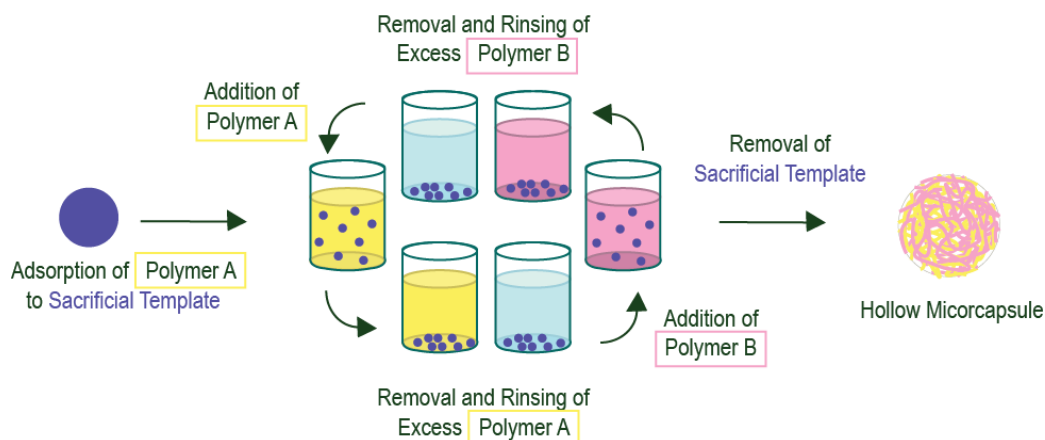


Figure 10. General Strategy for LbL Creation of Hollow Microcapsules. Figure created with Adobe Illustrator CC.

Research Summary

Gene therapy is an exciting area of research that can be described by the delivery of genetic material to help control diseases including multiple types of cancers, neurodegenerative diseases such as Parkinson's and Huntington's Disease, sickle-cell anemia, and cystic fibrosis. Many types of nucleic acids have been studied to treat disease however their use has been limited by inefficient delivery to the nucleus. The interactions between the nucleic acid drug and its receptor molecule within the cell are dependent upon the sequence and the structure of the nucleic acid. One type of nucleic acid structure that is particularly interesting are the G-quadruplexes formed from guanine rich sequences of DNA. These structures have been shown to play important roles in the cell including the provision of transcriptional regulation and telomeric maintenance. Additionally, the design of thrombin binding aptamers, a type of DNA drug, mimics the G-quadruplex structure. In recent years, the focus of nucleic acid delivery has been non-viral vectors constructed from synthetic polymeric due to inherent safety concerns of using viral vectors.

The compilation of this work seeks to blend polymer chemistry, biophysical chemistry and enzymology in a way that advances gene therapy as a viable tool for the treatment of a variety of diseases through the encapsulation and controlled release of G-quadruplex DNA structures. To complete this work, synthetic deoxyoligonucleotides of the human telomeric sequence were chosen as the nucleic acid drug for encapsulation and a structural study was performed first to determine the relative importance of the bases in the loop sequence region. G-quadruplex forming oligonucleotides were then encapsulated within two-component poly(methacrylic acid) (PMAA)/ poly(N-vinylpyrrolidone) (PVPON) microcapsules using a Layer-by-Layer (LbL) deposition strategy. Release of

the G-quadruplex structures using a controlled therapeutic ultrasound technique was then studied. It is important to note that this methodology can be easily refined for applications of in vivo targeting and synthesis of DNA and/or RNA as therapeutic agents that could be applied to several diseases.

CHAPTER 2

METHODS

The following chapter provides important background information relative to each technique as well as a general description of the procedures that were used in this body of work. Specific information about each of the experiments can be found within the chapters' specific for that method.

Preparation of Buffers

Buffers were freshly prepared for each experiment in MilliQ-ultrapure water at a volume slightly less than the desired total volume. After a 3-point calibration (pH 4.0, 7.0 and 10.0) with the pH meter, the pH of the solution was adjusted to the desired value using either HCl or NaOH. Buffer solutions were then transferred to a volumetric flask and diluted to the appropriate volume with MilliQ-ultrapure water. The buffer solutions were then filtered using a Millipore vacuum filtration apparatus with a 0.45 μm membrane filter. Buffers were stored at room temperature until use. The pH of each buffer was checked and appropriately adjusted before each experiment. Buffers were also checked periodically for bacterial growth. This was a rare occurrence for buffers that were properly filtered.

BPES buffers (0.01 M NaH_2PO_4 , 0.01 M Na_2HPO_4 , 0.001 M EDTA, and 100 mM NaCl) at pH 7.4 were prepared to reconstitute the DNA oligonucleotides. Phosphate

buffers (0.01 M NaH₂PO₄, 0.01 M Na₂HPO₄, and 100 mM NaCl) used to solvate the polymers used in this work were prepared at various pH levels as indicated in Chapter 4.

DNA Preparation

The following section describes the DNA preparation techniques used in both the characterization of G-quadruplex structure as a function of the loop sequence and the encapsulation of various DNA structures found in Chapters 3 and 4, respectively.

Synthetic Deoxyoligonucleotides

HPLC purified, G-quadruplex forming deoxyoligonucleotides were purchased from Midland Certified Reagents (Midland, TX). The oligonucleotides were re-suspended by adding an appropriate volume of BPES buffer (pH 7.4) to make a 1 mM (strand) stock solution. The G-quadruplex stock solutions were vortexed and allowed to sit overnight at 4 °C. The actual concentration of the G-quadruplex solution was checked using UV/vis spectroscopy. When the G-quadruplex solutions were not in use, they were stored at 4 °C.

Calf-thymus DNA

To prepare double-stranded DNA samples, calf thymus DNA (purchased from Sigma-Aldrich, St. Louis, MO) (ctDNA) fibers were weighed out (2:1 weight (mg) vs volume (mL) and added to a phosphate buffer (0.01 M NaH₂PO₄, 0.01 M Na₂HPO₄, 0.001 M EDTA). Solutions were allowed to solvate at 4 °C overnight until the DNA strands were completely dissolved. Once in solution, the DNA strands were sheared to shorter lengths through sonication using a Branson sonifier. The DNA was sonicated in 5

minute on/off intervals (to insure no overheating of the solution occurs) for a total sonication time of 30 minutes. To circumvent the heat evolved during this process, the DNA solution was kept in an ice bath. Additionally, nitrogen gas was bubbled through the sample throughout the sonication process to protect the blunt ends of the DNA from oxidation.

The sonicated solution was filtered using a 0.45 μm syringe filter and solid sodium chloride was added to increase the total salt concentration of the solution to 0.2 M NaCl. Several syringe filters were used to filter the entire solution due to clogging of the membrane. Back-pressure on the syringe pump during filtering is an indication that the membrane is clogged. The exact number of syringe filters needed is determined by the solution volume and viscosity. After filtering, the ctDNA sample was treated with RNase A to degrade any RNA present within the sample, followed by treatment with proteinase K to digest both the RNase as well as any other protein impurities in the DNA solution. An important feature of proteinase K is its auto-catalytic activity, meaning that it will digest itself, leaving no enzymes present in solution. RNase degradation was performed at 37 °C for 30 minutes and proteinase K digestion reacted for 2 hours at 37 °C.

After enzymatic digestions to remove RNA and protein, the DNA solution was extracted with a 1:1 chloroform/phenol solution. The DNA solution was vigorously mixed with an equal volume of the chloroform/phenol and the suspension decanted into two 50 ml glass test tubes. The layers were separated by centrifugation on the clinical centrifuge at 4 °C. The top layer containing the DNA was removed and returned to the separatory funnel. Care is taken not to contaminate the aqueous layer with the interface between the DNA and the organic layer. This step is repeated (~3 times) until the interface between the aqueous and organic layers is clear (not cloudy or white with pre-

cipitated protein). After the final centrifugation, the DNA layers were pooled in a 50-mL Falcon tube.

Precipitation of the ctDNA from the solution was achieved with the addition of -30 °C, salt-saturated ethanol. Centrifugation was used to pellet the precipitated DNA. The resulting DNA pellet was dried under vacuum. BPES buffer (0.01 M NaH₂PO₄, 0.01 M Na₂HPO₄, 0.001 M EDTA, and 100 mM NaCl) was added to the DNA pellet and allowed to solvate overnight at 4 °C. The DNA solution was pipetted into a dialysis bag and dialyzed against BPES buffer to remove any excess salts and small DNA fragments. The dialysis medium was exchanged with fresh BPES buffer a minimum of four times. The DNA was then filtered a second time using a 0.45- μ m syringe filter. The concentration of the stock DNA solution (in base pairs) by serial dilution by monitoring the UV/vis absorbance at 260 nm ($\epsilon = 13,200 \text{ M}^{-1} \text{ cm}^{-1}$).

Preparation of Polymer Solutions

The PMAA (100 kDa) and PVPON (1300 kDa) polymers used in this work were dissolved in the BPES buffer (0.01 M NaH₂PO₄, 0.01 M Na₂HPO₄, 0.001 M EDTA, and 100 mM NaCl) at pH 4.0 overnight, without stirring, to allow for complete solvation of the polymer chains. Due to the increased molecular weight of PVPON as compared to PMAA, the time to fully solvate PVPON will be greater than that for PMAA. Visual inspection of the solution for schlieren lines, which arise from mixing solutions with different refractive indexes, served as an indicator that the polymer had not yet been fully solvated by the buffer. After visual confirmation that the polymers were completely dissolved, the pHs of the solutions were adjusted to the desired value. Polymer solutions

were used within one week of their preparation and were stored at room temperature when not in use.

Differential Scanning Calorimetry

Differential scanning calorimetry (DSC) is a technique that measures the heat capacity change of a sample as a function of temperature (140, 141). In general, solutions of interest are placed in a sample cell, their corresponding buffers are placed in a reference cell and the temperature is increased over time. The heat energy needed to maintain a constant temperature in both cells is collected and then plotted as a function of temperature. The melting temperature of the system is determined from the curve peak. Additional processing of this data allows for the determination of thermodynamic parameters such as enthalpy (ΔH), entropy (ΔS), and Gibbs free energy (ΔG) (141).

The heats associated with G-quadruplex unfolding in this work were measured using a Microcal VP-DSC (Malvern Instruments, Northampton, MA). Scans were collected over a temperature range from 10-100 °C with a heating rate of 0.5 °C/min. The deoxyoligonucleotides used in these experiments ranged from 175 to 225 μM in strand concentration. At least five heating and cooling cycles were conducted for each sample to assess the reversibility of unfolding. Baseline scans were also completed for these experiments by placing the buffer in both the sample and reference cells. The baseline scans were completed using the same parameters as the sample solutions described above. Data were analyzed by 1) subtraction of the baseline scan from the raw sample data, 2) normalization to strand concentration and generation of heat capacity versus temperature plots, and 3) baseline correction of the heat capacity plots. Analyses of all DSC data were completed using Origin 7.0 VP-DSC software.

Circular Dichroism Spectroscopy

Circular dichroism (CD) is a spectroscopic technique that measures the absorption difference between left- and right-handed circularly polarized light. This phenomenon, known as ellipticity, occurs when molecules are chiral (142, 143). CD is most commonly used for the secondary structure prediction of proteins but it has also been proved useful for studying the structures of nucleic acids, specifically, the G-quadruplex forming structures. Like other spectroscopic techniques, the absorbance differential measured by CD can be taken as a function of temperature, or time, to derive information about the thermal stability or the kinetics of the system, respectively (144 – 146).

In this work, CD was used to confirm the G-quadruplex structure of 1) the loop sequence variants of the human telomere (Chapter 3) and 2) the G-quadruplex forming sequences released from PMAA/PVPON microcapsules (Chapter 4). For both studies, samples were scanned from 225-325 nm and the average of three scans was used for data analysis. The presence of a positive ellipticity band at 265 nm indicates the folding of the sequence into an all-parallel G-quadruplex structure and the presence of a negative peak at 265 nm with a positive peak at 295 nm indicates the folding of the sequence into an anti-parallel G-quadruplex structure (147).

Thermal stabilities of the loop sequence variants (Chapter 3) were also carried out in this work using CD spectroscopy. For these studies, the ellipticity was collected at 295 nm as a function of temperature from 10 to 90 °C. The temperature was increased at a rate of 1 °C/min and measurements were taken at every 1 °C. Prior to the first scan, samples were thermally equilibrated for 15 minutes with stirring. Samples were also equilibrated for one minute prior to each successive scan. A melting profile of the buffer was also collected and then baseline subtracted from each spectrum. The data was then nor-

malized to molar ellipticity by dividing the raw ellipticity data by the concentration of each sample multiplied by the pathlength of the cuvette that the data was collected in. The thermal stability, as defined by the melting temperature (T_m), was calculated from the midpoint of the sigmoidal transition using the first derivative method (148).

Advanced, three-dimensional melting profiles of the loop variant sequences (Chapter 3) as a function of both temperature and wavelength were also collected by CD in this work. For these studies, CD scans were collected for each sample from 220 to 320 nm over a range of temperatures. Starting at 4 °C, scans were collected every 2 degrees until the temperature reached 90 °C. The temperature was increased at a rate of 1 °C/min and sample was equilibrated at each temperature for 1 minute before completing the scan. Analysis of the three-dimensional melting profiles was completed using singular value decomposition as described in the follow section.

Analysis of Data by Singular Value Decomposition

Singular value decomposition (SVD) is a mathematical technique where complex data matrices can be analyzed for the presence of significant species (149, 150). In this work, SVD analysis is applied to three-dimensional melting profiles, collected by CD spectroscopy, to determine the number of significant spectral species present during the unfolding of G-quadruplex forming sequences the human telomere and its loop sequence variants (Chapter 3). An excellent review on SVD regarding the unfolding of deoxy-oligonucleotides can be found here (151).

To complete SVD analysis, the data collected for each sequence must first be arranged in a $i \times j$ matrix where i , represents the range of wavelengths that ellipticity was

collected at a certain temperature, j . The following equation was used in Matlab software (MathWorks, Natick, MA) to perform SVD on each data matrix:

$$SVD(A) = USV$$

In this equation, the $i \times j$ data matrix, represented by A , is equal to the product of three separate matrices, U , S , and V , each representing important information. Matrix U contains the basis spectra, matrix S contains the singular values, and matrix V contains the amplitude vectors. The total number of significant spectral species can be estimated through a combination of analyses of the following: 1) the different components of the S , $U \times S$, and V matrices, 2) the calculation of autocorrelation coefficients of the U and V matrices, and 3) the analyses of difference matrices plots calculated with a succinct number of singular values.

Autocorrelation coefficients calculated for the U and V matrices are inspected for the magnitude of their value. For a component of the U or V matrices to be considered spectrally significant, autocorrelation coefficients must be greater than 0.8. Autocorrelation of U and V matrices is performed using the following equation:

$$C(X_i) = \Sigma(X_{i,j})(X_i + 1_j)$$

The last component of SVD analysis consists of the plotting of difference matrices, calculated using the following equation:

$$D = A - US'V_T$$

Multiple difference matrices are calculated for each matrix A, by using a different number of singular values in each S' matrix. Each difference matrix is then evaluated by comparison to one another, through a contour plot. When the difference matrix contour plots present as random noise with no regular patterns, they have been calculated with the number of singular values that equals the spectrally significant components.

Encapsulation of DNA Within Sacrificial Cores

Calcium carbonate (CaCO_3) particles were chosen as the sacrificial cores in this work due to their biocompatibility as well as the ease in which they can be synthesized and then subsequently be dissolved and removed from the system. To condense the G-quadruplex forming oligonucleotides within CaCO_3 particles, equal volumes (1 mL) of 0.1 mg/mL calcium chloride, CaCl_2 , and 0.1 mg/mL sodium carbonate, Na_2CO_3 , were mixed with 1.0 μm oligonucleotide (10 μL) and enough DI water to bring the total volume to 3 mL. Each solution was added, sequentially, to a small cylindrical vial, commonly referred to as an "ITC tube", in the following order: DI water, CaCl_2 , oligonucleotide, and finally Na_2CO_3 . Prior to adding the solutions, the vial was equipped with a 'flea' stir-bar and placed upon a magnetic stir plate with the speed setting to 10.

The solutions were mixed continuously as they were being added to the vial. Upon the addition of Na_2CO_3 , a timer was started, and the solution mixed for exactly 40 seconds. The vial was removed from the stir plate, the stir-bar was removed using a magnetic rod, and the resulting CaCO_3 particle solution was split equally among two Eppendorf tubes (2.5 mL) using a Pasteur pipette. Care was taken not to scrape the bottom of the vial with the pipette as this could damage the structural integrity of the particles.

The Eppendorf tubes containing the CaCO₃ particle solutions were then pulsed on a portable, table-top centrifuge to separate the CaCO₃ particles from the supernatant. The supernatant was removed via a pasteur pipette and any remaining salts were removed by washing the CaCO₃ particles with DI water.

To wash the particles, DI water was added to the 1 mL line on the Eppendorf tube and the tubes were then vortexed to re-disperse the CaCO₃ particles. A second wash cycle, consisting of centrifuging the Eppendorf tubes to separate the CaCO₃ particles from the supernatant, replacement of the supernatant with DI water, and vortexing to re-suspend the CaCO₃ particles was completed. On the third wash cycle, the supernatant was removed from both Eppendorf tubes, however only one tube had its supernatant replaced with DI water. This tube was vortexed and then its contents were transferred to the second Eppendorf tube to combine the CaCO₃ particles into a single container. Once the CaCO₃ particles are combined into one Eppendorf tube, they are ready for immediate polymer deposition.

LbL Assembly of DNA Loaded Microcapsules

DNA loaded microcapsules were prepared using a hydrogen bonded, LbL self-assembly method (152, 153). To prepare the capsules, poly(methacrylic acid) (PMAA) and poly(N-vinylpyrrolidone) (PVPON) were sequentially layered on top of the DNA-loaded CaCO₃ sacrificial cores as prepared in the previous section of this chapter. The addition of one layer of PMAA and one layer of PVPON constitutes a single bilayer and the total number of bilayers added was dependent upon the particular study (Chapter 4). In this work, PMAA (average M_w 100,000 g mol⁻¹) and PVPON (average M_w 1,300,000 g mol⁻¹) were used for the fabrication of the multilayer composing the microcapsule

shell. The multilayer was stabilized further through the chemical cross-linking of the PMAA molecules with cystamine and the sacrificial cores were removed with treatment with EDTA. Specific information about each step is presented below.

All polymer depositions on the CaCO₃ cores used in this work were performed at pH 4.0. To facilitate the adsorption of positively charged PMAA to the DNA-loaded CaCO₃ cores, negatively charged polyethyleneimine (PEI, 0.25 mg/mL) was used as the initial polymer. Approximately 1 mL of PEI was added to the CaCO₃ cores in a 2.5-mL Eppendorf tube and was shaken for 15 minutes. Samples were then centrifuged using a short-spin pulse method and the excess PEI in the supernatant was carefully removed using a Pasteur pipette. To wash the excess PEI from the cores, the supernatant was replaced with approximately 1 mL of phosphate buffer at pH 4.0 and the cores were re-dispersed by vortexing the Eppendorf tube. The sample was then centrifuged and the supernatant removed as previously described to complete the wash step. The wash step was repeated a second time and two wash steps were performed between each subsequent polymer deposition.

To begin assembling the multilayer, approximately 1 mL of PMAA (0.1 mg/mL, pH 4) was added to the PEI-coated cores in the Eppendorf tube. PMAA was deposited for 10 minutes with constant shaking before the excess was removed by centrifugation and removal of the supernatant. After two wash steps, another polymer deposition step was performed using PVPON (0.1 mg/mL, pH 4). This pattern of polymer deposition followed by two wash steps was repeated until the desired number of polymer layers was reached. These polymer-coated CaCO₃ cores will hereby be referred to as core-shells.

Cross-linking of the PMAA molecules was achieved through a combination of two reactions. PMAA cannot directly bind the cystamine cross-linker and thus, the car-

boxylic acid side groups must first be modified so that they can react with the primary amine that is found on either side of the cystamine structure. This was achieved by converting the carboxylic acid side groups to an active ester through a reaction with 1-ethyl-3-(3-(dimethylamino)propyl)-carbodiimide hydrochloride (EDC). Core-shells were washed twice with phosphate buffer at pH 5.5 before approximately 1 mL of EDC (1 mg/mL, pH 5.5) was added. The EDC reacted for 35 minutes before it was removed by the centrifugal separation of the supernatant as described previously. After two wash steps with pH 5.5 phosphate buffer, the PMAA was then crosslinked by adding approximately 1 mL of cystamine dihydrochloride (1 mg/mL, pH 5.5) to the core-shells. The cystamine was removed from the core-shells after the desired length of cross-linking time.

Cross-linked core-shells were washed twice with phosphate buffer (pH 5.5) and approximately 1 mL ethyldiaminetetraacetic acid (EDTA, 1 mM, pH 5.5) was added to dissolve the cores. For this reaction, samples sat on the benchtop with no shaking. EDTA solutions were replaced after sufficient settling of the core-shells to allow the removal of the supernatant. The extent of dissolution was checked using optical microscopy and after complete dissolution, the EDTA supernatant was removed from the system, and the microcapsules washed twice with phosphate buffer at pH 5.5.

Prepared microcapsules were dialyzed against phosphate buffer at pH 7.4 to 1) remove excess EDTA, 2) remove excess CO_3^{3-} ions, and 3) re-equilibrate the system at a biologically relevant pH. After dialysis, the microcapsules were stored at room temperature until use. Optical microscopy was used to observe the shape and size of the resulting microcapsules. The concentration of the microcapsules in solution was estimated using a hemocytometer.

Zeta-Potential Studies

Measurement of the Zeta-potential (ζ -potential) is frequently used to estimate the net surface charge of a particle in a suspension (154, 155). In solution, charged particles are surrounded by a layer of counter-ions tightly bound to the charged surface known as the stem layer. This layer is then enveloped by a cloud-like region, known as the diffuse layer, containing both co- and counterions, relative to the surface charge of the particle. The diffuse layer expands several nanometers outward from the surface of the particle and together both layers are referred to as the electrical double layer. The stem and diffuse layers are illustrated in Figure 1 in blue and green, respectively.

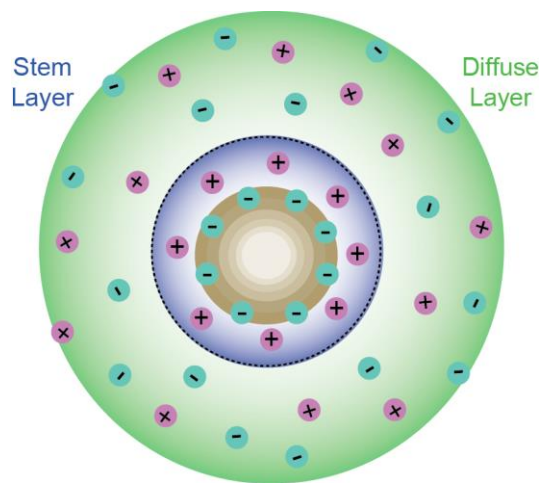


Figure 1. Co- and Counter-ion Distribution at the Surface of Charged Particles. Figure created using Adobe Illustrator CC.

The absolute value of the electric potential is directly proportional to the distance from the surface and this value approaches zero as the distance increases to include the neutral electric potential of the bulk solution. Zeta-potential of solutions are described as the electrical potential difference between the stem and diffuse layers. The potential in this region is thought to be a direct reflection of the surface charge on the particle, and thus represents the effective surface charge of the particle in solution (156).

Measurements of the ζ -potential of the various solutions in this work were calculated through an indirect measurement of the electrophoretic mobility of the microcapsules using a Nano Zetasizer (Malvern Instruments). Characterization of the relationship between the surface charge of the microcapsules and the pH was accomplished by collecting the ζ -potential of capsules after they are exposed to buffers of varying pH. The ζ -potential was determined by taking the average of three measurements, each set to collect an optimal number of scans based upon the signal to noise ratio of the spectra.

FTIR Studies

Fourier transform infrared spectroscopy (FTIR) is a method to identify functional groups of a molecule by monitoring the bond vibrations and stretching (157, 158). In this technique, an infrared interferon is collected and then Fourier transform (FT) is applied to the collected data to obtain the infrared spectrum (159). To confirm that the microcapsules have a two-component system, that is, to make sure they are composed of both PMAA and PVPON, the microcapsules were examined using Fourier Transform Infrared Spectroscopy (FTIR). Samples were prepared by freeze-drying overnight at the desired pH. The absorbance mode of an ATR-FTIR (Bruker, Alpha-FTIR) was used to collect data over a full range of wavelengths. A total of 128 scans were collected for each of the

background and sample measurements. All spectra were normalized and then baseline corrected before being analyzed.

Therapeutic Ultrasound Release of DNA

The ultrasound range for sound waves are those that have a frequency greater than 20 kHz and are not audible to the average adult. Medical ultrasound, or diagnostic ultrasound, is a technique that uses the vibrations from sound waves for imaging or other diagnostic purposes (160). Diagnostic ultrasound is performed at intensities that are less than 720 mW/cm^2 (161). When the intensity is increased above this threshold, up to 105 W/cm^2 , the technique is known as therapeutic ultrasound (162). Therapeutic ultrasound can be used to release the cargo of microcapsule through an effect known as inertial cavitation (163). In this process, high intensity focused ultrasound (HIFU) is applied to drug delivery vesicles, forming short-lived microbubbles. Collapse of the microbubbles emits a shockwave that can shear the molecules constructing the microcapsules when they are near one another. Perturbation of the polymers leads to degradation of the microcapsules and the subsequent release of cargo (164).

In this work, therapeutic levels of ultrasound were used to release DNA cargo from two-component PMAA/PVPON microcapsules. To prepare the microcapsule for ultrasound release, samples were dialyzed vs pH 7.4 phosphate buffer ($0.01 \text{ M NaH}_2\text{PO}_4$, $0.01 \text{ M Na}_2\text{HPO}_4$). After removal from dialysis, the microcapsules were diluted and sonicated at 40% power (57 W/cm^2) for 20 seconds. The extent of capsule rupture was monitored using optical microscopy. Capsule fragments present as small lines and semi-circles and are easily distinguishable from the intact spherical capsules.

CHAPTER 3

STABILITY OF THE Na^+ FORM OF THE HUMAN TELOMERIC G-
QUADRUPLEX: ROLE OF ADENINES IN STABILIZING G-QUADRUPLEX
STRUCTURE

by

BRENN A. TUCKER, JASON HUDSON, LEI DING, ED LEWIS, RICHARD D.
SHEARDY, EUGENIA KHARLAMPIEVA, DAVID E. GRAVES

Submitted to *ACS Omega*

Format adapted for dissertation

ABSTRACT

G-quadruplexes are higher order DNA structures that play significant roles in gene transcription and telomeric maintenance. The formation and stability of the G-quadruplex structures are under thermodynamic control and may be of biological significance for regulatory function of cellular processes. Here, we report the structural influence and energetic contributions of the adenine bases in the loop sequences that flank G-repeats in human telomeric DNA sequence. Spectroscopic and calorimetric techniques are used to measure the thermal stability and thermodynamic contributions to the stability of human telomeric G-quadruplexes that have been designed with systematic changes of A to T throughout the telomeric sequence. These studies demonstrate that the thermal stability of the G-quadruplex structure is directly related to the number and position of the adenines that are present in the telomeric sequence. The melting temperature (T_m) was reduced from 59 °C for the wild-type sequence to 47 °C for the sequence where all four adenines were replaced with thymines (0123TTT). Furthermore, the enthalpy required for transitioning from the folded to unfolded G-quadruplex structure was reduced by 15 kcal/mol when the adenines were replaced with thymines (37 kcal/mol for the wild-type telomeric sequence reduced to 22 kcal/mol for the sequence where all four adenines were replaced with thymines (0123TTT)). The CD melting studies for G-quadruplex sequences having a single A to T change showed significantly sloping pre-transition baselines and their DSC thermograms revealed biphasic melting profiles. In contrast, the deoxyoligonucleotides having sequences with two or more A to T changes did not exhibit sloping baselines or biphasic DSC thermograms. We attribute the biphasic unfolding profile and reduction in the enthalpy of unfolding to the energetic contributions of ade-

nine hydrogen bonding within the loops as well as the adenine stacking to the G-tetrads of the G-quadruplex structure.

INTRODUCTION

Guanine rich nucleic acids are capable of forming higher order DNA structures called G-quadruplexes.^{1,4} Analyses of the human genome have established the presence of a large number of highly conserved guanine-rich sequences that have the potential to form G-quadruplex structures.⁵⁻⁷ These regions were found in certain oncogenic promoter regions and at the telomeric ends of the chromosome; providing evidence for *in vivo* biological functions of G-quadruplex structures. The potential for G-quadruplex structures to serve regulatory functions have made them attractive targets for the development of therapeutic drugs to modulate genetic transcription and telomeric extension.⁶⁻⁹ At the core of G-quadruplex structure are the planar G-tetrads composed of four guanines that are held together by Hoogsteen bonding and further stabilized by G-tetrad stacking. *In vitro*, G-quadruplexes may be constructed via intermolecular or intramolecular interactions of G-rich DNA sequences with significant variations in sequence and molecularity. G-rich oligonucleotides of sufficient length have the innate ability to form unimolecular G-quadruplexes that have demonstrated a high degree of topological variations that are dependent on both the base sequence and cationic environment.^{10,11}

Human telomeric DNA is a non-coding region at the end of the chromosome that consists of repetitive sequences that are approximately 5 to 15 kilobases in length with the tandem repeat of 5'- (TTAGGG)_n-3'. The terminal end of this sequence has a 3'- single stranded overhang ranging from 35 to 600 nucleotides in length that has been demonstrated to form stable G-quadruplex structures both *in vitro* and *in vivo*.¹²⁻¹⁵ The formation of the G-quadruplex structure has been demonstrated to inhibit the attachment of telomerase, thus halting the enzymatic extension of the telomere that is often associat-

ed with cancerous cells.¹⁶⁻¹⁸ The unimolecular human telomeric G-quadruplex structure has three stacked G-tetrads connected by loops comprised of a 5'-TTA-3' sequence. The nature of the loop connectivity gives rise to a number of alternate conformations that have been characterized both by NMR and X-ray crystallography.¹⁹⁻²⁴ The most notable structural differences are between the sodium and potassium cationic forms. Sodium-based buffers result in an all antiparallel strand orientation with glycosidic bond angles in the *anti*-conformation. However, the loop connectivity may differ and be all lateral loops, the “chair” conformation, or have two lateral loops and one diagonal loop, the “basket” conformation.^{19,20} Both of these folding topologies and their loop connectivity are illustrated in Figure 1. Potassium-based buffers result in more complex G-quadruplex structures that are characterized by two lateral loops and one loop that shows a chain reversal that is oriented on the edge of the tetrad core. The result is a mixed strand polarity that has both antiparallel and parallel characteristics with one guanine in a *syn*-conformation and the remaining three in an *anti*-conformation.²¹⁻²⁴ Nevertheless, G-quadruplex structures have the amazing ability to form topologically diverse structures that are quite stable under biologically relevant temperatures and conditions. The stabilities of G-quadruplex structures are derived from contributions of the G-tetrad Hoogsteen base pairing and hydrophobic stacking of successive G-tetrads.^{25,26}

The energetics of G-quadruplex unfolding and the enthalpic (ΔH_{unfold}) and entropic (ΔS_{unfold}) contributions to the thermal stability have been reported by numerous research groups using a variety of biophysical methods.^{18,25,27-29} There are variations in the unfolding energies reported for G-quadruplex forming sequences. These variations arise from subtle differences in base sequences as well as buffer conditions.^{25,27} Herein, we

present an analysis of the thermal stabilities and the energies of unfolding of the wild-type human telomeric sequence 5'- (AGGGTTAGGGTTAGGGTTAGGG-3' using circular dichroism spectropolarimetry (CD) and differential scanning calorimetry (DSC). Starting the wild-type sequence, a series of deoxyoligonucleotides were designed and to probe contributions that the adenines within the loops had on the structural and energetic contributions (see Table I for sequences). The buffer conditions (100 mM NaCl supplemented buffer) and loop length (3 nucleotides) were consistent for CD and DSC measurements on each of the DNA sequences. In an effort to discern the number of structurally relevant and or intermediate components present or arising during the unfolding event, 3-dimensional CD melting curves were generated and analyzed by singular value decomposition (SVD).

METHODS

Oligonucleotide Preparation and Nomenclature for A to T Conversion in G-quadruplex Sequences

Synthetic oligonucleotides with the selected adenine to thymine base changes were purchased from Midland Certified Reagents (Midland, TX). The deoxyoligonucleotides were dissolved in 100 mM NaCl BPES buffer (0.01 M NaH₂PO₄, 0.01 M Na₂HPO₄, 0.001 M EDTA) and allowed to equilibrate overnight at 4 °C. Prior to their use, stock solutions were filtered using 0.45 micron Millipore syringe filters and the concentrations were determined by UV-visible spectrophotometry at 90 °C to ensure that any secondary structure was fully denatured. The molar extinction coefficients were calculated using the nearest neighbor method as previously described.³⁰ The DNA solutions were then annealed at a cooling rate of 0.5 degrees/min using a MJ Research Mini-Cycler (Bio-Rad Laboratories). Confirmation that each of the DNA sequences were in the G-quadruplex conformation was carried out by circular dichroism (CD) spectropolarimetry, scanning from 225-325 nm and observing the presence of a positive ellipticity at 295 nm.

Changes to the loop sequences were designed such that the A residue(s) were sequentially replaced with T residues, starting at the 5' end (referred to as loop 0) and at each of the subsequent loops (loop 1-3). The sequence changes and nomenclature used to distinguish each of them are illustrated in Table 1.

Circular Dichroism Spectropolarimetry

Circular Dichroism (CD) melting studies were conducted using an AVIV 400 CD spectropolarimeter (AVIV Biomedical, Inc., Lakewood, NJ) at a strand concentration of 3 μM in a 1 cm path length quartz cuvette. The deoxyoligonucleotide solutions were al-

lowed to equilibrate in the cuvette with stirring for fifteen minutes prior to each measurement. The thermal difference spectra revealed the largest change at 295 nm for all sequences and the CD signal at 295 nm was monitored as a function of temperature. The temperature ranged from 10 to 90 °C at a rate of 1 °C/min. Measurements were taken at every 1 °C after a one-minute equilibration time. A buffer melting baseline was subtracted from each spectrum and data normalized to molar ellipticity. The melting temperature (T_m) was defined as the midpoint of the transition calculated by the first derivative of the sigmoidal curve. Model dependent van't Hoff analyses of the melting curves were not performed due to the presence of sloping pre-transition baselines and undetermined heat capacity changes upon melting of the G-quadruplex structures.

Differential Scanning Calorimetry

The heat associated with the unfolding of the G-quadruplex was measured using a Microcal VP-DSC (Malvern Instruments, Northampton, MA), at strand concentrations ranging from 175 to 225 μ M. Experiments were conducted with a heating rate of 0.5 °C/min over a range from 10-100 °C. A minimum of five heating and cooling cycles was conducted for each sample to assess reversibility of the unfolding. Buffer versus buffer scans were conducted in an identical manner for the subtraction of the reference scan.¹⁸ DSC data were analyzed using Origin 7.0 VP-DSC software with the following procedure. The third buffer/buffer scan was subtracted from the raw data and then normalized to strand concentration to provide heat capacity versus temperature plots. These data were corrected for baseline effects by using the iterative baseline function integrated within the Origin 7.0 VP-DSC software.

The baseline procedure was conducted by allowing the software to detect the linear portions of the pre- and post-transitions of the baseline and was only manually adjusted when there were obvious deficiencies in the selected position. The pre- and post-transition baselines were connected using the cubic function and the resulting baseline was subtracted from the data. The user has a number of baseline connecting functions to choose from and can inadvertently subtract important energetic contributions from the data. This is particularly true for transitions that exhibit non-zero changes in heat capacity for the folded and unfolded structures or sloping baselines. For the studies presented here, the cubic and progress baseline functions resulted in baselines that had minimal effects on the transition. However, the progress baseline function was less effective in providing a reliable baseline for the deoxyoligonucleotides with single adenine to thymine changes that exhibited pre-transition baseline slopes. Therefore, the cubic baseline function was consistently used for all of the sequences contained within this study. After baseline subtraction, the transition was deconvoluted using the minimum number of Gaussian curves necessary to achieve a good fit.

The total area under the curve was integrated to provide the enthalpy of unfolding (ΔH_{unfold}) as defined by the thermodynamic relationship:

$$\Delta H_{\text{cal}} = \int \Delta C_p(T) dT$$

The free energy (ΔG) of unfolding can be calculated from the Gibb's free energy equation:

$$\Delta G = \Delta H - T\Delta S$$

or alternatively at any reference temperature:

$$\Delta G(T) = \Delta H \left[1 - \frac{T}{T_m} \right]$$

The midpoint of the transition is defined as the melting temperature (T_m) and corresponds to a population of 50% folded and 50% unfolded G-quadruplex structure.^{18,28}

Singular Value Decomposition Analysis

CD melting data were collected over a range of wavelengths (320 to 220 nanometers) and used to create a three-dimensional melting profile for analysis by singular value decomposition (SVD).²⁸ Melting profiles were collected every 2 degrees from 4 to 90 °C with a temperature slope of 1 °C/min. Three data points were collected every nanometer from 320 to 220 nm for each degree and averaged. Samples were allowed to equilibrate for 1 minute at each temperature prior to data collection. The resulting data were arranged in a $i \times j$ matrix with j being the number of different temperature scans collected over i , number of wavelengths. SVD was performed on each data matrix using Matlab software (MathWorks, Natick, MA) by applying the following equation:

$$SVD(A) = USV$$

where A equals the three-dimensional $i \times j$ data matrix, U equals the resulting matrix containing the basis spectra, S equals a diagonal matrix containing singular values, and V equals a matrix containing the amplitude vectors. Autocorrelation of U and V matrices were performed using the following equation:

$$C(Xi) = \Sigma(X_{i,j})(X_i + 1_j)$$

Difference matrices were calculated using the following equation:

$$D = A - US'V_T$$

RESULTS

Conformational Analysis and Thermal Denaturation by Circular Dichroism Spectropolarimetry

The conformation of the wild type and A to T converted G-quadruplex sequences were analyzed by CD spectroscopy. The CD spectra are provided in Figure 2 and are assembled with respect to the number of A to T loop changes (i.e. either single loop change or multiple loop changes). The wild type spectrum (black) is included in both panels for comparison. All of the deoxyoligonucleotide sequences exhibited a significant positive ellipticity band at 295 nm corresponding to antiparallel strand orientation. Depending on the position of the A to T loop change, differences in the magnitude of the positive ellipticity band were observed. Similarly, variations in the magnitude of the band at 265 nm (minima) and the secondary maxima around 245 nm were observed. The single A to T loop conversions resulted in minimal wavelength shifts but displayed differences in the magnitudes of both the maxima and minima. In the cases of multiple loop changes, greater deviations from the wild type were observed with all of the sequences that were examined resulting in a higher magnitude of the positive ellipticity at 295 nm. In addition, a slight shift to higher wavelengths for the minimum at 265 nm and secondary maximum at 245 nm were observed. Interestingly, the minimum did not go below the zero baseline and was no longer a negative ellipticity for the 0123TTT and 13TTT (A to T) converted sequences. These CD spectra represent the average solution conformation and are influenced by the syn/anti-base conformations as well as base stacking interactions.³¹⁻

³⁵ Currently, there are no empirical procedures for the direct analysis of G-quadruplex CD spectra that provide details of the folding topology in its entirety. Chaires and coworkers have provided considerable insights into gleaned G-quadruplex unfolding

mechanisms by CD spectropolarimetry.^{26,35,36} In this study, CD spectra are used to qualitatively determine the nature of strand polarity for the folded structures.^{35,36} For these Na⁺-induced G-quadruplex sequences, all are indicative of antiparallel conformations.

Melting studies derived by monitoring the change in CD signal at 295 nm were conducted to probe the effects of A to T loop conversions on the thermal stabilities for each of the G-quadruplex structures. Overlays for the single loop changes and multiple loop changes are provided in Figure 3. The curves appear to be monophasic and the T_m was calculated by taking the first derivative of the sigmoidal melting curve. The wild type G-quadruplex resulted in a melting temperature of 58 °C. The melting temperatures of the majority G-quadruplexes having A to T loop changes were within ± 4 °C from the wild type. These results are summarized in Table 2. In the case of the 0123TTT deoxyoligonucleotide where all 4 adenine residues are replaced with thymine, a significant reduction in the thermal stability of the G-quadruplex structure is observed with a T_m of 44 °C, a decrease in thermal stability of 14 °C. In contrast to this trend, when the sequence of loop 2 was changed from TTA to TTT, a slight enhancement in the thermal stability ($T_m = 62$ °C) relative to the wild type was observed. Whereas all other A to T loop changes resulted in reduced thermal stability relative to the wild type sequence, the A to T conversion of loop 2 was the only G-quadruplex that showed an increase (4 °C) in stability over the wild-type sequence.

In addition to the differences in the melting temperatures, the sequences containing A to T conversions in the loop sequence exhibited differences in the pre-transition baselines. In the case of G-quadruplex sequences having single A to T conversions, “sloping” pre-transition baselines were observed; the most significant deviations observed for the wild-type and the OTTT sequence. In contrast, deoxyoligonucleotides with

multiple A to T loop conversions did not exhibit sloping pre-baseline transitions. Sloping baselines are problematic for model dependent van't Hoff analyses and could potentially induce systematic errors in calculating melting temperatures; hence, the CD data were not analyzed using a model dependent analysis for the determination of the thermodynamic contributions to the unfolding process.

Calorimetric Analysis of G-quadruplex Unfolding.

Differential scanning calorimetry (DSC) was used to measure the heat of unfolding for each of the G-quadruplex sequences. The advantage of using DSC is that the measurement is model independent and does not rely on van't Hoff plots to determine the enthalpy of the transition from the folded to unfolded state. A representative thermogram for the wild-type human telomeric G-quadruplex sequence in 100 mM NaCl BPES buffer is shown in Figure 4. These data reveal the transition to be biphasic with a shoulder occurring prior to the larger transition that has a T_m of 59 °C. It is necessary to include two Gaussian curves (red lines) to deconvolute the raw data (black line) and achieve a suitable fit for the complete transition. The calorimetric enthalpy was calculated by the integrating the area under the curve and was determined to be 37.4 kcal/mol for the unfolding direction. Thermograms for deoxyoligonucleotides containing both the single loop and multiple loop A to T modifications are shown in Figures 5 and 6, respectively. Melting temperatures and calorimetric enthalpies were calculated in a manner similar to the wild-type sequence and their results are reported in Table 2.

Comparison of the melting temperatures derived from the CD data with the DSC are in good agreement, with the most significant variations being observed for the single loop changes. The variations for these T_m 's may be due to the pre-transition baselines in

the CD data and/or shoulder peaks that are observed for the DSC data. Analysis of the enthalpy of unfolding comparing the wild-type with the A to T loop changes sequences provides a suitable probe for determining the thermodynamic contributions of the adenine bases within the TTA loops on G-quadruplex stability. We observed the enthalpy of unfolding to be systematically reduced as the number of A to T changes was increased, indicating the role that adenine stacking plays on stabilizing the G-tetrads. The energetic contribution toward stability that is provided by an adenine within the loop was determined to be approximately 1 to 2 kcal/mol. For example, the 2TTT sequence melting temperature was 62 °C and the 0123TTT sequence was destabilized to 47 °C. The number of transitions that are necessary to fit the DSC data was reduced to 1 when the sequences with multiple loop A to T changes were examined. The DSC data were in good agreement with the CD data for A to T loop changes that resulted in the highest and lowest observed thermal stabilities.

It should be noted that none of the DSC transitions could be fit with a simple 2-state model that assumes a negligible heat capacity change. Analyses of the raw data prior to baseline correction revealed non-zero heat capacity changes. G-quadruplex sequences possessing a single A to T loop changes exhibited pre-transition baseline sloping effects that made ΔC_p values difficult to determine. In contrast, the DNA sequences with multiple A to T loop changes did not have sloping pre-transition baselines and changes in heat capacities were easily determined, ranging from 0.7 to 1.0 cal/molK. Isothermal titration calorimetric studies have demonstrated non-zero heat capacity changes for G-quadruplex structures.³⁷ Taking into account the non-zero heat capacity changes and the apparent non-two-state unfolding mechanism, we limited our analysis to quantitation of

the enthalpy of unfolding by integrating the area under the transition in an effort to limit the bias and assumptions embedded in the integrated models for data fitting.

Singular Value Decomposition of G-quadruplex Unfolding.

Singular value decomposition (SVD) of three-dimensional CD melting data are utilized to determine the number of significant spectral species that are present during the unfolding of the human telomeric G-quadruplex sequence and the selected deoxyoligonucleotides with single or multiple A to T loop changes (Figure 7).^{34,38} The number of significant spectral species are estimated by analyzing the different components of the S, UxS, and V matrices, calculating the auto-correlation coefficients of the U and V matrices, and analyses of the plots of difference matrices calculated with a succinct number of singular values. The S matrix is evaluated by plotting the singular values versus the component number and counting the number of singular values that rise above the baseline. The UxS matrix is representative of the basis spectra and the columns of the UxS matrix are plotted as a function of wavelength. Each trace in the plot depicts a component involved in the unfolding mechanism and those arising above the baseline are considered spectrally significant. The V matrix columns are plotted as a function of temperature and, similar to the UxS matrix, each trace represents a different component in the unfolding process. The components that give distinct traces without noise are considered spectrally significant. Autocorrelation coefficients are calculated for each column of both the U and V matrices and values greater than 0.8 indicate that the respective component is spectrally significant. A final check to determine the significance of each spectral component is achieved by calculating difference matrices and evaluating them through a contour plot. If the difference plot is calculated with the same number of singular values

as number of spectrally significant components, then the resulting contour plot will present as random noise.³⁸⁻⁴⁰ Difference plots that do not present as random noise are therefore calculated with the wrong number of singular values.

For the unfolding of the wild-type telomeric G-quadruplex in a Na⁺ environment, the SVD data reveal a minimum of three spectral species as shown in Figure 8. The autocorrelation values for the first three columns of both the U and V matrices were larger than 0.8 also indicative of the presence of three spectrally significant species. A summary of the singular values and the U and V matrix autocorrelation values for the wild-type G-quadruplex sequence is provided in Table 3. The difference matrix plots for the wild-type sequence calculated with three singular values resulted in contour plots of random noise while plots created with one, two, or four singular values yielded contour plots with defined contour lines (data not shown). Hence, these data are indicative of a minimum of three spectrally significant species in the unfolding of the wild-type human telomeric sequence.

A summary of these data for all of the G-quadruplex A to T loop modified sequences is presented in Table 4. For all sequences with A to T loop modifications, a minimum of three spectrally significant species were found in all cases with three exceptions - 1TTT, 12TTT, and 23TTT. These sequences were shown to have a minimum of four spectrally distinct species.

DISCUSSION

The work that is described in this manuscript specifically focuses the contributions of adenine within the conserved TTA loop sequences. Spectroscopic and calorimetric methods to investigate the stabilizing effects imposed by the of adenines base stacking on G-quadruplex structure(s). These studies focused on the changes to structures and thermodynamic stabilities resulting from systematic A to T changes in the human telomeric G-quadruplex loop sequences. Considerable work has been published that focuses on the effects of loop sequence and length on G-quadruplex stability.³⁹⁻⁴⁴ Structural analyses by CD of the wild-type human telomeric DNA sequence and concomitant sequences containing A to T loop changes reveal that under Na⁺ conditions, all of the selected sequences used in this study formed antiparallel G-quadruplex structures as indicated by their positive maximum at 295 nm and a negative minimum at 265 nm.⁴⁴⁻⁴⁶ The CD spectra for deoxyoligonucleotides with base changes in the TTA loops (A to T conversions) are all consistent with antiparallel topology; however, subtle differences are observed in the magnitudes and the wavelength of the maxima and minima. In the case of single A to T loop conversion, differences in magnitudes of the maxima at 295 and 245 nm and minimum at 265 nm, relative to the wild-type, are observed. In the modified sequences with two or more A to T loop conversions, differences in the magnitudes for all maxima and minima are observed. Additionally, slightly higher shifts in wavelengths for the maximum and minimum are observed. The CD spectra are clearly influenced by sequence effects, most likely because of the geometries associated with differences between adenine base stacking with G-tetrads that are adjacent to the loops in the folded structures in the case of the wild-type sequence or the lack thereof when the adenine is replaced with thymine. CD analyses of G-quadruplexes are most suited for classifying the strand

polarities (parallel and antiparallel orientations) and observing changes in G-quadruplex structure, and cannot distinguish between conformations or structural isoforms of the same strand polarity. However, when analyzed in conjunction with the DSC data, we speculate that the changes in the CD spectra are likely due to the disruption of the stacking interactions resulting from the removal of the adenine bases from the loop sequences. It has been previously reported that changing the thymine(s) in the loop sequences to cytosines result in structural changes to the G-quadruplex formed when in the presence of potassium.⁴⁷ The loss of adenine stacking interactions may result in structural distortion of the G-tetrads that result in subtle structural changes relative to the wild-type sequence that would give rise to the observed variations in the CD spectra.

Thermodynamic Profiles for the Unfolding of the G-quadruplexes

The large hypochromic effect on the CD signal at 295 nm observed for the denaturation of G-quadruplex structures has been extensively used to study their thermal stability.^{29,48-53} Figure 3 depicts the CD melting experiments conducted on deoxyoligonucleotides containing loops with A to T converted sequences with the calculated melting temperatures summarized in Table 2. Systematic changes of the adenine to thymine in the loop sequence (TTA) results in changes in the stabilities of the sequence-modified G-quadruplexes. The majority of the modified deoxyoligonucleotides showed slightly lowered melting temperatures with the exception being the modified sequence with all four A bases replaced by T (0123TTT), resulting in a significantly less stable G-quadruplex structure with a T_m of 44 °C, a change of 14 °C lower than the wt-sequence melting of 58 °C. In contrast, the A to T converted loop 2 sequence (2TTT) had a slightly enhanced stabilization with an observed melting temperature of 62 °C, 4 °C higher than the wild-

type sequence. All of the transitions appeared to be monophasic and were characterized by sigmoidal curves. However, a closer examination of the baselines showed that there were differences for the single-loop and multiple-loop modified sequences. All of the single-loop modified sequences had severely sloping pre-transition baselines, whereas the multiple-loop modifications exhibited minimal sloping effects observed for the baselines. There are a number of potential factors that may cause sloping pre-transition baselines, such as a temperature dependence of the solvent, heat capacity effects, loss of base stacking interactions, or the presence of intermediates in the unfolding mechanism. The lack of clearly defined pre- and post-transition baselines is problematic for calculating thermodynamic parameters by van't Hoff analysis and may not represent the true enthalpy of the unfolding process.⁵⁴⁻⁵⁶ We utilized the model independent method of DSC to directly measure the heat of unfolding to characterize the thermodynamic parameters of the unfolding process. A biphasic transition profile was observed for the wild type human telomeric sequence and is depicted in Figure 4. Deconvolution of the DSC thermogram required two transitions with melting T_m 's of 39 °C and 59 °C for the first and second transitions, respectively. This biphasic melting profile has been observed for similar G-quadruplex sequences in K^+ buffer.^{40,57,58} In addition to telomeric sequences, two distinct unfolding events were also observed for the c-MYC promoter region G-quadruplex as reported by Freyer and coworkers.⁵⁹ Chaires and coworkers addressed the apparent discrepancies reported for G-quadruplex stability and kinetics and noted that the basis for these discrepancies to be a combination of strand concentrations, sequence variations, differences in buffer solution conditions, and methodologies employed to determine the parameters. The published thermodynamic data for the unfolding of human telomeric G-

quadruplexes was reported to vary in T_m values from 56 to 63.7 °C in 100 mM Na⁺ buffer and that enthalpy values varied dramatically from 38 to 72.7 kcal/mol.^{18,27}

The thermal unfolding of the sequences with A to T loop modifications revealed that the low temperature transition was reduced in magnitude for the single loop A to T modification and was not observed at all for the multiple A to T loop modification. The telomeric sequence where the 5'-A base was converted to 5'-T (0T) most resembled the wild-type and the additional single loop A to T change resulted in transition profiles that were broadened with only minor features present corresponding to the low temperature transition. The sequences with multiple A to T loop modifications were all easily fit with a single transition and lacked any evidence of the low temperature transition that was observed for the wild-type and single loop modifications. Not only did the presence of the adenine bases contribute to the shape of the melting transition, but also contributed to the calculated unfolding enthalpies. The unfolding enthalpies for the wt-sequence and A to T loop modified sequences are summarized in Table 2 reveals that as the number of adenines modified to thymines are increased, the unfolding enthalpy decreases. When all of the adenines are converted to thymines (0123TTT sequence), the enthalpy of the transition was reduced to from 37 kcal/mol (as observed for the wild-type sequence) to 22 kcal/mol for the 0123TTT sequence, a change in unfolding enthalpy of 15 kcal/mol. Hence, the adenines within the G-quadruplex loops play a significant role in stabilizing the G-quadruplex structure. Adenine bases stacking on adjacent G-tetrads are known to be significant contributors to G-quadruplex stability and our results provide a quantitative measure of those interactions.⁶⁰ An outlier was the 2TTT sequence that exhibited an enhanced thermal stability of 62 °C. We speculate that replacement of the A with a T in loop 2 may allow for a more favorable stacking of the 5'-A with the bottom G-tetrad of

the G-quadruplex. In addition to the adenine-G-tetrad stacking interactions, adenine in the TTA loops also contribute ionic and hydration effects providing favorable energetic contributions toward G-quadruplex stability; however, these effects are thought to contribute only modestly to the unfolding enthalpy.^{33,55,61} Calculation of the free energy at a reference temperature is a more useful measure of G-quadruplex stability as compared with melting temperatures. The calculated free energies at 25 °C for the wild-type and A to T modified sequences are provided in Table 2. The enhanced thermal stability of the 2TTT sequence is not as significant when comparing the free energies of unfolding for the wild-type and modified 2TTT sequences, with both free energies calculated to be 3.8 kcal/mol. The remaining modified sequences show a systematic reduction in the free energy with the fully A to T modified sequence (0123TTT) possessing the lowest calculated free energy at 25 °C of 1.5 kcal/mol.

Energetic Nature of the Unfolding Transition

The molecular basis for the low temperature transition observed for the DSC profiles is complex. As previously mentioned, direct comparisons with published results are often difficult due to slight variations in the G-quadruplex sequences, structures, buffer conditions, and preparation methodologies. One possibility that may explain the observed biphasic melting profile could be the presence of multiple conformers and/or intermediate species within the solution that thermally denature independent of each other. The Na⁺ form of the human telomeric G-quadruplex has been shown to form both the “chair” and/or “basket” folding topologies in solution.² It is feasible that conversion of A to T in one or more of the loop regions may influence the folding topologies such that the G-quadruplex structure that is formed will favor one or the other (basket or chair) con-

formation. However, if that were the case, we would not expect the T_m of the low temperature transition to deviate as much as 15 °C as observed in the case of the 2TTT loop. The T_m of the low temperature transitions that are apparent in the wild-type and single-loop conversions appear to be linked to the high temperature transition and were never clearly resolved with a baseline between the transitions. Furthermore, we are not aware of any published biphasic DSC thermograms of G-quadruplexes that have been resolved by stabilizing one of the transitions relative to the other using variations in cation concentration, scan rates, or sequence variations.^{26,61-63}

An additional possibility for the biphasic profile is the presence of intermediates in the unfolding pathway. In 2011, Chaires and coworkers proposed that the human telomeric G-quadruplex does not unfold in a two-state manner, suggesting that there are significantly populated intermediates states.^{26,35} Our analyses of three-dimensional CD data by SVD reveal that all A to T loop-altered sequences unfold along a pathway containing at least three spectral species. Our results are consistent with previous G-quadruplex folding studies wherein magnetic tweezers were used to reveal the presence of intermediate species along the unfolding pathway of the human telomere G-quadruplex DNA in the presence of Na^+ .⁶⁴ SVD analysis of CD data collected as a function of temperature for the human telomere G-quadruplex in the presence of K^+ has also been previously reported. This study also revealed the presence of an intermediate species along the unfolding pathway of the G-quadruplex.⁴⁰

In addition, fluorescence studies have also been reported that both Na^+ and K^+ forms of the G-quadruplex have populated intermediate states and/or rapid equilibrium between multiple conformers.^{65,66} Specifically, single molecule FRET studies have been performed on the human telomeric G-quadruplex in the presence of Na^+ that have shown

the existence of four populated species during G-quadruplex folding including an anti-parallel basket, and anti-parallel chair, an unfolded single strand, and a transient state that could include a G-triplex or a (2+2) anti-parallel structure.^{67,68} It is safe to assume that the CD techniques used in this study are not sensitive enough to discern between two G-quadruplex structures that are energetically similar. In this case, fast conversion between the anti-parallel chair and basket conformations would not be observable in the SVD analysis of the deoxyoligonucleotide sequences harboring the A to T converted loops and they would appear as one significant spectral species. Indeed, intermediates encountered by the CD experiments may be calorimetrically silent; either the intermediate concentrations are too low to detect or they have enthalpies that are indistinguishable. We speculate that the biphasic melting profiles of the human telomeric sequence used for this study are due to the presence of unfolding intermediates and are characterized by the loss the enthalpic contributions of the loop base stacking interactions represented by the low temperature transition.

The single loop A to T conversions significantly reduced the magnitude of the low temperature transition, whereas conversions from A to T of multiple loop sequences resulted in a complete loss of the low temperature transition. Conversion of the terminal 5'-A (0T) to 5'-T, that is not a loop base, had only a minimal effect on the biphasic profile and closely resembled the wild-type. The unfolding of a G-quadruplex structure may involve a process wherein the loop structures and interactions begin to denature prior to the denaturation of the G-tetrad core. The disruption of adenine-guanine stacking interactions and/or hydrogen bonding between the bases in the loops would have enthalpic consequences and could be observed by DSC. It is important to distinguish that neither

the low or high temperature transitions of the denaturing profile represents the intermediate structure. Instead, the initial unfolding step may be loop structure destabilization (low temperature transition), followed by the breaking of the G-tetrad core of the G-quadruplex structure (high temperature transition). The deoxyoligonucleotides where multiple loops have A to T conversions are observed to have only high temperature transitions yet could not be adequately fit with a simple two-state model. This suggests that the G-quadruplex unfolds by a similar mechanism with initial loop denaturing followed by denaturing of the G-tetrad at higher temperatures, but the low temperature transitions are no longer apparent because the adenine-guanine base stacks that are responsible for the low temperature transition are no longer present in the sequence.

The present study has focused on the spectroscopic and calorimetric analysis of the unfolding of the human telomeric sequence and provided insight into the energetic contributions of the adenine bases present in the loop sequences. Systematically changing the adenines present in the TTA loop sequences have provided insights into the role of adenines within the loops for stabilizing the G-quadruplex structure and their enthalpic contribution as observed by their biphasic melting profile. The results of this study demonstrate that the adenines within the G-quadruplex loops play a significant role in influencing the stability and energetics of the G-quadruplex structure. Additionally, these results support previously published work that suggests G-quadruplex thermodynamic stability is a combination of loop sequence effects and G-tetrad formation.

REFERENCES

1. Simonsson, T. (2001) G-quadruplex DNA structures – Variations on a theme, *J. Biol. Chem.* 382, 621-628.
2. Burge, S., Parkinson, G.N., Hazel, P., Todd, A.K., and Neidle, S. (2006) Quadruplex DNA: Sequence, topology and structure. *Nucleic Acids Res.* 35, 5402-5415.
3. Bončina M, Lah J, Prislán I, and Vesnaver G. (2012) Energetic basis of human telomeric DNA folding into G-quadruplex structures. *J. Am. Chem. Soc.* 134, 9657-9663.
4. Paeschke, K., Simonsson, T., Postberg, J. Rhodes, D., and Lipps, H.J. (2005) Telomere end-binding proteins control the formation of G-quadruplex DNA structures in vivo. *Nature Struct. & Molec. Biol.* 12, 847-854.
5. Todd, A.K., Johnston, M., and Neidle, S. (2005) Highly prevalent putative quadruplex sequence motifs in human DNA. *Nucleic Acids Res.* 33, 2901-2907.
6. Huppert, J.L. and Balasubramanian, S. (2005) Prevalence of quadruplexes in the human genome. *Nucleic Acids Res.* 33, 2908-2916.
7. Eddy, J. and Maizels, N. (2008) Conserved elements with potential to form polymorphic G-quadruplex structures in the first intron of human genes. *Nucleic Acids Res.* 36, 1321-1333.
8. Balasubramanian, S. and Neidle, S. (2009) G-quadruplex nucleic acids as therapeutic targets. *Curr. Opin. Chem. Biol.* 13, 345-353.
9. DeClan, A., Lacroix, L., Douarre, C., Tamime-Smaali, N., Treniesaux, C., Riou, J-F., and Mergny, J-L. (2008) Targeting telomeres and telomerase. *Biochimie*, 90, 131-155.

10. Gellert, M., Lipsett, M.N. and Davies, D.R. (1962) *Helix formation by guanylic acid. Proc. Natl. Acad. Sci. U.S.A.* 48, 2013-2018.
11. Bhattacharyya, D., Arachchilage, G.M., and Basu, S. (2016) Metal cations in G-quadruplex folding and stability. *Front. Chem.* 4, 1-14.
12. Williamson, J.R., Raghuraman, M.K. and Cech, T.R. (1989) Monovalent cation-induced structure of telomeric DNA: The G-quartet model. *Cell*, 59, 871-880.
13. Chang, CC., Kuo, I.C., Ling, I.F., Chen, C.T., Chen, H.C., Lou, P.J., Lin, J.J., and Chang, T.C. (2004) Detection of quadruplex DNA structures in human telomeres by a fluorescent carbazole derivative. *Anal. Chem.* 70, 4490-4494.
14. Tsai, Y.C., Qi, H. and Liu, L.F. (2007) Protection of DNA ends by telomeric 3' G-tail sequences. *J. Biol. Chem.*, 282, 18786-18792.
15. O'Sullivan, R.J., Karlsader, J. (2010) Telomeres: Protecting chromosomes against genome instability. *Nat. Rev. Mol. Cell Biol.* 11, 171-181.
16. Greider, C.W. and Blackburn, E.H. (1996) Telomeres, telomerase and cancer. *Sci. Am.* 274, 92-97.
17. Boukamp, P. and Mirancea, N. (2007) Telomeres rather than telomerase a key target for anticancer therapy? *Exp. Dermatol.* 16, 71-79.
18. Lane, A.N., Chaires, J.B., Gray, R.D. and Trent, J.O. (2008) Stability and kinetics of G-quadruplex structures. *Nucleic Acids Res.* 36, 5482-5515.
19. Wang, Y. and Patel, D.J. (1993) Solution structure of the human telomeric repeat d[AG₃](T₂AG₃)₃ G-tetraplex. *Structure*, 1, 263-282.
20. Lim, K.W., Ng, V.C., Martin-Pintado, N., Heddi, B. and Phan, A.T. (2013) Structure of the human telomere in Na⁺ solution: An antiparallel (2+2) G-quadruplex scaffold reveals additional diversity. *Nucleic Acids Res.* 41, 10556-10562.

21. Hud, N.V. and Plavec, J. (2006) The role of cations in determining quadruplex structure and stability, in *Quadruplex Nucleic Acids* (Neidle, S. and Balasubramanian, S., Eds) pp 100-130, Royal Soc. Chemistry, Cambridge.
22. Ambrus, A., Chen, D., Dai, J., Bialis, T., Jones, R.A. and Yang, D. (2006) Human telomeric sequence forms a hybrid-type intramolecular G-quadruplex structure with mixed parallel/antiparallel strands in potassium solution. *Nucleic Acids Res.* *34*, 2723-2735.
23. Parkinson, G.N., Lee, M.P. and Neidle, S. (2002) Crystal structure of parallel quadruplexes from human telomeric DNA. *Nature*, *417*, 876-880.
24. Adrian, M., Heddi, B. and Phan, A.T. (2012) NMR spectroscopy of G-quadruplexes. *Methods*, *57*, 11-24.
25. Hardin, C.C., Perry, A.G. and White, K. (2000) Thermodynamic and kinetic characterization of the dissociation and assembly of quadruplex nucleic acids. *Biopolymers*, *56*, 147-194.
26. Gray, R.D., Trent, J.O. and Chaires, J.B. (2014) Folding and unfolding pathways of the human telomeric G-quadruplex. *J. Mol. Biol.* *426*, 1629-1650.
27. Chaires, J.B. (2009) Human telomeric G-quadruplex: Thermodynamic and kinetic studies of telomeric quadruplex stability. *FEBS J.* *277*, 1098-1106.
28. Olsen, C.M., Lee, H.T. and Marky, L.A. (2009) Unfolding thermodynamics of intramolecular G-quadruplexes: base sequence contributions of the loops. *J. Phys. Chem B.*, *113*, 2587-2595.
29. Boncina, M., Vesnaver, G., Chaires, J.B. and Lah, J. (2016) Unraveling the thermodynamics of the folding and interconversion of human telomere G-quadruplexes. *Angew. Chem.* *126*, 10496-10500.

30. Cantor, C.R., Warshaw, M.M. and Shapiro, H. (1970) Oligonucleotide interactions, 3. Circular dichroism studies of the conformation of deoxyoligonucleotides. *Biopolymers*, 9, 1059-1077.
31. Viglasky, V. and Hianik, T. (2013) Potential uses of G-quadruplex-forming aptamers. *Gen. Physiol. Biophys.* 32, 149-172.
32. Mergny, J-L., Phan, A-T., Lacroix, L. (1998) Following G-quartet formation by UV-spectroscopy. *FEBS Lett.* 435, 74-78.
33. Ponikova, S., Antalík, M. and Hianik, T. (2008) A circular dichroism study of the stability of guanine quadruplexes of thrombin DNA aptamers at presence of K⁺ and Na⁺ ions. *Gen. Physiol. Biophys.* 27, 271-277.
34. Haq, I., Chowdhry, B.Z. and Chaires, J.B. (1997) Singular value decomposition of 3-D DNA melting curves reveals complexity in the melting process. *Eur. Biophys. J.* 26, 419-426.
35. Gray, R.D. and Chaires, J.B. (2011) Analysis of multidimensional G-quadruplex melting curves in *Curr. Protoc. Nucleic Acid Chem.* 45, 17.4.1-17.4.16.
36. Buscaglia, R., Gray, R.D. and Chaires, J.B. (2013) Thermodynamic characterization of human telomere quadruplex unfolding. *Biopolymers*, 99, 1006-1018.
37. Majhi, P.R., Qi, J., Tang, C.F. and Shafer, R.H. (2008) Heat capacity changes associated with guanine quadruplex formation: An isothermal titration calorimetry study. *Biopolymers*, 89, 302-309.
38. Wall, M.E., Rechtsteiner, A., and Rocha, L.M. (2003) Singular value decomposition and principle component analysis in *A Practical Approach to Microarray Data Analysis* (Norwell, M.A. ed), pp 91-109.

39. Guedin, A., De Cian, A., Gros, J., Lacroix, L. and Mergny, J.L. (2008) Sequence effects in single-base loops for quadruplexes. *Biochimie*, *90*, 686-696.
40. Antonacci, C., Chaires, J.B. and Sheardy, R.D. (2007) Biophysical characterization of the human telomeric (TTAGGG)₄ repeat in potassium solution. *Biochemistry* *46*, 4654-4660.
41. Petraccone, L., Erra, E., Nasti, L., Galeone, A., Randazzo, A., Mayol, L., Barone, G. and Giancola, C. (2003) Effect of a modified thymine on the structure and stability of [d(TGGGT)]₄ quadruplex. *Int. J. Biol. Macromol.* *31*, 131-137.
42. Hazel, P., Huppert, J., Balasubramanian, S., and Neidle, S. (2004) Loop-length dependent folding of G-quadruplexes. *J. Am. Chem. Soc.* *126*, 16405-16415.
43. Rachwal, P.A., Brown, T. and Fox, K.R. (2007) Sequence effects of single base loops in intramolecular quadruplex DNA. *FEBS Lett.* *581*, 1657-1660.
44. Risitano, A. and Fox, K.R. (2004) Influence of loop size on the stability of intramolecular DNA quadruplexes. *Nucleic Acids Res.* *32*, 2598-2606.
44. Ren, J., Qu, X., Trent, J.O. and Chaires, J.B. (2002) Tiny telomere DNA. *Nucleic Acids Res.* *30*, 2307-2315.
45. Lee, J.Y., Yoon, J., Kihm, H.W. and Kim, D.S. (2008) Structural diversity and extreme stability of unimolecular *Oxytricha nova* telomeric G-quadruplex. *Biochemistry*, *27*, 3389-3396.
46. Dapic, V., Abdomerovic, V., Marrington, R., Peberdy, J., Roger, A., Trent, J.O. and Bates, P.J. (2003) Biophysical and biological properties of quadruplex oligodeoxyribonucleotides. *Nucleic Acids Res.* *31*, 2097-2107.

47. Wolna, A.H., Fleming, A.M. and Burrows, C.J. (2014) Single-molecule analysis of thymine dimer-containing G-quadruplexes formed from the human telomere sequence. *Biochemistry*, *53*, 7484-7493.
48. Vorlickova, M., Bednarova, K., Kejovska, I. and Kypr, J. (2007) Intramolecular and intermolecular guanosine quadruplexes of DNA in aqueous salt and ethanol solutions. *Biopolymers*, *86*, 1-10.
49. Sun, X.G., Cao, E.H., He, Y.J. and Qin, J.F. (1999) Spectroscopic comparison of different DNA structures formed by oligonucleotides. *J. Biomol. Struct. Dynam.* *16*, 863-872.
50. Zhang, X.Y., Cao, E.H., Zhang, Y., Chou, C. and Bai, C. (2003) K⁺ and Na⁺-induced self assembly of telomeric oligonucleotides d(TTAGGG)_n. *J. Biomol. Struct. Dynam.* *20*, 693-702.
51. Peng, C.G. and Damha, M.J. (2007) G-quadruplex induced stabilization by 2'-deoxy-2'-fluoro-D-arabinonucleic acids (2'-F-ANA). *Nucleic Acids Res.* *35*, 4977-4988.
52. Kumar, N. and Maiti, S. (2008) A thermodynamic overview of naturally occurring intramolecular DNA quadruplexes. *Nucleic Acids Res.* *36*, 5610-5622.
53. Balkwill, G.D., Garner, T.P. and Serle, M.S. (2009) Folding of single-stranded DNA quadruplexes containing an autonomously stable mini-hairpin loop. *Mol. Biosyst.* *5*, 542-547.
54. Marchand, A. and Gabelica, V. (2016) Folding and misfolding pathways of G-quadruplex DNA. *Nucleic Acids Res.* *44*, 10999-11012.
55. Chaires, J.B. (1997) Possible origins of differences between van't Hoff and calorimetric enthalpy estimates. *Biophys. Chem.* *28*, 15-23.

56. Allen, D.L. and Pielak, G.J. (1998) Baseline length and automated fitting of denaturation data. *Protein Sci.* 7, 1262-1263.
57. Olsen, C.M. and Marky, L.A. (2010) Monitoring the temperature unfolding of G-quadruplexes by UV and circular dichroism spectroscopies and calorimetry techniques. *Methods Mol. Biol.* 608, 147-158.
58. Hudson, J.S., Brooks, S.C. and Graves, D.E. (2009) Interactions of actinomycin D with human telomeric G-quadruplex DNA. *Biochemistry*, 48, 4440-4447.
59. Freyer, M.W., Buscaglia, R., Kaplan, K., Cashman, D., Hurley, E.H. and Lewis, E.A. (2007) Biophysical studies of the c-MYC NHEIII1 promoter: model quadruplex interactions with a cationic porphyrin. *Biophys. J.* 92, 2007-2015.
60. Schultze, P., Macaya, R.F. and Feigon, J. (1994) Three-dimensional solution structure of the thrombin-binding DNA aptamer d(GGTTGGTGTGGTTGG). *J. Mol. Biol.* 235, 1532-1547.
61. Olsen, C.M., Gmeiner, W.H. and Marky, L.A. (2006) Unfolding of G-quadruplexes: energetic, and ion and water contributions of G-quartet stacking. *J. Phys. Chem. B.* 110, 6962-6969.
62. Mashimo, T., Yagi, H., Sannohe, Y., Rajendran, A., and Sugiyama, H. (2010) Folding pathways of human telomeric type-1 and type-2 G-quadruplex structures. *J. Am. Chem. Soc.* 132, 14910-14918.
63. Rosu, F., Gabelica, V., Poncelet, H. and De Pauw, E. (2010) Tetramolecular G-quadruplex formation pathways studied by electrospray mass spectrometry. *Nucleic Acids Res.*, 38, 5217-5225.
64. Chu, J.F., Chang, T.C. and Li, H.W. (2010) Single-molecule TMP studies on the conversion of human telomeric DNA. *Biophys. J.* 98, 1608-1616.

65. Lee, J.Y. and Kim, D.S. (2009) Dramatic effect of single-base mutation on the conformational dynamics of human telomeric G-quadruplex. *Nucleic Acids Res.* *37*, 3625-3634.
66. Shirude, P.SI and Balasubramanian, S. (2008) Single molecule conformational analysis of DNA G-quadruplexes. *Biochimie*, *90*, 1197-1206.
67. Noer, S.L., Gudnason, P.S., Aznauryan, M., Mergny, J.L., Birkedal, V. (2016) Folding dynamics and conformational heterogeneity of human telomeric G-quadruplex structures in Na⁺ solutions by single molecule FRET microscopy. *Nucleic Acids Res.* *44*, 464-471.
68. Sondergaard, S., Aznauryan, M., Hastrup, E.K., Schiott, B., Birkedal, V. and Corry, B. (2015) *Chemphyschem*, *16*, 2562-2570.

FIGURE LEGENDS

Figure 1. Cartoon representing the chair (left) and basket (right) conformations of the Na⁺ human telomeric G-quadruplex. The blue circles represent the guanines and the red circles represent the adenines.

Figure 2. CD wavelength scans for the human telomeric G-quadruplex d[AGGG(TTAGGG)₃] (red line) and the A to T converted loop sequences. Panel A represents the sequences that possess single adenine to thymine base changes. Panel B represents the sequences with multiple A to T modified loops.

Figure 3. Composite CD melting curves of the human telomeric sequence and A to T modified loop sequences in 100 mM NaCl BPES buffer at pH 7.0. Panel A contains the CD melting curves for the wild type sequence (red line) and the single A to T modified base sequences. Panel B contains the CD melting curves for the G-quadruplex sequences with multiple A to T base changes. Melting temperatures were calculated from the first derivative of the sigmoidal curve. Data were normalized to molar ellipticity and not converted to fraction folded/unfolding in order to retain the pre-transition baseline sloping characteristics.

Figure 4. A DSC thermogram of the wild type human telomeric G-quadruplex DNA in 100mM NaCl and 10 mM BPES buffer at pH 7.0. The observed transition (black line) is biphasic with a lower temperature transition at 39 °C and higher temperature transition at

59 °C. The observed data were fit to two transitions (red lines) and the total area under the curve integrated to provide the enthalpy of unfolding (ΔH_{unfold}).

Figure 5. Representative DSC thermograms for the single A to T base modifications of the telomeric G-quadruplex. The black lines represent the raw DSC data and the red lines represent the number of transitions. (Panel A) Conversion of the 5'-A to 5'-T (0T); (Panel B) A to T modification of loop 1 (1TTT); (Panel C) A to T modification of loop 2 (2TTT); (Panel D) A to T conversion of loop 3 (3TTT).

Figure 6. Representative DSC thermograms for multiple A to T loop conversions for the telomeric G-quadruplex sequence. The black lines represent the raw DSC data and the red lines represent the number of transitions. (Panel A) wild type; (Panel B) A to T modifications of loop 0 and loop 1 (01TTT); (Panel C) A to T modifications of loop 0 and loop 2 (02TTT); (Panel D) A to T modifications of loop 2 and loop 3 (23TTT); (Panel E) A to T modifications of loop 1 and loop 2 (12TTT); (Panel F) A to T modifications of loop 1 and loop 3 (13TTT); (Panel G) A to T modifications of loop 2 and loop 3 (23TTT); (Panel H) A to T modifications of loops 0, 1, and 2 (012TTT); (Panel I) A to T modifications of all adenines in the sequence to thymine (0123TTT).

Figure 7. Three-dimensional CD plot for the thermal denaturation of wild-type human G-quadruplex. Each line represents a traditional CD scan at a particular temperature.

Figure 8. SVD analysis of wild-type human telomeric G-quadruplex. (Panel A) S matrix plot of singular values; (Panel B) V matrix plot of the vector amplitudes; (Panel C) Representative basis spectra obtained by multiplying the U and S matrices together.

Table 1. Sequences showing the A to T base modifications in the loops of the human telomeric G-quadruplex sequences used in this study. Red indicates A to T conversion.

Sequence	Loop Modification	Nomenclature
5'-AGGGTTAGGGTTAGGGTTAGGG-3'	-	wild-type
5'- T GGGTTAGGGTTAGGGTTAGGG-3'	0	0T
5'-AGGGTT T GGGTTAGGGTTAGGG-3'	1	1TTT
5'-AGGGTTAGGGTT T GGGTTAGGG-3'	2	2TTT
5'-AGGGTTAGGGTTAGGGTT T GGG-3'	3	3TTT
5'- T GGGTT T GGGTTAGGGTTAGGG-3'	0,1	01TTT
5'- T GGGTTAGGGTT T GGGTTAGGG-3'	0,2	02TTT
5'- T GGGTTAGGGTTAGGGTT T GGG-3'	0,3	03TTT
5'-AGGGTT T GGGTT T GGGTTAGGG-3'	1,2	12TTT
5'-AGGGTT T GGGTTAGGGTT T GGG-3'	1,3	23TTT
5'-AGGGTTAGGGTT T GGGTT T GGG-3'	2,3	13TTT
5'-AGGGTT T GGGTT T GGGTT T GGG-3'	1,2,3	123TTT
5'- T GGGTT T GGGTT T GGGTT T GGG-3'	0,1,2,3	0123TTT

Table 2. Summary of differential scanning calorimetry (DSC) and circular dichroism (CD) thermal denaturation of telomeric G-quadruplex (sodium form) deoxyoligonucleotides containing A to T modifications in one or more loops. All deoxyoligonucleotides are in 10 mM BPES with 0.1 M NaCl at a pH of 7.0.

Sequence	DSCa			CDb	
	Number of Transitions	T_m (°C)	ΔH_{unf} (kcal/mol)	$\Delta G_0(298K)$ (kcal/mol)	T_m (°C)
wt G-quad	2	59 ± 0.8	37.4 ± 3.2	3.8 ± 0.2	58 ± 1.8
0T	2	59 ± 1.8	36.1 ± 2.6	3.7 ± 0.3	53 ± 0.8
1TTT	2	55 ± 0.6	35.7 ± 2.1	3.2 ± 0.2	53 ± 1.4
2TTT	2	62 ± 1.2	34.3 ± 3.2	3.8 ± 0.3	62 ± 2.2
3TTT	2	55 ± 1.3	34.6 ± 2.5	3.2 ± 0.4	54 ± 1.5
01TTT	1	55 ± 1.5	19.2 ± 1.8	1.7 ± 0.1	52 ± 0.9
02TTT	1	54 ± 0.6	23.5 ± 2.9	2.0 ± 0.3	53 ± 1.1
03TTT	1	54 ± 1.1	21.6 ± 2.2	1.9 ± 0.1	51 ± 1.3
12TTT	1	59 ± 2.0	32.3 ± 2.0	3.3 ± 0.2	58 ± 1.6
13TTT	1	59 ± 1.4	32.1 ± 1.8	3.3 ± 0.4	57 ± 0.7
23TTT	1	57 ± 1.6	30.0 ± 2.7	2.9 ± 0.3	59 ± 2.2
123TTT	1	59 ± 1.1	28.0 ± 3.2	2.9 ± 0.2	58 ± 0.8
0123TTT	1	47 ± 0.9	22.3 ± 2.2	1.5 ± 0.4	44 ± 1.1

aDifferential scanning calorimetry experiments were performed in 10 mM phosphate buffer (BPES) (pH = 7.0), 0.001 M disodium EDTA, and 0.1 M sodium chloride. For the DSC experiments, the DNA concentration strand concentrations ranging from 175 to 225 μM . Experiments were conducted with a heating rate of 0.5 $^{\circ}\text{C}/\text{min}$ over a range from 10-100 $^{\circ}\text{C}$. A minimum of five heating and cooling cycles was conducted for each sample to assess reversibility of the unfolding.

bCircular dichroism spectropolarimetry melts were performed in 10 mM phosphate buffer (BPES) (pH = 7.0), 0.001 M disodium EDTA, and 0.1 M sodium chloride at a DNA strand concentration of 3 μM in a 1 cm path length quartz cuvette. The temperature ranged from 10 to 90 $^{\circ}\text{C}$ at a rate of 1 $^{\circ}\text{C}/\text{min}$. Measurements were taken at every 1 $^{\circ}\text{C}$ after a one-minute equilibration time. A minimum of three melts were performed per experiment and data averaged.

Table 3. Summary of singular values and autocorrelation data for the wild-type human telomeric G-quadruplex DNA sequence.

Order	Singular Value	U-Correlation	V-Correlation
1	288.5280	0.978185	0.970595
2	88.5680	0.984135	0.969943
3	25.3149	0.991713	0.907941
4	6.3224	0.719899	-0.117919

Table 4. Singular Value Decomposition and autocorrelation data for the wild-type human telomeric G-quadruplex DNA sequence and selected sequences having A to T modifications in one or more loops.

Sequence	S	UxS	V	Autocorrelation	Difference	Minimum
	Matrix	Matrix	Matrix	Coefficient	Matrix	Spectral
						Species
wt G-quad	3	3	3	3	3	3
0T	3	4	3	3	4	3
1TTT	4	4	4	4	4	4
2TTT	4	3	3	3	3	3
3TTT	4	4	3	4	3	3
01TTT	4	3	3	3	3	3
02TTT	4	3	3	3	3	3
03TTT	4	3	3	4	4	3
12TTT	5	4	4	4	4	4
13TTT	5	4	4	4	4	4
23TTT	4	4	3	3	4	3
123TTT	4	4	3	3	4	3
0123TTT	4	4	4	3	3	3

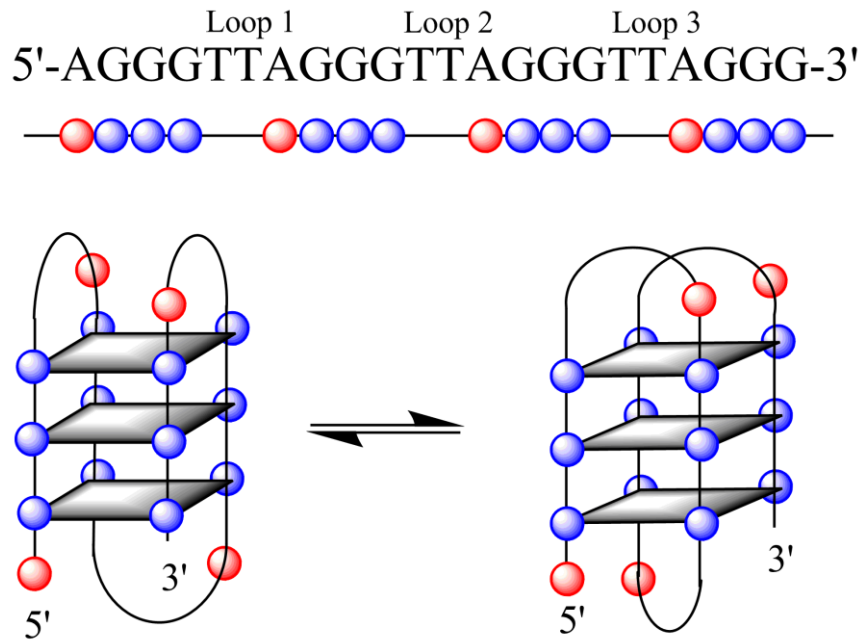


Figure 1. Cartoon representing the chair (left) and basket (right) conformations of the Na⁺ human telomeric G-quadruplex. The blue circles represent the guanines and the red circles represent the adenines.

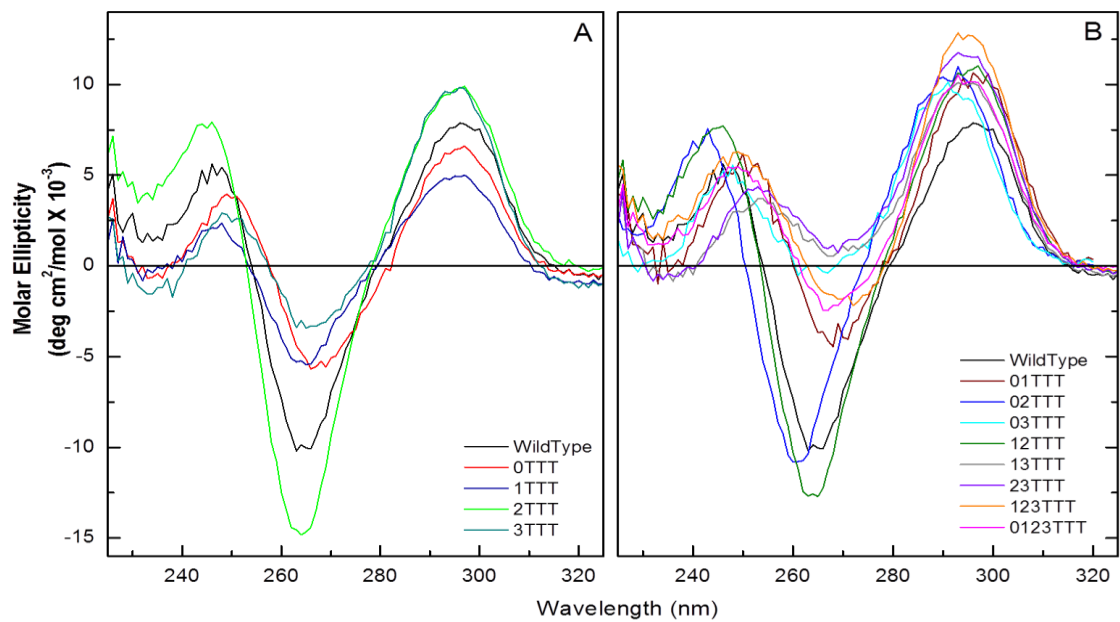


Figure 2. CD wavelength scans for the human telomeric G-quadruplex d[AGGG(TTAGGG)₃] (red line) and the A to T converted loop sequences. Panel A represents the sequences that possess single adenine to thymine base changes. Panel B represents the sequences with multiple A to T modified loops.

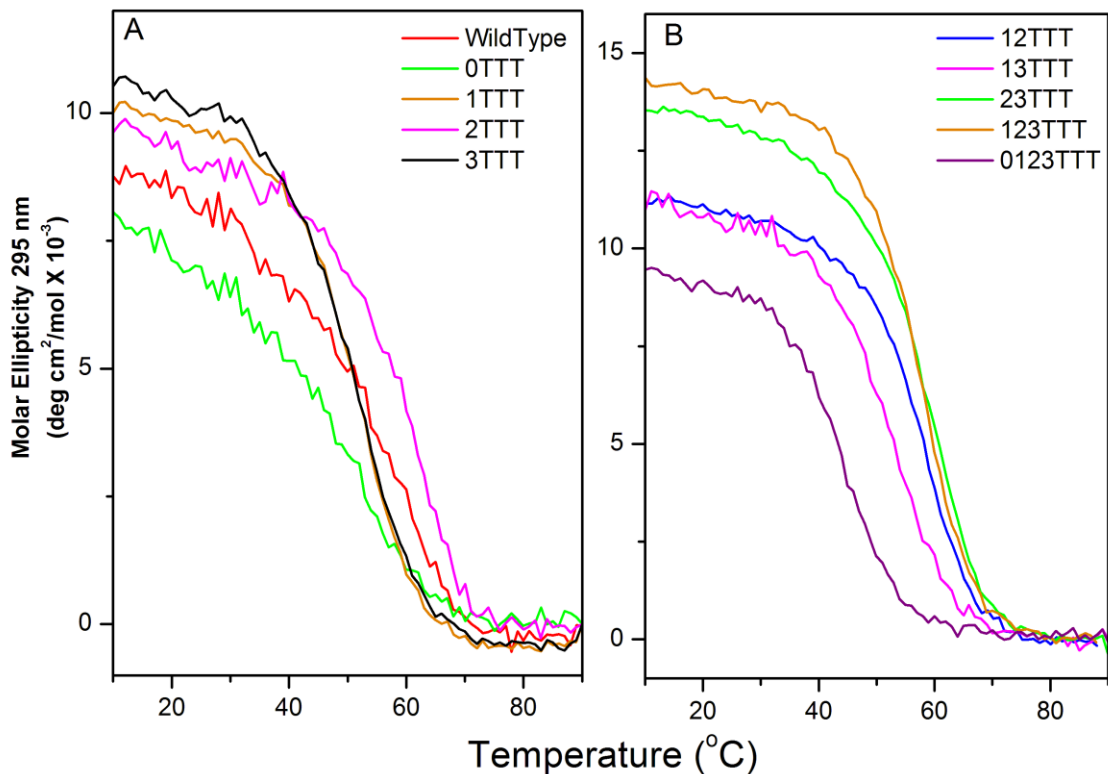


Figure 3. Composite CD melting curves of the human telomeric sequence and A to T modified loop sequences in 100 mM NaCl BPES buffer at pH 7.0. Panel A contains the CD melting curves for the wild type sequence (red line) and the single A to T modified base sequences. Panel B contains the CD melting curves for the G-quadruplex sequences with multiple A to T base changes. Melting temperatures were calculated from the first derivative of the sigmoidal curve. Data were normalized to molar ellipticity and not converted to fraction folded/unfolding in order to retain the pre-transition baseline sloping characteristics.

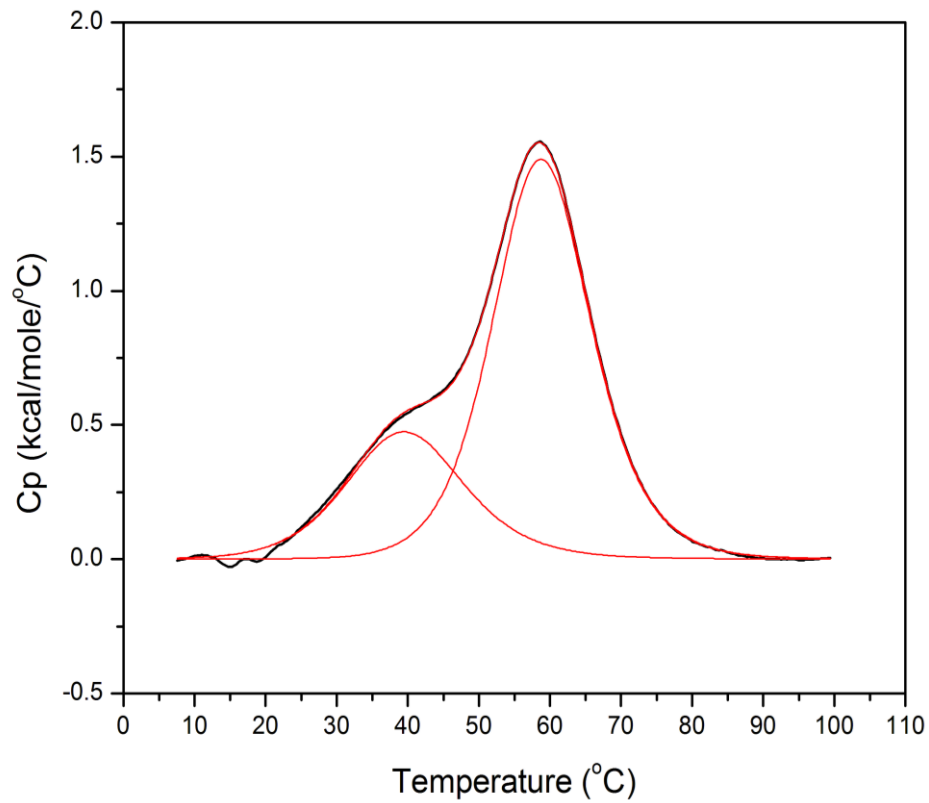


Figure 4. A DSC thermogram of the wild type human telomeric G-quadruplex DNA in 100mM NaCl BPES buffer at pH 7.0. The observed transition (black line) is biphasic with a lower temperature transition at 39 °C and higher temperature transition at 59 °C. The observed data were fit to two transitions (red lines) and the total area under the curve integrated to provide the enthalpy of unfolding (ΔH_{unfold}).

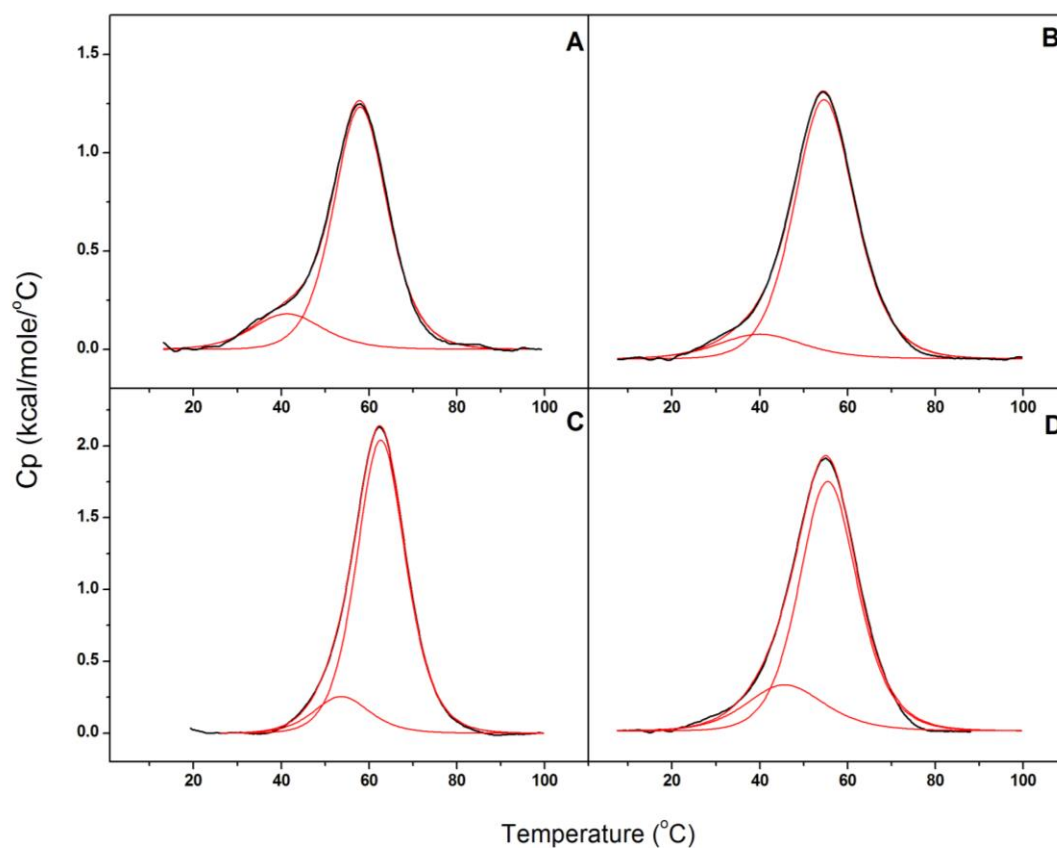


Figure 5. Representative DSC thermograms for the single A to T base modifications of the telomeric G-quadruplex. The black lines represent the raw DSC data and the red lines represent the number of transitions. (Panel A) Conversion of the 5'-A to 5'-T (0T); (Panel B) A to T modification of loop 1 (1TTT); (Panel C) A to T modification of loop 2 (2TTT); (Panel D) A to T conversion of loop 3 (3TTT).

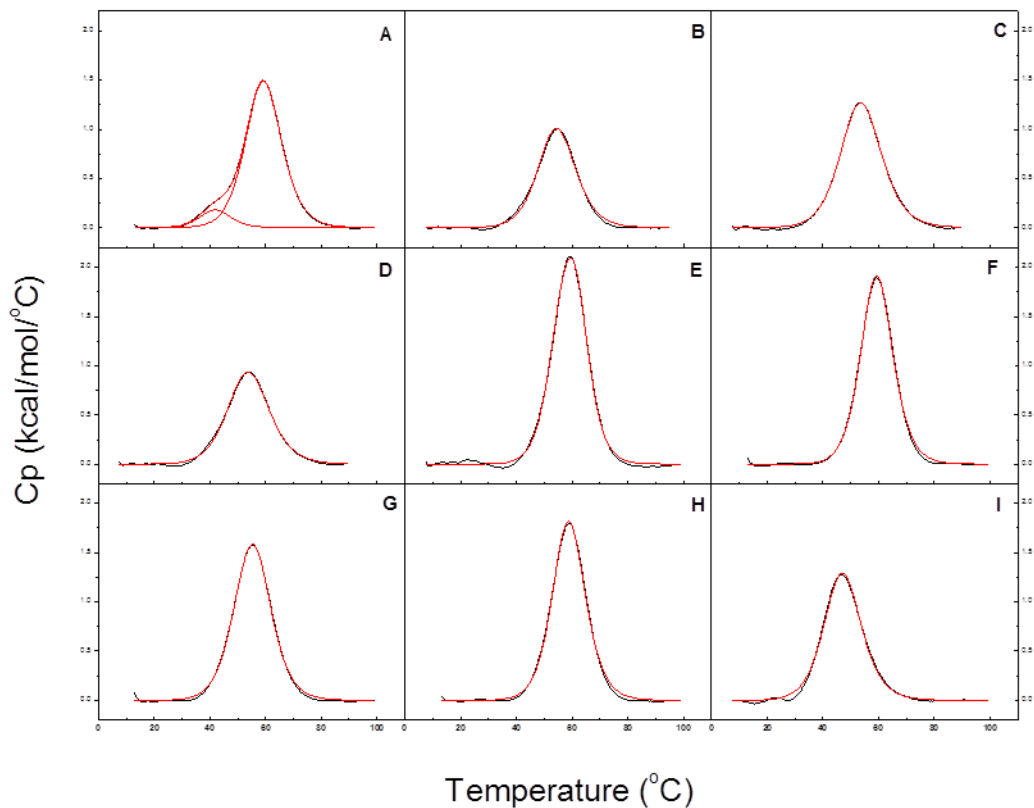


Figure 6. Representative DSC thermograms for multiple A to T loop conversions for the telomeric G-quadruplex sequence. The black lines represent the raw DSC data and the red lines represent the number of transitions. (Panel A) wild type; (Panel B) A to T modifications of loop 0 and loop 1 (01TTT); (Panel C) A to T modifications of loop 0 and loop 2 (02TTT); (Panel D) A to T modifications of loop 2 and loop 3 (23TTT); (Panel E) A to T modifications of loop 1 and loop 2 (12TTT); (Panel F) A to T modifications of loop 1 and loop 3 (13TTT); (Panel G) A to T modifications of loop 2 and loop 3 (23TTT); (Panel H) A to T modifications of loops 0, 1, and 2 (012TTT); (Panel I) A to T modifications of all adenines in the sequence to thymine (0123TTT).

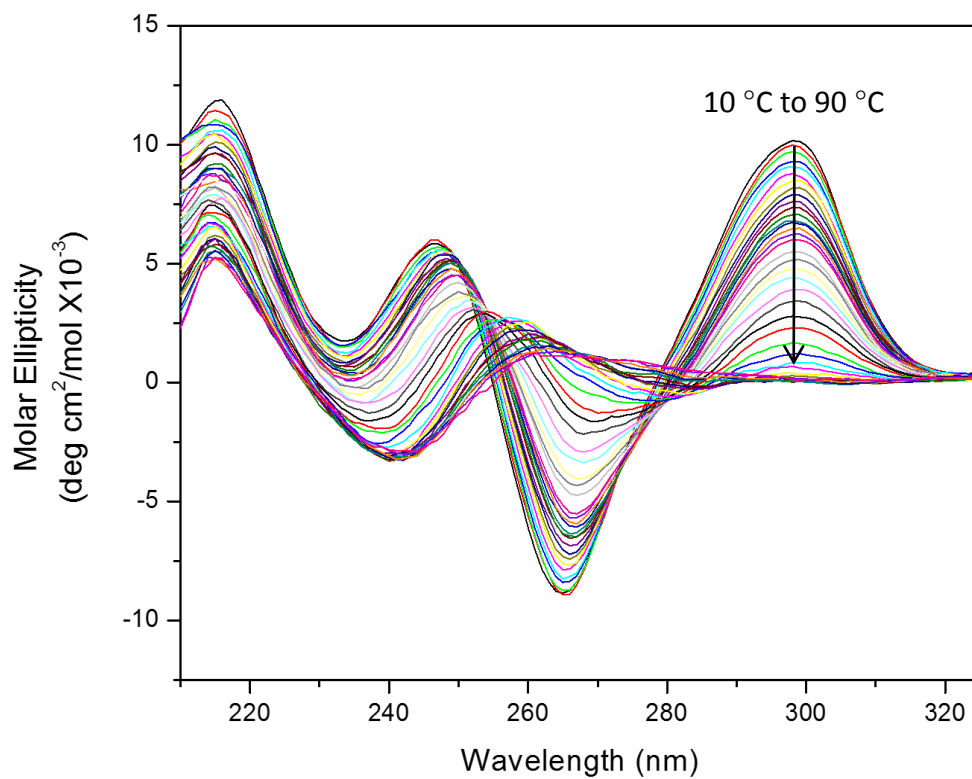


Figure 7. Three-dimensional CD plot for the thermal denaturation of wild-type human G-quadruplex. Each line represents a traditional CD scan at a particular temperature.

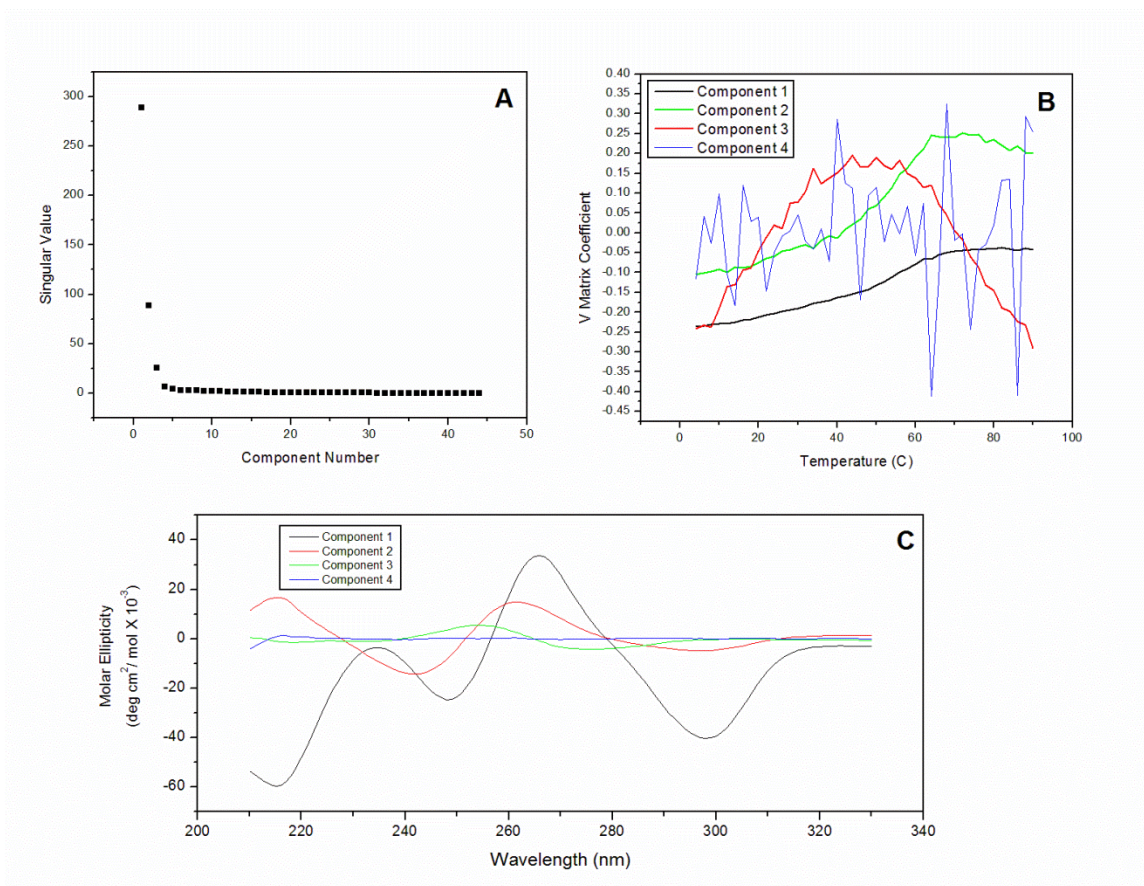


Figure 8. SVD analysis of wild-type human telomeric G-quadruplex. (Panel A) S matrix plot of singular values; (Panel B) V matrix plot of the vector amplitudes; (Panel C) Representative basis spectra obtained by multiplying the U and S matrices together.

CHAPTER 4

ENCAPSULATION AND CONTROLLED RELEASE OF NUCLEIC ACIDS
THROUGH TWO-COMPONENT PMAA/PVPON MICROCAPSULES

by

BRENNA A. TUCKER, JUN CHEN, VERONIKA KOZLOVSKAYA, DAVID E.
GRAVES, and EUGENIA KHARLAMPIEVA

In preparation for *Biomacromolecules*

Format adapted for dissertation

INTRODUCTION

Nucleic acids have been shown to play a key role in a variety of different biological processes within cells including the storage and transfer of genetic information. Due to their biological relevance and interesting secondary structures, nucleic acids have been well characterized^{1,2} and investigated in a wide range of applications.^{3,4,5} In recent years, the delivery of therapeutic nucleic acids to modify gene expression⁶ has emerged as a promising way to treat a varied range of inherited or acquired diseases.^{7,8} Despite their potential, nucleic acid therapeutics have not been widely used for treating diseases due to a series of extracellular and intracellular barriers preventing effective delivery of nucleic acid to the desired sites.⁷

When 'naked' DNA, or DNA that exists freely in solution, is administered as a therapeutic it can be rapidly degraded by nucleases in the plasma or the extracellular matrix.⁹ In addition, it is highly possible that any non-degraded DNA is cleared rapidly from circulation.¹⁰ Specifically, lack of endosomal escape, degradation by lysosomes,¹¹ and insufficient cytosolic transport are significant barriers to overcome when free DNA is uptaken by the cells.¹² These barriers result in lowered levels of gene transfection.^{12,13} To solve this, both viral- and non-viral vectors have been developed to entrap nucleic acids, travel to the cell nucleus, and deliver the nucleic acid of interest to its desired location.^{14,15}

Viral vectors have been developed to deliver DNA, however, several limitations have been associated with the use of viral vectors including, low capacity, challenges in scale-up, high cost, and risk of mutagenesis. Furthermore, vector-inactivating immune responses are frequently observed with repeated administrations or prior exposures which limits the efficacy of these drugs.⁷ Non-viral vectors synthesized from a variety of dif-

ferent cationic lipids or polymers can condense the DNA into micro- or nanoparticles and offers a reprieve from the limitations of viral vectors.¹⁶ Unfortunately, commercially available cationic non-viral vectors, such as Lipofectamine 2000 or PEI, have been shown to cause high cytotoxicity.^{13,17} Also, previous studies have discussed the possibility of changes the native properties and functions of DNA upon direct electrical conjugation of the non-viral vectors to the DNA.¹⁸ Consequently, it is of significant importance to develop safe and biocompatible non-viral vector that can encapsulate DNA inside the carriers without changing the structural integrity of the DNA.

Layer-by-layer (LbL) assembly of microcapsules have emerged as promising non-viral vectors for DNA delivery due to the biocompatibility, micron-sized interior cavity, and trigger responsive nanometer-sized shell of the capsules.^{19,20,21} For example, negatively charged DNA has been incorporated into LbL multilayers or LbL capsule shells by electrostatic interactions with positively charged layers as building block.^{22,23} DNA has also been incorporated within the interior of degradable microcapsules by loading DNA into calcium carbonate microparticles followed by coating of enzyme degradable LbL multilayers and dissolution of the calcium carbonate microparticles.²⁴⁻²⁷ Though the feasibility of encapsulation of DNA inside/within the capsules/capsule shells have been reported, only a few reports have shown the functionality of DNA after released from the capsule and most the previous studies regarding to gene delivery have been focused on bio/redox degradable carriers.⁶ Although enzyme triggered release have been proved efficient, gene vectors that are responsive to different triggers must be combined to better control the DNA release kinetics. Thus, the design of multi stimuli-responsive gene vectors has become a research area of interest.

Recently, we have developed pH responsive LbL capsules of two component poly(methacrylic acid) (PMAA) and poly(vinylpyrrolidone) (PVPON) hydrogen bonded multilayers crosslinked with ethylenediamine.²⁸ We have demonstrated that these capsules can entrap molecules with molecular weights as low as 20,000 g mol⁻¹ at physiological pH.²⁸ In addition, we have also reported that one component PMAA hydrogel particles can release cargo upon intracellular GSH can be obtained when the crosslinking agent was changed from ethylenediamine to cystamine.²⁹ Recent studies have also shown that LbL capsules can be designed to be ultrasound responsive and release their cargos by regulating mechanical stability of the capsules. Ultrasound has been widely used in gene delivery, because the stimulation offers a traceable, localized and non-invasive way to release therapeutic cargos. More important, the use of ultrasound has been shown to assist in the cellular/brain uptake of the DNA³⁰ as well as enhance microbubble mediated gene delivery.³¹ Therefore, inspired by our previous works and by research in the literature, we aim to develop enzyme- and ultrasound- responsive PMAA/PVPON two-component capsules as a novel type of DNA delivery vector.

In the work presented here, we study the conditions for fabrication of PMAA/PVPON dual-responsive capsules as well as the encapsulation and controlled release of nucleic acids through ultrasound and glutathione (GSH) incubation. To our knowledge, this is the first example of multi-responsive LbL microcapsules developed as a G-quadruplex delivery system and this is the first reporting of ultrasound triggered release of functional G-quadruplex from LbL microcapsules. The microcapsules and approach shown here may provide promising potential for the design of DNA vaccines and medicines for a wide range of immunotherapies, cancer therapy and/or tissue regeneration therapies in the future.

EXPERIMENTAL

Materials

Poly(methacrylic acid) (PMAA, average M_w 100,000 g mol⁻¹), Poly(methacrylic acid) (PVPON, average M_w 1,300,000 g mol⁻¹), Poly(ethylene imine) (PEI; average M_w 70,000 g mol⁻¹), L-glutathione reduced (GSH), and cystamine dihydrochloride (CS) were purchased from Sigma-Aldrich. 1-ethyl-3-(3-(dimethylamino)propyl)-carbodiimide hydrochloride (EDC) was purchased from Chem-Impex International. Monobasic sodium phosphate (NaH₂PO₄), dibasic sodium phosphate (Na₂HPO₄), ethylenediaminetetraacetic acid (EDTA), sodium chloride (NaCl), calcium chloride (CaCl₂), sodium carbonate (Na₂CO₃), and calf thymus DNA (ctDNA) were purchased from Fisher Scientific. DNA oligonucleotides (5'-AGGGTTAGGGTTAGGGTTAGGG-3') were purchased from Midland Certified Reagents (USA).

Preparation of double-stranded calf thymus DNA.

Calf thymus DNA was weighed out and dissolved in BPE buffer at 4 °C overnight. Once the DNA was in solution, it was then sonicated using a Branson sonifier for 5 minute on/off intervals for a total of 30 minutes. The DNA was kept over an ice bath and nitrogen gas was bubbled through the sample throughout the sonication process. A syringe filter (0.45 µm) was then used to filter the sonicated solution and then the salt concentration was increased to 0.2 M by the addition of solid NaCl. The DNA sample was then treated with RNase at 37 °C for 30 minutes followed by treatment with proteinase K at 37 °C for 2 hours. The DNA sample was then extracted with an equal volume of chloroform in a separatory funnel before being split into two 50-mL Falcon tubes. The tubes were centrifuged at 4 °C for 5 minutes and the top layers from each tube were add-

ed back to the separatory funnel. This process was repeated until the interface between the DNA solution and the chloroform was clear and not cloudy. The DNA layers were then pooled together and precipitated by adding salt-saturated ethanol to the solution. The precipitated DNA was separated by centrifugation and dried using a vacuum. The dried DNA pellet was dissolved in BPES buffer and then placed into dialysis against BPES buffer. After a minimum of 4 buffer changes, the DNA was collected from dialysis, filtered again using a 0.45 μm syringe filter, and stored at 4 °C for future use. The average length of the calf thymus DNA was determined by an agarose gel to be approximately 700 base pairs. The concentration of the DNA sample per duplex was determined by monitoring the UV/Vis absorbance at 260 nm ($\epsilon = 13,200 \text{ M}^{-1} \text{ cm}^{-1}$).

Preparation of DNA oligonucleotides

G-quadruplex forming oligonucleotides were resuspended in sodium phosphate buffer (50 mM NaH_2PO_4 , 50 mM Na_2HPO_4 , 150 mM NaCl , and 0.01 mM EDTA) and stored at 4 °C overnight. Beer-Lambert's law was used to determine the concentration of DNA per strand of G-quadruplex by measuring the absorbance at 260 nm at room temperature ($\epsilon = 228,500 \text{ M}^{-1} \text{ cm}^{-1}$). When not in use, oligonucleotide solutions were stored at 4 °C.

Encapsulation of DNA into calcium carbonate cores

G-quadruplex oligonucleotides (1 mM) were encapsulated into calcium carbonate cores by combining 150 μL CaCl_2 (1mM) with 690 μL ultrapure water and 150 μL Na_2CO_3 (1 mM) under rapid stirring for 40 seconds. G-quadruplex-loaded cores were removed from the stir plate, centrifuged to remove the supernatant, and washed by adding

ultrapure water and vortexing the sample. Then, the G-quadruplex-loaded cores were washed with water a second time and then examined under the microscope to determine their size and aggregation state. The supernatants from the wash step were saved for further analysis of the capsule loading capacity of G-quadruplex. Empty cores were also prepared using this same strategy except 10 uL of the buffer was added to the cores instead of the DNA.

Double stranded calf thymus DNA was encapsulated by mixing 450 uL CaCl₂ (1mM), 2.07 mL ultrapure water, and 450 uL ctDNA (6.1 mM). Once this solution spun uniformly, 450 uL Na₂CO₃ (1 mM) was added and after 40 seconds, the cores were collected and washed as described previously. To make the control empty calcium carbonate cores for this system, 450 uL of sodium phosphate buffer was added instead of the ctDNA.

Synthesis of G-quadruplex loaded (PMAA/PVPON)*n* biodegradable capsules

The DNA-loaded calcium carbonate cores were sequentially exposed to different polymers to prepare the capsules using a cyclic procedure where the sample is vortexed, centrifuged to exchange the supernatant for either wash buffer or a polymer, and then vortexed and centrifuged again. Specifically, to make the PMAA/PVPON biodegradable capsules, PEI (0.25 mg/mL, pH 4) was added as the initial polymer layer and then PMAA (0.1 mg/mL, pH 4) and PVPON (0.1 mg/mL, pH 4) layers were alternated to deposit on the DNA-loaded cores until the desired number of polymer layers was reached. Core-shells were washed with buffer twice between the additions of each polymer layer. After the desired number of bilayers was added, core-shells were allowed to mix with 1-ethyl-3-(3-(dimethylamino)propyl)-carbodiimide hydrochloride (EDC) (1 mg/mL, pH 5.5) for

35 minutes before being crosslinked with cystamine dihydrochloride (1 mg/mL, pH 5.5) for either 24 or 48 hours. The cross-linked core-shells were washed twice with buffer (NaH₂PO₄, pH 5.5) before EDTA (1 mM, pH 5.5) was added to dissolve the cores. The dissolution of the cores was checked daily using the microscope. After all cores had dissolved, the two-component (PMAA/PVPON)_n capsules were washed and dialyzed versus buffer (pH 7.4). Capsules were removed from dialysis, washed with buffer (pH 7.4), and stored for use.

Characterization of (PMAA/PVPON)₁₃ capsules using FTIR

Fourier Transform Infrared Spectroscopy (FTIR) was used to analyze the chemical composition of PMAA/PVPON capsules. Empty and G-quadruplex loaded (PMAA/PVPON)₁₃ hydrogel capsules at pH 7.5 as well as G-quadruplex forming oligonucleotides at pH 7.5 were used in this study. To prepare the samples for FTIR 0.5 mL of each at pH 7.5 were freeze-dried overnight. Spectra were collected in absorbance mode using an ATR-FTIR (Bruker, Alpha-FTIR). The number of scans collected for each of the background and sample measurements equaled 128. The resulting spectrum was normalized and baseline corrected before being analyzed for peaks.

Characterization of (PMAA/PVPON)_n capsules by Scanning Electron Microscopy

Scanning electron microscopy (SEM) was used to look at the morphology of the empty and G-quadruplex loaded (PMAA/PVPON)₁₃ capsules. For this work a FEI Quanta FEG SEM microscope at 10 kV was used. Capsules were dialyzed against water to prepare them for SEM, and then a drop of the diluted capsule solution was placed on a

silicon wafer and allowed to dry overnight. A Denton sputter-coater was used to coat the dried capsule samples with a ~5 mm thick layer of gold immediately before imaging.

Characterization of (PMAA/PVPON)_n capsules using Zeta-sizer

To characterize the ζ -potential of the capsules, the Nano Zetasizer (Malvern) was run on both G-quadruplex loaded and ctDNA loaded (PMAA/PVPON)_n capsules, where $n = 13$, exposed to buffers of varying pH. To expose the capsules to a new pH, the capsules were centrifuged and the supernatant was replaced with a phosphate buffer of the desired pH. The capsules were allowed to equilibrate for 10 minutes before being vortexed and inserted into the sample chamber. The ζ -potential was determined by taking the average of three measurements each consisting of 20 runs.

Ultrasound controlled release of G-quadruplex DNA from the (PMAA/PVPON)_n capsules

G-quadruplex loaded (PMAA/PVPON)_n capsules, where $n = 10, 13, \text{ or } 16$, were burst using the ultrasound waves of a sonication probe. The capsules were washed with NaCl-free phosphate buffer (pH 7.4) 3 times and allowed to equilibrate for 10 minutes upon the final wash. The sonication probe was then inserted into the capsule solution and run at 40% power (57 W/cm^2) for 20 seconds. Water and 70% ethanol were used to wash the sonication probe both before and after use.

Turbidity Measurements of GSH treated (PMAA/PVPON)₁₃ capsules

Turbidity measurements were performed to track the GSH-induced degradation of (PMAA/PVPON)₁₃ capsules at 37 °C using fluorescence spectroscopy (Varian, Cary Eclipse). The scattering intensity of the capsules suspended in phosphate buffer (2×10^5

capsules μL^{-1}) at pH 7.4 with or without 5 mM GSH was measured at $\lambda = 700$ nm. The ratio of the particle scattering intensity at a certain interval to that of the initial nondegraded particles was used to calculate the relative turbidity.

Enzymatic release of G-quadruplex DNA from (PMAA/PVPON)₁₃ capsules

Glutathione (GSH) was used to reduce the disulfide bonds of the cystamine cross-linker allowing for the degradation and release of cargo from (PMAA/PVPON)₁₃ hydrogel capsules. G-quadruplex-loaded capsules were incubated at 37 °C with pH 7.5 GSH (5 mg/mL). Release of DNA was monitored at various time points by using UV/Vis spectroscopy. Capsule samples were centrifuged and the supernatant was collected for measurements before being returned to the capsules.

Quantification of G-quadruplex DNA release

Prior to the ultrasound/enzyme treatment, the capsules were centrifuged (5,000 rpm for 10 minutes) and the supernatant was collected, monitored for any absorbance at 260 nm using a spectrophotometer to determine any initial amounts of G-quadruplex present, and returned to the capsules. After ultrasound/enzyme treatment, the release of G-quadruplex was determined using the absorbance at 260 nm and the molar absorptivity coefficient ($228,500 \text{ M}^{-1}\text{cm}^{-1}$).

Probing structural changes of G-quadruplex DNA after release

DNA released from the capsules was examined for any structural changes to probe the resulting functionality of the released cargo. After confirming release of DNA through UV/Vis spectroscopy, G-quadruplex DNA was monitored using circular dichro-

ism (CD) and compared to CD scans of free G-quadruplex to determine if there were any changes to the secondary structure. Changes in intensity and shifting of peaks would indicate changes to the secondary structure. Free and released G-quadruplex scans were obtained from an average of 3 scans collected from 320-220 nm with a 1 nm step and a 1 sec response time.

Quantification of dsDNA release

The amount of dsDNA released from the capsules was determined through fluorescence measurements of DNA loaded capsules after ultrasound treatment. Samples were excited at 520 nm and the emission spectrum was recorded from 530 nm to 750 nm. A 1x1 mm square cuvette was used for all measurements and a 1% v/v amount of EtBr was added to each sample before collecting the emission data. Samples equilibrated for 10 minutes before data collection. A calibration curve was collected for varying amounts of ctDNA and the emission at 605 nm was used to calculate the ctDNA concentration in each sample from the slope of the calibration curve. To examine how encapsulation affects the structure of double stranded calf thymus DNA, agarose gel electrophoresis was run on released ctDNA using free ctDNA as a control. Damage to the DNA structure would be indicated by the appearance of bands that do not align with the control.

RESULTS AND DISCUSSION

In this work, we address the barriers of using nucleic acids as drugs by synthesizing two-component (PMAA/PVPON)_n hydrogel capsules loaded with different types DNA for use as an improved delivery vehicle for nucleic acids. A two-component capsule system utilizing LbL technology to alternatively deposit poly(methacrylic acid) (PMAA) and poly(N-vinylpyrrolidone) (PVPON) was chosen due to the biocompatibility of these polymers.^{29,32,33,34} For this work, we have focused on the encapsulation of G-quadruplex forming oligonucleotides which are unique DNA structures formed from guanine-rich sequences of DNA that can be found within promotor regions of oncogenes as well as in the telomeric regions of the chromosome.^{35,36} We chose the G-quadruplex because it is nuclease resistant, plays a role in transcriptional regulation, and is structurally similar to the thrombin binding aptamer (TBA).^{37,38} TBA is a G-quadruplex forming sequence of DNA that is commonly used as an anti-coagulant during surgeries.³⁹ Encapsulation of G-quadruplex oligonucleotides can be applied to the encapsulation of TBA and contribute to the continuous optimization of TBA delivery. The encapsulation of G-quadruplex DNA to use as a therapeutic is therefore a novel concept that will allow new directions for the use of G-quadruplex structures. To show the versatility of this system, we also encapsulated dsDNA and present that work here.

Synthesis and Characterization of G-quadruplex-loaded (PMAA/PVPON)₁₃ capsules

We have previously demonstrated that increasing the molecular weight of PVPON within cross-linked PMAA hydrogel films decreases the ability of the PVPON to be released by the system after the pH is increased above the pKa of PMAA.⁴⁰ When the molecular weight of PVPON in PMAA/PVPON films was increased to 1,300,000 g mol⁻¹

¹, it was found that approximately 18% of the PVPON was released due to the increased chain entanglements relative to smaller PVPON chains.⁴⁰ Knowing this, we chose to use PMAA with a MW of 100,000 g mol⁻¹ and PVPON with a MW of 1,300,000 g mol⁻¹ to create two-component (PMAA/PVPON)₁₃ hydrogel capsules and encapsulate G-quadruplex DNA within them as described in the experimental section. It is expected that in our current work, an increase in the cross-linking time of PMAA will decrease the PVPON that is released from the capsules relative to our previous experiments.⁴⁰ An overview of the nucleic acid loaded capsule synthesis can be found in Figure 1. Briefly, porous calcium carbonate sacrificial cores were co-precipitated with G-quadruplex forming oligonucleotides before PMAA (100,000 g mol⁻¹) and PVPON (1,300,000 g mol⁻¹) were sequentially deposited to a total of 13 bilayers at pH 4.0 to facilitate the hydrogen bonding between PMAA and PVPON layers. A combination of EDC and cystamine were used to cross-link the PMAA molecules making up the capsule shell for 48 hours at pHs 5 and 5.5, respectively. After cross-linking of the core-shells, capsules were obtained by treatment with EDTA to dissolve the CaCO₃ cores.

To confirm that both polymers were present within the capsules and thus two-component hydrogel capsules were produced, FTIR was run on both empty and G-quadruplex loaded (PMAA/PVPON)₁₃ capsules, freeze dried at pH 7.4. The FTIR spectrum for the empty capsules, shown by the red trace in Figure 2a, revealed major peaks centered around 1525 cm⁻¹ and 1640 cm⁻¹ corresponding to the presence of both the ionized carboxylate groups from PMAA (1525 cm⁻¹) and the carbonyl groups of PVPON (1640 cm⁻¹). The presence of the carbonyl stretch of PVPON within the FTIR indicates that PVPON is not released from the PMAA cross-links after dissolution of the cores and remains trapped within the PMAA cross-links. These results agree with our previous

studies on the ability to use LbL technology to create two-component PMAA/PVPON hydrogel capsules.⁴⁶ The successful entrapment of PVPON within the PMAA cross-links is attributed to maintaining the hydrogen bonding of the PMAA/PVPON multilayers during capsule cross-linking. This is easily achievable by keeping the pH of the capsule solution less than the pKa of PMAA (~6.0) during cross-linking.⁴⁶ In the work presented here, the cross-linking solution was kept at a pH of 5.5. Interestingly, when the capsules were loaded with G-quadruplex DNA, a broadening of the peaks occurred as can be seen in the black trace in Figure 2a. The spectrum for the G-quadruplex loaded capsules contains discernable shoulders and the presence of PMAA and PVPON can still be detected at 1525 cm^{-1} and 1640 cm^{-1} , respectively, within the broadened peak. To discern why this broadening of peaks occurred, G-quadruplex forming oligonucleotides were also freeze-dried at pH 7.4 and run on the FTIR as shown in Figure 2b. The spectrum for the free oligonucleotide showed a broad peak centered around 1700 cm^{-1} corresponding to carbonyl groups found in the guanine bases of the DNA. This peak can also be seen in Figure 2a in the black trace for G-quadruplex loaded capsules. Taken together, these results indicate that loading the capsules with G-quadruplex does not affect the ability to form two-component (PMAA/PVPON)₁₃ hydrogel capsules.^{40,45}

To determine the effects of G-quadruplex encapsulation upon the surface charge of the capsules, the zeta-potential of both empty and G-quadruplex loaded (PMAA/PVPON)₁₃ capsules was determined using a Nano Zetasizer (Malvern). Figure 3a shows the trends between zeta-potential and pH for empty capsules. When the pH is greater than 4, the capsules possess an overall negative zeta-potential and as the pH decreases lower than 4, the capsules possess an overall positive zeta-potential. When the pH equals 4 the overall zeta-potential on the capsules is neutral. This trend can be ex-

plained by the different protonation states of carboxylic acid functional groups within the PMAA residues.⁴¹ At higher pHs, the carboxylic acid is ionized to carboxylate consistent with the observed negative zeta-potential. These results are in good agreement with previously reported data.²⁹ Similar results were found for the G-quadruplex loaded capsules. Figure 2b shows the trend of zeta-potential versus the biologically relevant pHs 5.5 and 7.5 for both empty and G-quadruplex loaded capsules. Both types of capsules have a negative surface charge at pHs 5.5 and 7.5, however, capsules loaded with G-quadruplex oligonucleotides were found to have an increased negative surface charge relative to the empty capsules at each pH studied. It is well established DNA is negatively charged at neutral pH due to the phosphate ions comprising its backbone and that the magnitude of this charge can be controlled by the salt concentration.⁴² Because the solution conditions contain no added salt, it is safe to assume the G-quadruplex oligonucleotides in this work are negatively charged. It is also well established that the pKa of the individual nucleotide bases are largely overwhelmed by the phosphate pKa (~1) when they are assembled into DNA strands and therefore we would not expect the magnitude of the negative charge on the G-quadruplex oligonucleotides to shift over the range of pH values studied.⁴³ Taking this information collectively, we suggest the negative increase in zeta-potential upon G-quadruplex loading is explained by the presence of negatively charged G-quadruplex oligonucleotides within the shell of the capsules.

We also studied the effect of pH on the size of the G-quadruplex loaded capsules. The size of the capsules was determined at pHs 5.5 and 7.4 by averaging of 35 different capsule size measurements. The capsules had an average size of $1.9 \pm 0.2 \mu\text{m}$ at pH 5.5 and they increased slightly to $2.5 \pm 0.4 \mu\text{m}$ when the pH was increased to 7.4 giving a swelling fold increase of approximately 1.3. These results are in good agreement with

previously published studies on the effects of pH on size of two-component (PMAA/PVPON)_n hydrogel capsules.⁴⁵ SEM images of G-quadruplex loaded capsules in their dry state are shown in Figure 4. From these images, it is apparent that the capsules have very thin shells.

Release of G-quadruplex DNA through ultrasound treatment

We have recently reported the successful rupture of two-component tannic acid (TA)/PVPON capsules through exposure to ultrasound⁴⁴ and are interested in applying this technique to different capsule systems. To study the ability of our capsule system to release G-quadruplex upon ultrasound stimuli, G-quadruplex loaded (PMAA/PVPON)₁₃ capsules were fabricated and exposed to ultrasound at pH 7.5. A schematic for the stimuli-responsive release of DNA cargo is shown in Figure 5.

Prior to ultrasound exposure, G-quadruplex loaded (PMAA/PVPON)₁₃ capsule samples were counted, centrifuged, and the supernatant examined by UV/Vis for any initial amount of DNA present. After exposure, the supernatant was monitored using UV/Vis to calculate the moles of G-quadruplex released per capsule in the sample. As reported in Table 1, it was found that approximately $6.52 \times 10^{-18} \pm 3.9 \times 10^{-19}$ moles of G-quadruplex oligonucleotides were released per capsule. Considering that the size of the capsules at pH 7.4 was calculated to be $2.5 \pm 0.5 \mu\text{m}$, a volume of 6.54×10^{-14} L can be estimated for the capsules. With this information, we then calculated the average concentration of G-quadruplex oligonucleotides released per capsule and found that value to be about $100 \pm 6 \mu\text{M}$. Previously, double- and single stranded DNA was encapsulated within single component PMAA capsules using porous silica spheres as the core template.⁴⁵ With this approach, it was found that the upper limit to the number of 20-mer ssDNA

chains that could be adsorbed to the surface of the silica template, and thus become encapsulated, approached 10,000 chains per capsule. In comparison, we show a significant increase in the number of 24-mer G-quadruplex oligonucleotide chains that can be loaded per capsule, an impressive 4 million G-quadruplex molecules per capsule. This increase in encapsulation can be attributed to the use of a co-precipitation technique, which is better able to condense the oligonucleotides within the CaCO₃ cores, as compared to surface adsorption methods.

To study any effects shell thickness has upon cargo release, two-component (PMAA/PVPON)_n capsules loaded with G-quadruplex oligonucleotides with varying number of bilayers were also synthesized. G-quadruplex loaded (PMAA/PVPON)_n capsules where n= 10 or 16 were exposed to ultrasound in addition to the 13 bilayer capsules. It was found that the moles of G-quadruplex released is independent of the number of bilayers (Table 1). The concentration of G-quadruplex DNA in each capsule was calculated using total number of capsules in each sample, the moles of DNA released after ultrasound exposure, and the volume of the respective capsule sample. The concentration of DNA inside capsules was also found to be independent as the number of bilayers increased from 10 to 13 which is not surprising considering that there was a negligible volume change of the capsules as the number of bilayers increased. With the increased average capsule size of the 16 bilayer capsules, the average concentration of G-quadruplex per capsule is decreased to $6.47 \times 10^{-18} \pm 0.09 \times 10^{-18}$ moles of G-quadruplex oligonucleotides. It should be noted that the mesh size of the capsules would be expected to increase with increasing number of bilayers and constant cross-linking conditions. If the mesh size had increased to allow leaking of the DNA cargo, then the total number of moles of DNA released per capsule would decrease with increasing number of bilayers. This trend

was not observed and it can be concluded that the mesh size of the capsules is sufficient to keep the G-quadruplex encapsulated until a stimuli-responsive release event is triggered.

To determine if ultrasound would be harmful to the DNA cargo, we first studied the effect of various ultrasound parameters on the resulting structure of G-quadruplex oligonucleotides. Solutions of free G-quadruplex forming oligonucleotides were exposed to 40% ultrasound power for either 20, 40, or 60 seconds and then these solutions were monitored using circular dichroism to determine if there were any changes to the secondary structure of the G-quadruplex (Figure 6a). A control solution of G-quadruplex oligonucleotides with no exposure to ultrasound was used to compare any differences found within the spectra after the oligonucleotides were exposed to ultrasound. The control solution displayed major peaks at 245 nm and 300 nm and a trough at 265 nm, indicative of a G-quadruplex structure in the basket conformation.⁴⁶ After ultrasound exposure, the expected characteristic peaks for a G-quadruplex oligonucleotide in a basket conformation were present for all solutions (Figure 6a). The lack of changes between the control G-quadruplex solution and the solutions exposed to ultrasound indicates that the G-quadruplex is stable enough to undergo ultrasound treatment at 40% power for up to 60 seconds and remain in its folded state. This is in good agreement with previous reports on the effects of sonication on G-quadruplex structure.⁴⁷ From this data, we conclude that our capsule system should be exposed to 40% ultrasound for 20 second intervals to release the G-quadruplex from the capsules.

Circular dichroism was also used to monitor any changes to the secondary structure of the G-quadruplex oligonucleotides before and after encapsulation (Figure 6b). A solution of free G-quadruplex was run as a positive control and the characteristic peaks

and trough (245 nm, 295 nm, and 265 nm, respectively) for a G-quadruplex basket structure can be seen in the blue trace.⁴⁶ Prior to GSH triggered release of G-quadruplex from (PMAA/PVPON)₁₃ capsules, the G-quadruplex oligonucleotides were encapsulated and released from CaCO₃ cores to determine if the initial encapsulation by the cores altered the secondary structure of the DNA. The G-quadruplex oligonucleotides were released from the cores through EDTA treatment and are represented by the green trace in Figure 6b. These samples were also shown to retain their secondary structure as indicated by the characteristic peaks that match that of the blue trace. Similar results were also found for G-quadruplex oligonucleotides released from (PMAA/PVPON)₁₃ capsules by ultrasound stimuli as indicated by the red trace in Figure 6b. From these results, we can conclude that our capsule system and ultrasound release mechanism is not-harmful the G-quadruplex oligonucleotides released from (PMAA/PVPON)₁₃ capsules because they remain folded state even after exposure to ultrasound.

Release of G-quadruplex DNA through GSH treatment

To study the ability of reduced glutathione (GSH) to cleave the disulfide bonds crosslinking the PMAA strands of the capsule shell, G-quadruplex loaded capsules were added to 5mM GSH and the turbidity of the solution was monitored at 700 nm using a Varian Cary Fluorometer. It is expected that as the crosslinks between the PMAA strands degrade, the capsules fall apart and the polymers resolubilize, causing a decrease in turbidity.^{29,48} It was observed that after treatment with GSH, empty (PMAA/PVPON)₁₃ capsules had a relative decrease in turbidity by 45% over a time frame of 8 hours (Figure 7). Interestingly, when loaded with G-quadruplex, the capsules were observed to have a lessen decrease in relative turbidity over the same time range, by

approximately 30% (Figure 7). Visual observation of the both empty and G-quadruplex loaded capsules after treatment with 5 mM GSH revealed that the solutions were opaque, indicating the presence of capsules in the solution. These solutions were examined using optical microscopy and were found to contain both fully rounded capsules as well as caved in capsules and capsule fragments (data not shown). We conclude that under these conditions, there is an insufficient amount of GSH present to reduce all the disulfide cross-links. The lack of capsule degradation observed is credited to the highly cross-linked, two-component capsule shell. The difference in overall relative turbidity decrease between the G-quadruplex loaded capsules compared to empty capsules is attributed to the presence of G-quadruplex within the capsules shell. It is possible that the presence of DNA stabilizes the capsule shell or that the DNA interacts with GSH in such a way to inhibit cleavage of the disulfide cross-links holding the capsule shell together.

To determine if the capsules could degrade at higher concentrations of GSH, the same turbidity experiments were repeated using 20 mM GSH. After incubation with GSH, visual inspection of the capsules revealed a clear solution, indicating that the capsules had completely degraded. This was confirmed by optical microscopy in which no capsules or capsule fragments could be observed. It is important to note that even though the capsules were shown to break apart, exposure to extremely high concentrations of GSH, such as in this experiment, would not occur in the cell under normal respiration.^{49,50} We can conclude from these results that due to the heavy cross-linking, two-component (PMAA/PVPON)₁₃ capsules cross-linked for 48 hours will not fully degrade when in the presence of cellular concentrations of GSH.

Encapsulation and ultrasound release of dsDNA-loaded (PMAA/PVPON)₁₃ capsules

To explore the versatility of our two-component (PMAA/PVPON)₁₃ capsules, we also used this system to encapsulate double-stranded calf thymus DNA (ctDNA). As summarized in Figure 1, dsDNA was coprecipitated within CaCO₃ particles and PEI was added as a precursor layer before PMAA and PVPON were alternatively deposited at pH 4 to a total of 13 bilayers. The multilayers were crosslinked for 48 hours, and finally, cores were dissolved with EDTA at pH 5.5 to yield dsDNA loaded (PMAA/PVPON)₁₃ capsules. Figure 8a shows confocal images of dsDNA-loaded (PMAA/PVPON)₁₃ capsules at pH 7.4 in the presence of ethidium bromide (EtBr), a well-known DNA intercalator.⁵¹ EtBr contains fluorescent properties and the red in Figure 8a originates from EtBr bound to dsDNA.⁵¹ Visual observation of both empty and dsDNA-loaded capsules treated with EtBr confirmed that only capsules containing dsDNA can trap EtBr (Figure 8b). When EtBr was added to empty capsules, the red color coming from the EtBr was washed away after several rinses. However, when EtBr was added to dsDNA-loaded capsules, the red color persisted after several rinses indicating that EtBr is too small to be trapped within our capsules without the presence of dsDNA for it to interact with (Figure 8b). We therefore can conclude that the presence of the red fluorescence throughout the capsules in Figure 8a indicates that dsDNA can be encapsulated using our (PMAA/PVPON)₁₃ hydrogel system. These results agree with previous studies on the encapsulation of dsDNA by polyelectrolyte multilayer capsules.^{52,53} The encapsulation of ctDNA is unique in the fact that it exists as a range of different lengths and shows an additional feature of our capsules to be able to encapsulate molecules of different molecular weights.

We then examined the ability of our capsules to release dsDNA upon ultrasound exposure as described earlier for release of G-quadruplex oligonucleotides. Solutions of dsDNA loaded (PMAA/PPON)₁₃ capsules were counted, exposed to ultrasound at 40% power for 20 seconds, and then the supernatant was examined for the presence of dsDNA released from the capsules. Because the molar extinction coefficient of ctDNA is much lower than that of the G-quadruplex, (6,600 M⁻¹cm⁻¹ versus 228,500 M⁻¹cm⁻¹, respectively)⁵⁴ the absorbance is much lower for ctDNA, making it harder to detect by UV/Vis spectroscopy. To solve this, the binding of EtBr to DNA and their subsequent linear spectroscopic relationship⁵¹ was taken advantage of as a way to monitor the amount of ctDNA present in the supernatant. It was found that $6.73 \times 10^{-18} \pm 0.52 \times 10^{-18}$ moles of dsDNA were released per capsule. When the volume of the capsules is considered, the concentration of dsDNA per capsule can be calculated to be 105 ± 8 μM. Interestingly, these values are extremely similar to those obtained for G-quadruplex loaded (PMAA/PVPON)₁₃ capsules ($6.52 \times 10^{-18} \pm 3.9 \times 10^{-19}$ moles G-quadruplex/capsule and 100 ± 6 μm G-quadruplex/capsule) which might indicate that we have reached a maximum effective loading capacity⁵¹ for this capsule system.

To determine how ultrasound exposure affects the shearing of dsDNA, we monitored samples of free dsDNA before and after ultrasound treatment on an agarose gel (Figure 8c).⁵⁵ The gel was imaged using a BioRad Gel Dock station and the lanes, numbered 1 through 3, contained a low mw DNA ladder ranging from 25 to 700 base pairs, a control sample of dsDNA without exposure to ultrasound, and dsDNA exposed to 40% ultrasound for 20 seconds, respectively. From lane 2, we can see that most the free ctDNA before ultrasound exposure ranges from 400 to 700 base pairs, corresponding to an average molecular weight range of 260 – 455 kDa. Similarly, the dsDNA after ultra-

sound exposure in lane 3, demonstrates a banding pattern that shows most of the dsDNA is between 400 and 700 base pairs long. We did notice, however, a difference in the banding associated with DNA strands 75 base pairs long before and after ultrasound exposure. The intensity of the bands around 75 base pairs decreases slightly after ultrasound exposure in lane 3, compared to the control dsDNA without ultrasound exposure in lane 2. From these results, we conclude that the ultrasound settings were strong enough to minimally disrupt the shorter lengths of the ctDNA. However, this observation could be decreased by the encapsulation of the DNA and is not expected to influence the delivery of dsDNA using this capsule system.

CONCLUSIONS

New roles for nucleic acids have emerged, however, challenges with delivery have limited their use as drugs. We address the need for improved delivery of nucleic acids in this work through the development of two-component (PMAA/PVPON)₁₃ capsules that can be used for the encapsulation and release of various DNA structures including G-quadruplex and double-stranded helices. We show that (PMAA/PVPON)₁₃ capsules loaded with either G-quadruplex or ctDNA have a higher effective loading capacity compared to previous studies, decreasing to the number of capsules required per dose. In addition, we show that these capsules are responsive toward ultrasound exposure allowing for a controlled delivery of cargo. At the same time, the capsules were shown to be minimally responsive to GSH concentrations within the intracellular range. This observation leads to a novel dual release mechanism where capsules in the cell can release some cargo before a controlled burst release of cargo is triggered by external ultrasound devices.

FIGURES

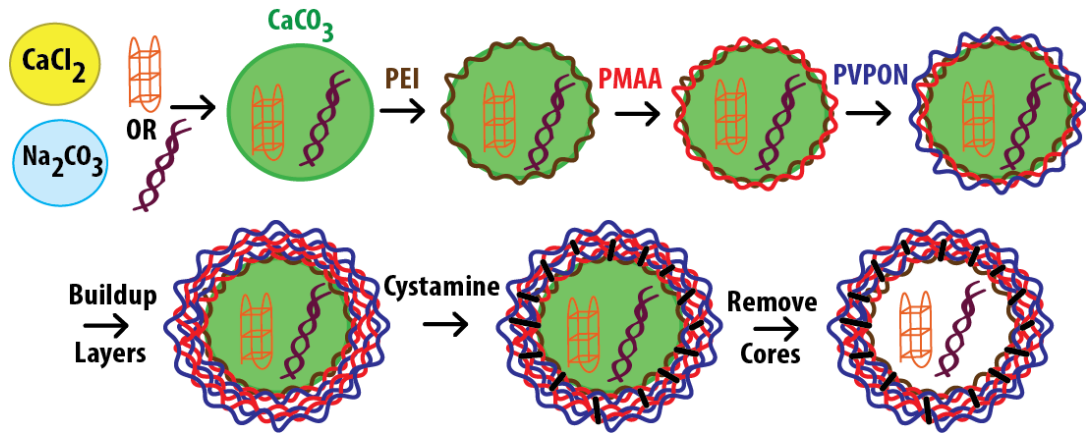


Figure 1. (PMAA/PVPON) $_n$ multilayers were formed on spherical CaCO_3 cores using hydrogen-bonded layer-by-layer assembly. PMAA strands were crosslinked using cystamine and then the cores were dissolved to form capsules.

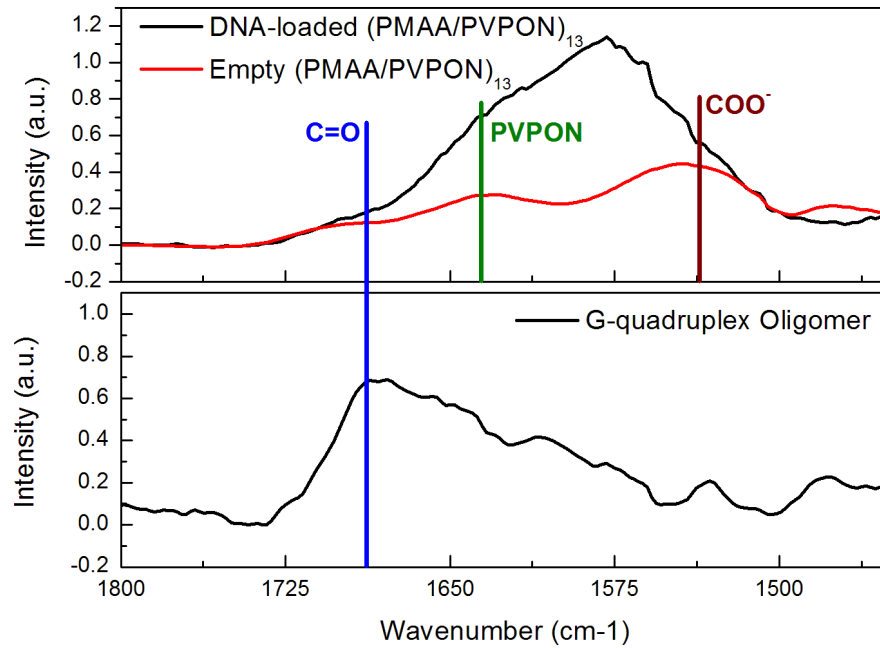


Figure 2. FTIR confirmation of two-component (PMAA/PVPON)₁₃ hydrogel capsules. FTIR was run on empty (PMAA/PVPON)₁₃ capsules (red line), G-quadruplex loaded (PMAA/PVPON)₁₃ capsules (black line), and on G-quadruplex forming oligonucleotides (blue line) at pH 7.5 as shown above. Peaks centered around 1550 cm⁻¹ and 1660 cm⁻¹ indicate the presence of both PMAA and PVPON, respectively.

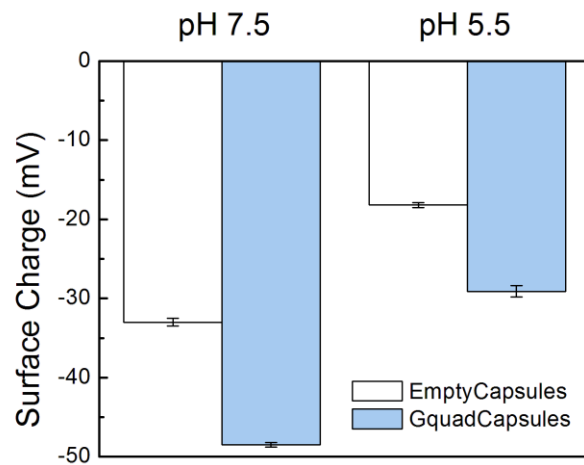
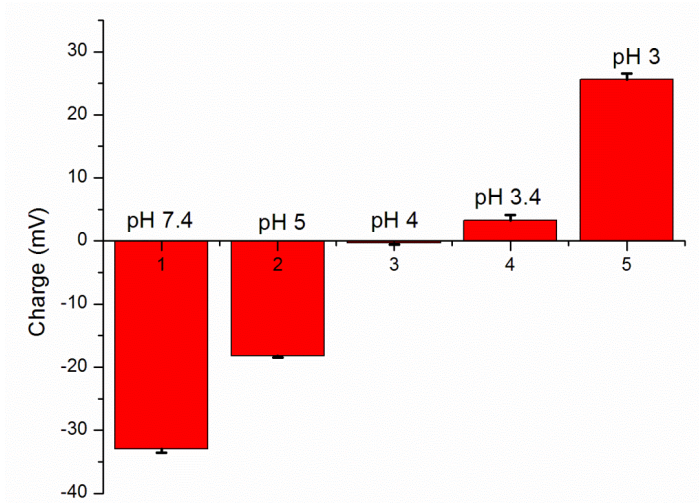


Figure 3. Relationship between the pH and surface charge of the (PMAA/PVPON)13 capsules.

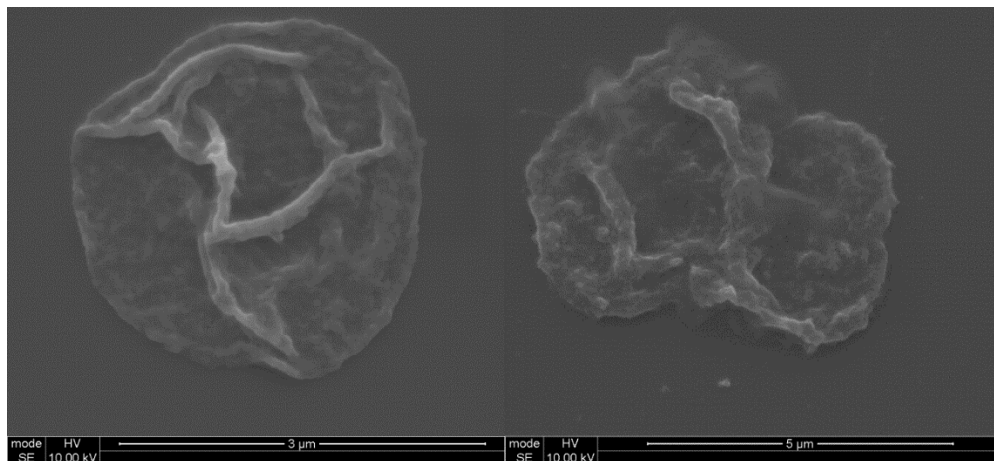


Figure 4. Scanning electron microscopy of (PMAA/PVPON)_n capsules loaded with G-quadruplex DNA (a) and dsDNA (b).

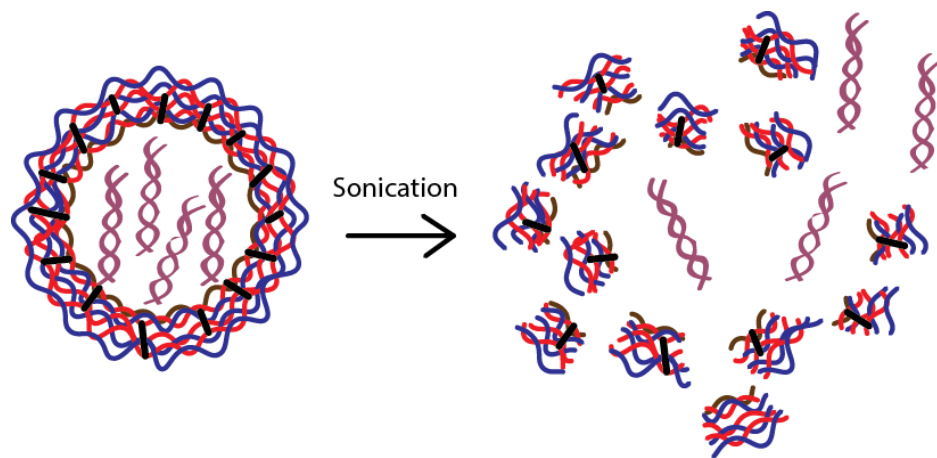


Figure 5. Cargo release schematic. (PMAA/PVPON)_n capsules can release their cargo by either sonication or GSH enzymatic degradation as indicated above.

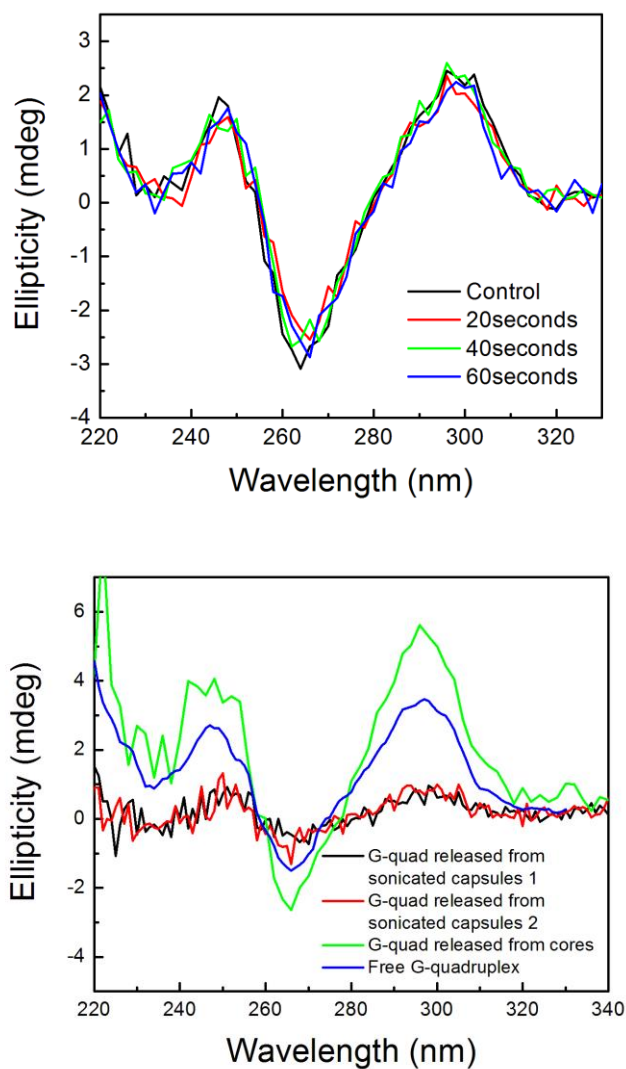


Figure 6. Confirmation of G-quadruplex structure. G-quadruplex forming oligonucleotides were exposed to ultrasound waves and then analyzed using circular dichroism spectroscopy for the retention of its secondary structure. G-quadruplex samples were exposed to the ultrasound waves for various times as indicated above. After 1 minute of exposure, the oligonucleotide continued to show characteristic peaks for a G-quadruplex secondary structure.

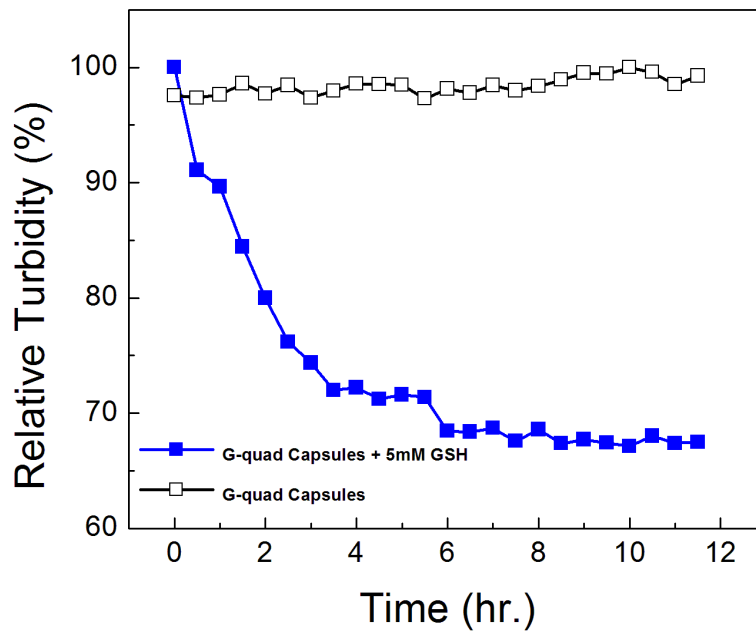


Figure 7. Reduced glutathione (GSH) was used to cleave the disulfide bonds that cross-link the PMAA strands of the capsule shell. Capsules loaded with G-quadruplex DNA were added to 5mM GSH and the turbidity of the solution was monitored at 700 nm using a Varian Cary Fluorometer. As the crosslinks between the PMAA strands degrade, the capsules fall apart and the turbidity of the solution decreases. The capsules loaded with G-quadruplex DNA decreased in turbidity by 30% over a time frame of 8 hours.

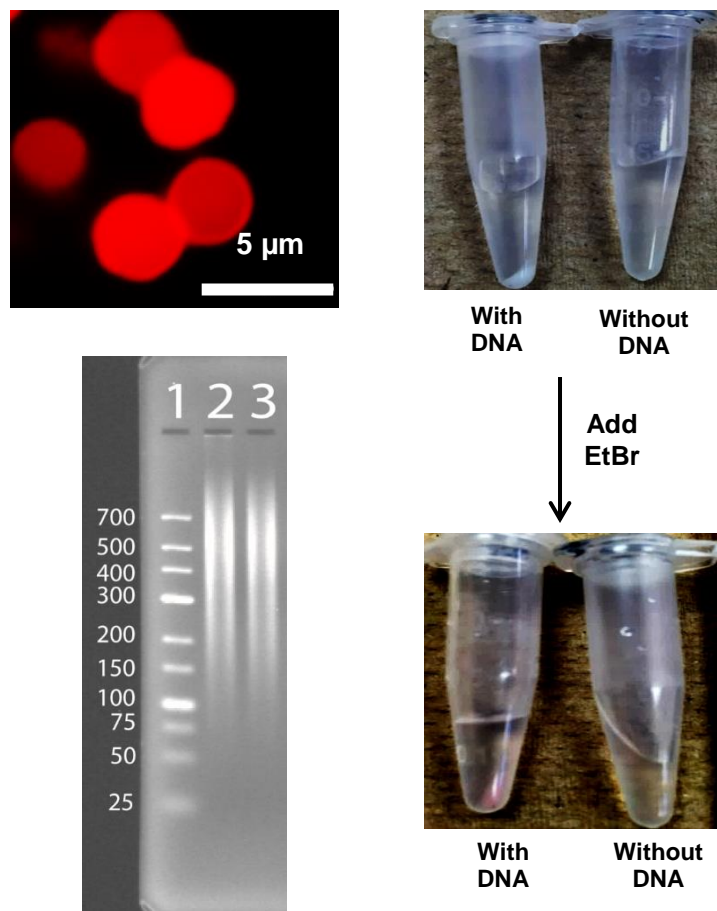


Figure 8. Optimization of capsule synthesis. (a-c) ctDNA-loaded (PMAA/PVPON)13 capsules at pH 7.5 with changes to the cross-linking density or core dissolution step. (a) Capsules cross-linked for 24 hours and cores dissolved in 0.1M EDTA at pH 7.5. (b) Capsules cross-linked for 48 hours and were dissolved in 0.1M EDTA at pH 7.5. (c) Capsules cross-linked for 48 hours and cores dissolved in 0.1M EDTA at pH 5.0. (d) The percentage of DNA-loaded capsules increases with changes to the capsule synthesis as indicated by panels (a-c). Images in (e) and (f) show of capsules as prepared in (c) at pH 7.5 and 5.5, respectively.

Table 1. Relationship between encapsulation efficiency and number of bilayers.

Number of Bilayers	Moles G-quad/ Capsule	Capsule size at pH 7.4 (Volume)	[G-quad]/ Capsule
10	6.26E-18	2.5 ± 0.4um (6.54E-14L)	96 μM
13	6.52E-18 ± 3.9E-19	2.5 ± 0.4um (6.54E-14L)	100 ± 6 μM
16	6.47E-18 ± 8.6E-20	2.7 ± 0.4um (8.24E-14L)	86 ± 4 μM

REFERENCES

- (1) Breslauer, Kenneth J., et al. Predicting DNA Duplex Stability From the Base Sequence. *Proc. Natl. Acad. Sci. U.S.A.* **1986**, *83* (11), 3746-3750.
- (2) Rich, A.; Zhang, S. Z-DNA: The Long Road to Biological Function. *Nat. Rev. Genet.* **2003**, *4* (7) 566.
- (3) Lu, C.-H.; Willner, B.; Willner, I. DNA Nanotechnology: From Sensing and DNA Machines to Drug-Delivery Systems. *ACS Nano* **2013**, *7* (10), 8320-8332.
- (4) Ivanov, A. P.; Actis, P.; Jönsson, P.; Klenerman, D.; Korchev, Y.; Edel, J. B. On-Demand Delivery of Single DNA Molecules Using Nanopipets. *ACS Nano* **2015**, *9* (4), 3587-3595.
- (5) Anderson, D. G. Polymeric Materials for Gene Delivery and DNA Vaccination. *Advanced Materials* **2009**, *21* (8), 847-867.
- (6) Bauhuber, S.; Hozsa, C.; Breunig, M.; Göpferich, A. Delivery of Nucleic Acids Via Disulfide- Based Carrier Systems. *Adv. Mater.* **2009**, *21*, 3286-3306.
- (7) Mastorakos, P.; Da Silva, A. L.; Chisholm, J.; Song, E.; Choi, W. K.; Boyle, M. P.; Morales, M. M.; Hanes, J.; Suk, J. S. Highly Compacted Biodegradable DNA Nanoparticles Capable of Overcoming the Mucus Barrier for Inhaled Lung Gene Therapy. *Proc. Natl. Acad. Sci. U.S.A.* **2015**, *112* (28), 8720-8725.
- (8) Alton, E. W. F. W.; Armstrong, D. K.; Ashby, D.; Wolstenholme-Hogg, P.; et al. Repeated Nebulisation of Non-Viral Gene Therapy in Patients with Cystic Fibrosis: A Randomised, Double-Blind, Placebo-Controlled, Phase 2b Trial. *Lancet Respir. Med.* **2015**, *3* (9), 684-691.
- (9) Herweijer, H.; Wolff, J. A. Progress and Prospects: Naked DNA Gene Transfer and Therapy. *Gene Ther.* **2003**, *10* (6), 453.
- (10) Wang, W.; Balk, M.; Deng, Z.; Wischke, C.; Gossen, M.; Behl, M.; Ma, N.; Lendlein, A., Engineering Biodegradable Micelles of Polyethylenimine-Based Amphiphilic Block Copolymers for Efficient DNA and siRNA Delivery. *J. Controlled Release* **2016**, *242*, 71-79.
- (11) Beavers, K. R.; Werfel, T. A.; Shen, T.; Kavanaugh, T. E.; Kilchrist, K. V.; Mares, J. W.; Fain, J. S.; Wiese, C. B.; Vickers, K. C.; Weiss, S. M. Porous Silicon and Polymer Nanocomposites for Delivery of Peptide Nucleic Acids as Anti- MicroRNA Therapies. *Adv. Mater.* **2016**, *28* (36), 7984-7992.

- (12) Lambrecht, L.; Lopes, A.; Kos, S.; Sersa, G.; Pr eat, V.; Vandermeulen, G. Clinical Potential of Electroporation for Gene Therapy and DNA Vaccine Delivery. *Expert Opin. Drug Delivery* **2016**, *13* (2), 295-310.
- (13) Molla, M. R.; Levkin, P. A. Combinatorial Approach to Nanoarchitectonics for Nonviral Delivery of Nucleic Acids. *Adv. Mater.* **2016**, *28* (6), 1159-1175.
- (14) Lehto, T.; Ezzat, K.; Wood, M. J.; Andaloussi, S. E. Peptides for nucleic acid delivery. *Advanced Drug Delivery Reviews* **2016**, *106*, 172-182.
- (15) Luo, D.; Saltzman, W. M. Synthetic DNA delivery systems. *Nat. Biotech.* **2000**, *18* (1), 33-37.
- (16) Molla, M. R.; Levkin, P. A. Combinatorial Approach to Nanoarchitectonics for Nonviral Delivery of Nucleic Acids. *Adv. Mater.* **2016**, *28* (6), 1159-1175.
- (17) Keeney, M.; Ong, S.-G.; Padilla, A.; Yao, Z.; Goodman, S.; Wu, J. C.; Yang, F. Development of Poly(β -Amino Ester)-Based Biodegradable Nanoparticles for Nonviral Delivery of Minicircle DNA. *ACS Nano* **2013**, *7* (8), 7241-7250.
- (18) Richardson, J. J.; Choy, M. Y.; Guo, J.; Liang, K.; Alt, K.; Ping, Y.; Cui, J.; Law, L. S.; Hagemeyer, C. E.; Caruso, F. Polymer Capsules for Plaque-Targeted In Vivo Delivery. *Adv. Mater.* **2016**, *28* (35), 7703-7707.
- (19) Richardson, J. J.; Choy, M. Y.; Guo, J.; Liang, K.; Alt, K.; Ping, Y.; Cui, J.; Law, L. S.; Hagemeyer, C. E.; Caruso, F. Polymer Capsules for Plaque-Targeted In Vivo Delivery. *Adv. Mater.* **2016**, *28* (35), 7703-7707.
- (20) Kozlovskaya, V.; Higgins, W.; Chen, J.; Kharlampieva, E. Switching Shape of Layer-by-Layer Hydrogel Microcontainers. *Chem. Commun.* **2011**, *47* (29), 8352-8354.
- (21) Chen, J.; Kozlovskaya, V.; Goins, A.; Campos-Gomez, J.; Saeed, M.; Kharlampieva, E. Biocompatible Shaped Particles from Dried Multilayer Polymer Capsules. *Biomacromolecules* **2013**, *14* (11), 3830-3841.
- (22) Cavalieri, F.; Postma, A.; Lee, L.; Caruso, F. Assembly and Functionalization of DNA-Polymer Microcapsules. *ACS Nano* **2009**, *3* (1), 234-240.
- (23) Kakade, S.; Manickam, D. S.; Handa, H.; Mao, G.; Oupick y, D., Transfection Activity of Layer-by-Layer Plasmid DNA/Poly(Ethylenimine) Films Deposited on PLGA Microparticles. *Int. J. Pharm.* **2009**, *365* (1), 44-52.
- (24) Shchukin, D. G.; Patel, A. A.; Sukhorukov, G. B.; Lvov, Y. M. Nanoassembly of Biodegradable Microcapsules for DNA Encasing. *J. Am. Chem. Soc.* **2004**, *126* (11), 3374-3375.

- (25) Zelikin, A. N.; Li, Q.; Caruso, F. Degradable Polyelectrolyte Capsules Filled with Oligonucleotide Sequences. *Angew. Chem.* **2006**, *45* (46), 7743-7745.
- (26) Ng, S. L.; Such, G. K.; Johnston, A. P.; Antequera-García, G.; Caruso, F. Controlled Release of DNA from Poly(Vinylpyrrolidone) Capsules Using Cleavable Linkers. *Biomaterials* **2011**, *32* (26), 6277-6284.
- (27) Borodina, T.; Markvicheva, E.; Kunizhev, S.; Möhwald, H.; Sukhorukov, G. B.; Kreft, O. Controlled Release of DNA from Self-Degrading Microcapsules. *Macromol. Rapid Commun.* **2007**, *28* (18-19), 1894-1899.
- (28) Chen, J.; Kozlovskaya, V.; Zavgorodnya, O.; Hasan, M. B.; Kharlampieva, E. Entrapment of Various Hydrophilic Molecules into Two Component Hydrogel Capsules. **2017**, *In preparation*.
- (29) Xue, B.; Kozlovskaya, V.; Liu, F.; Chen, J.; Williams, J. F.; Campos-Gomez, J.; Saeed, M.; Kharlampieva, E. Intracellular degradable hydrogel cubes and spheres for anti-cancer drug delivery. *ACS Appl. Mater. Interfaces* **2015**, *7* (24), 13633-13644.
- (30) Hynynen, K. Ultrasound for drug and gene delivery to the brain. *Adv. Drug Deliv. Rev.* **2008**, *60* (10), 1209-1217.
- (31) Lawrie, A.; Brisken, A.; Francis, S.; Cumberland, D.; Crossman, D.; Newman, C. Microbubble-enhanced ultrasound for vascular gene delivery. *Gene Ther.* **2000**, *7* (23), 2023-2027.
- (32) Kozlovskaya, V., Wang, Y., Higgins, W., Chen, J., Chen, Y., & Kharlampieva, E. pH-triggered shape response of cubical ultrathin hydrogel capsules. *Soft Matter* **2012**, *8*, 9828-9839.
- (33) Kozlovskaya, V.; Alexander, J.; Wang, Y.; Kunczewicz, T.; Liu, X.; Godin, B.; Kharlampieva, E. Internalization of Red Blood Cell-mimicking Hydrogel Capsules with pH-triggered Shape Responses. *ACS Nano* **2014**, *8* (6), 5725-5737.
- (34) Kozlovskaya, V.; Chen, J.; Tedjo, C.; Liang, X.; Campos-Gomez, J.; Oh, J.; Saeed, M.; Lungu, C. T.; Kharlampieva, E. pH-Responsive Hydrogel Cubes for Release of Doxorubicin in Cancer Cells. *J. Mater. Chem. B* **2014**, *2*, 2494-2507.
- (35) Biffi, G.; Tannahill, D.; McCafferty, J.; Balasubramanian, S. Quantitative visualization of DNA G-quadruplex structures in human cells. *Nat. Chem.* **2013**, *5*, 182-186.
- (36) Maizels N, Gray LT (2013) The G4 Genome. *PLoS Genet* 9(4): e1003468.
- (37) Rhodes, D.; Lipps, H. J. G-quadruplexes and their regulatory roles in biology, *Nucleic Acids Res.* **2015**, *43* (18), 8627-8637.

- (38) Macaya, R. F.; et al. Thrombin-binding DNA aptamer forms a unimolecular quadruplex structure in solution. *Proc. Natl. Acad. Sci.* **1993**, *90* (8), 3745-3749.
- (39) Tombelli, S.; Minunni, M.; Mascini, M. Analytical applications of aptamers. *Biosens. Bioelectron.* **2005**, *20* (12), 2424-2434.
- (40) Kozlovskaya, V.; Zavgorodnya, O.; Ankner, J. F.; Kharlampieva, E. Controlling internal organization of multilayer poly(methacrylic acid) hydrogels with polymer molecular weight. *Macromolecules* **2015**, *48* (23), 8585-8593.
- (41) Kharlampieva, E.; Ankner, J.F.; Rubinstein, M.; Sukhishvili, S. A. *Phys. Rev. Lett.* **2008**, *100* (12), 128303.
- (42) Bloomfield, V. A. DNA condensation by multivalent cations. *Biopolymers* **1997**, *44*, 269–282.
- (43) Verdolino, V.; Cammi, R.; Munk, B. H.; Schlegel, H. B. Calculation of pKa Values of Nucleobases and the Guanine Oxidation Products Guanidinohydantoin and Spiroiminodihydantoin using Density Functional Theory and a Polarizable Continuum Model. *J. Phys. Chem. B* **2008**, *112* (51), 16860-16873.
- (44) Chen, J.; Ratnayaka, S.; Alford, A.; Kozlovskaya, V.; Liu, F.; Xue, B.; Hoyt, K.; Kharlampieva, E. Theranostic multilayer capsules for ultrasound imaging and guided drug delivery. *ACS Nano* **2017**, *11*, 3135-3146.
- (45) Zelikin, A. N.; Becker, A. L.; Johnston, A. P. R.; Wark, K. L.; Turatti, F.; Caruso, F. A General Approach for DNA Encapsulation in Degradable Polymer Microcapsules. *ACS Nano* **2007**, *1* (1), 63-69.
- (46) Kypr, J.; Kejnovská, I.; Renčiuk, D.; Vorlíčková, M. Circular dichroism and conformational polymorphism of DNA, *Nucleic Acids Res.* **2009**, *37* (6), 1713–1725.
- (47) Zhao, H.; Shen, K. G-quadruplex DNA-based asymmetric catalysis of michael addition: Effects of sonication, ligands, and co-solvents. *Biotech. Progress* **2016**, *32*, 891–898.
- (48) Xue, B.; Wang, W.; Qin, J. J.; Nijampatnam, B.; Murugesan, S.; Kozlovskaya, V.; Zhang, R.; Velu, S. E.; Kharlampieva, E. Highly efficient delivery of potent anti-cancer iminoquinone derivative by multilayer hydrogel cubes. *Acta Biomater.* **2017**, *58*, 386-398.
- (49) Jones, D. P.; Carlson, J. L.; Mody, V. C.; Cai, J.; Lynn, M. J.; Sternberg, P. Redox state of glutathione in human plasma. *Free Radic. Biol. Med.* **2000**, *28* (4), 625-635.
- (50) Meister, A., & Anderson, M. E. Glutathione. *Annu. Rev. Biochem.* **1983**, *52*, 711-760.

- (51) Lepecq, J.; Paoletti, C. A fluorescent complex between ethidium bromide and nucleic acids. *J. Mol. Bio.* **1967**, 27 (1), 87-106.
- (52) Zelikin, A. N.; Li, Q.; Caruso, F. Degradable Polyelectrolyte Capsules Filled with Oligonucleotide Sequences. *Angew. Chemie.* **2006**, 118, 7907–7909.
- (53) DeGeest, B. G.; Skirtach, A. G.; Mamedov, A. A.; Antipov, A. A.; Kotov, N. A.; DeSmedt, S. C.; Sukhorukov, G. B. Ultrasound-Triggered Release from Multilayered Capsules. *Small* **2007**, 3, 804–808.
- (54) Reichmann, M. E., et al. A further examination of the molecular weight and size of desoxyntose nucleic acid. *J. Amer. Chem. Soc.* **1954**, 76 (11), 3047-3053.
- (55) Sutherland, J. C.; Lin, B.; Monteleone, D. C.; Mugavero, J.; Sutherland, B. M.; Trunk, J. Electronic imaging system for direct and rapid quantitation of fluorescence from electrophoretic gels: Application to ethidium bromide-stained DNA. *Anal. Biochem.* **1987**, 163 (2), 446-457.

CHAPTER 5

CONCLUSIONS AND OUTLOOK

Conclusions

In this work, the thermal stability and the energetics of unfolding of synthetic G-quadruplex forming deoxyoligonucleotides of the human telomeric sequence were studied, specifically as a function of the influence of the adenine bases in the loop sequence. The wild-type sequence of this G-quadruplex structure was then encapsulated by two-component PMAA/PVPON microcapsules prepared by LbL techniques. Release of the DNA cargo was then studied using therapeutic levels of ultrasound or GSH enzymatic degradation. The encapsulation of double stranded ctDNA was also performed in this work to test the ability of this system to be applied to multiple types of DNA drugs. The conclusions from these experiments are summarized below.

In Chapter 3, a set of synthetic deoxyoligonucleotides of the human telomeric sequence were purchased with systematic mutations of a single adenine, or multiple adenines, within the loop sequence region to thymine. CD spectra were used to probe the secondary structure of each sequence and it was found that all sequences could fold into a G-quadruplex structure. CD melting profiles were then collected to determine the thermal stability of each sequence relative to the wildtype sequence. It was shown that most loop mutants exhibited lower melting temperatures relative to the wildtype sequence except for the loop 2 single mutant, which displayed a slightly increased melting temperature. The energetics associated with the unfolding of each sequence were then monitored by DSC. Results from these studies showed that melting thermograms for the wild-type

human telomeric G-quadruplex sequence, as well as the single loop mutants, were biphasic in nature, indicating the presence of an unfolding intermediate. As the number of modified loops increased to two or more, the thermograms were fit by a single monophasic curve, however these curves could not be fit by a simple two-state transition either. The enthalpies associated with the unfolding of each sequence were found to decrease as the number of adenine to thymine mutations increased which confirmed the correlating decrease in thermal stability as observed by CD melting profiles. The possibilities of intermediates along the unfolding transition was explored by SVD of three-dimensional CD data (wavelength, ellipticity, and temperature). Results from deconvolution of this data are consistent with the presence of intermediates during the unfolding for the wild-type G-quadruplex as well as the loop modified G-quadruplexes. When taking this data together, it was concluded that stacking of adenine bases contributes to the overall stability of the G-quadruplex structure.

In Chapter 4, the wildtype G-quadruplex sequence was encapsulated by two-component PMAA/PVPON microcapsules and then release was explored using either therapeutic ultrasound or GSH enzymatic degradation of the cystamine crosslinker. Characterization of the capsules using FTIR confirmed the presence of both PMAA and PVPON within the microcapsule. Measurement of the Zeta-potential as a function of pH was collected to estimate the effective surface charge of the microparticles. Results from these studies showed that the effective surface charge on the capsules was positive at pH values less than 5 and negative at pH values greater than 5, consistent with the protonation and ionization of the carboxylic acid groups on PMAA, respectively. At pH values of 5, the capsules were neutral in effective surface charge. Due to the increase in magnitude of the Zeta-charge of G-quadruplex loaded microcapsules over empty microcap-

sules, it was concluded that the stability of the capsules is increased by the presence of G-quadruplex deoxyoligonucleotides within the capsule interior and the capsule shell.

When using GSH enzymatic degradation of the disulfide bonds in cystamine to release the cargo, it was shown that the capsules were not able to be degraded by intracellular concentrations of GSH (1-10 mM) and the DNA was unable to be released from the microcapsules. The release of the DNA cargo was then studied by applying therapeutic ultrasound to the capsules at a strength of 57 W/cm^2 for 20 seconds. Assuming complete release of cargo by this release method, it was found that $6.52 \times 10^{-18} \pm 3.9 \times 10^{-19}$ moles of G-quadruplex were released per capsule with 13 bilayers of PMAA/PVPON.

Outlook

The completion of this work contributes to the advancement of DNA drug delivery with the successful creation of two-component PMAA/PVPON microcapsules that can deliver DNA cargo through controlled release methods. This methodology can be easily refined for applications that require other types of nucleic acids or those that require the specificity of in vivo targeting. For example, the versatility of this system was shown through the encapsulation of both G-quadruplex and double stranded DNA structures. Encapsulation of RNA and other types of nucleic acid hybrids would further expand the applications of this capsule system. In addition, modification of the polymer side chains to include more functional groups or to introduce a targeting moiety before polymer deposition would allow the microcapsules to increase their specificity and delivery abilities. Another avenue for this project could be the synthesis of nucleic acids within the microcapsules. The ability to synthesize nucleic acids within the microcapsules increases the amount of cargo that can be delivered. Studies on these capsules can then

be completed to determine how effectively they are able to deliver DNA to the nucleus of cells at a therapeutic level.

GENERAL REFERENCES

- 1) Mendel, G. (1866). Experiments in Plant Hybridization. *Read at the February 8th, and March 8th, 1865, meetings of the Briinn Natural History Society.*
- 2) Avery, O. T., Macleod, C. M., & McCarty, M. (1944). Studies on the Chemical Nature of the Substance Inducing Transformation of Pneumococcal Types. *The Journal of Exp. Medicine.* 79(2), 137-159.
- 3) Garrod, A. (1902). The Incidence of Alkaptonuria: A Study in Chemical Individuality. *The Lancet*, 160(4137), 1616-1620.
- 4) Bernfield, M. R., & Nirenberg, M. W. (1965). RNA Codewords and Protein Synthesis: The Nucleotide Sequences of Multiple Codewords for Phenylalanine, Serine, Leucine, and Proline. *Science*, 147(3657), 479-484.
- 5) Ulmer, J., Donnelly, J., Parker, S., Rhodes, G., Felgner, P., Dwarki, V., Et, A. (1993). Heterologous protection against influenza by injection of DNA encoding a viral protein. *Science*, 259(5102), 1745-1749.
- 6) Luo, D., & Saltzman, W. M. (2000). Synthetic DNA delivery systems. *Nature Biotechnology*, 18, 33-37.
- 7) Phillips, A. J. (2001). The challenge of gene therapy and DNA delivery. *The Journal of Pharmacy and Pharmacology*, 53, 1169-1174.
- 8) Patil, S. D., Rhodes, D. G., & Burgess, D. J. (2005). DNA-based therapeutics and DNA delivery systems: A comprehensive review. *The AAPS Journal*, 7(1), E61-E77.

- 9) Opalinska, J. B., Gewirtz, A. M. (2002). Nucleic-acid therapeutics: basic principles and recent applications. *Nature Reviews Drug Discovery*, 1, 503-514.
- 10) Rimmele, M. (2003). Nucleic Acid Aptamers as Tools and Drugs: Recent Developments. *ChemBioChem*, 4(10), 963-971.
- 11) Lipfert, J., Doniach, S., Das, R., & Herschlag, D. (2014). Understanding Nucleic Acid–Ion Interactions. *Ann. Rev. Biochem.* 83, 813-841.
- 12) Dahm, R. (2007). Discovering DNA: Friedrich Miescher and the early years of nucleic acid research. *Human Genetics*, 122(6), 565-581.
- 13) His W (1897a) Aus dem wissenschaftlichen Briefwechsel von F. Miescher. In: His W et al (eds) Die Histochemischen und Physiologischen Arbeiten von Friedrich Miescher, vol 1. F. C. W. Vogel, Leipzig, pp 33–138
- 14) Altmann R (1889) Ueber Nucleinsäuren. *Arch. f. Anatomie u. Physiol*:524-536.
- 14) Watson, J. D., & Crick, F. H. (1953). The Structure of DNA. *Cold Spring Harbor Symposia on Quantitative Biology*, 18(0), 123-131.
- 15) Watson, J. D., & Crick, F. H. (1953). Genetical Implications of the Structure of Deoxyribonucleic Acid. *Nature*, 171(4361), 964-967.
- 16) Watson, J. D., & Crick, F. H. (1953). Molecular Structure of Nucleic Acids: A Structure for Deoxyribose Nucleic Acid. *Nature*, 171(4356), 737-738.
- 17) Franklin, R. E., & Gosling, R. G. (1953). The structure of sodium thymonucleate fibres. I. The influence of water content. *Acta Crystallographica*, 6(8), 673-677.
- 18) Franklin, R. E., & Gosling, R. G. (1953). The structure of sodium thymonucleate fibres. II. The cylindrically symmetrical Patterson function. *Acta Crystallographica*, 6 (8), 678-685.

- 19) Franklin, R. E., & Gosling, R. G. (1953). Molecular Configuration in Sodium Thymonucleate. *Nature*, 171 (4356), 740-741.
- 20) Klug, A. (1968). Rosalind Franklin and the Discovery of the Structure of DNA. *Nature*, 219 (5156), 808-810.
- 21) Kim, S. H., Quigley, G., Suddath, F. L., Mcpherson, A., Sneden, D., Kim, J. J., Rich, A. (1972). The Three-Dimensional Structure of Yeast Phenylalanine Transfer RNA: Shape of the Molecule at 5.5-Å Resolution. *PNAS*, 69(12), 3746-3750.
- 22) Robertus, J. D., Ladner, J. E., Finch, J. T., Rhodes, D., Brown, R. S., Clark, B. F., & Klug, A. (1974). Structure of yeast phenylalanine tRNA at 3 Å resolution. *Nature*, 250 (5467), 546-551.
- 23) Stout, C., Mizuno, H., Rubin, J., Brennan, T., Rao, S., & Sundaralingam, M. (1976). Atomic coordinates and molecular conformation of yeast phenylalanyl tRNA. An independent investigation. *Nucleic Acids Res.* 3 (4), 1111-1124.
- 24) Sussman, J. L., Holbrook, S. R., Warrant, R., Church, G. M., & Kim, S. (1978). Crystal structure of yeast phenylalanine transfer RNA. *The Journal of Molecular Biology*, 123(4), 607-630.
- 25) Drew, H., Takano, T., Tanaka, S., Itakura, K., & Dickerson, R. E. (1980). High-salt d(CpGpCpG), a left-handed Z' DNA double helix. *Nature*, 286(5773), 567-573. doi:10.1038/286567a0
- 26) Dickerson, R. E., & Klug, A. (1983). Base sequence and helix structure variation in B and A DNA. *The Journal of Molecular Biology*, 166(3), 419-441. doi:10.1016/s0022-2836(83)80093-x

- 27) Dickerson, R. E., Drew, H. R., Conner, B. N., Wing, R. M., Fratini, A. V., & Kopka, M. L. (1982). The anatomy of A-, B-, and Z-DNA. *Science*, 216(4545), 475-485. doi:10.1126/science.7071593
- 28) Wahl, M. C., & Sundaralingam, M. (1997). Crystal structures of A-DNA duplexes. *Biopolymers*, 44(1), 45-63. doi:10.1002/(sici)1097-0282(1997)44:1<45::aid-bip4>3.0.co;2-#
- 29) Haniford, D. B.; Pulleyblank, D. E. (1983). The In-Vivo Occurrence of Z DNA. *J Biomolecular Structure Dyn.* 1(3), 593-609.
doi:10.1080/07391102.1983.10507467
- 30) Yakovchuk, P. (2006). Base-stacking and base-pairing contributions into thermal stability of the DNA double helix. *Nucleic Acids Research*, 34(2), 564-574.
doi:10.1093/nar/gkj454
- 31) Šponer, J., Leszczynski, J., & Hobza, P. (2001). Electronic properties, hydrogen bonding, stacking, and cation binding of DNA and RNA bases. *Biopolymers*, 61(1), 3-31.
- 32) Hunter, C. A. (1993). Sequence-dependent DNA structure: the role of base stacking interactions. *Journal of Molecular Biology* 230(3), 1025-1054.
- 33) Rachofsky, E. L., Osman, R., & Ross, J. A. (2001). Probing structure and dynamics of DNA with 2-aminopurine: effects of local environment on fluorescence. *Biochemistry*, 40(4), 946-956.
- 34) Gervasio, F. L., Carloni, P., & Parrinello, M. (2002). Electronic structure of wet DNA. *Physical Review Letters*, 89(10), 108102.
- 35) Freier, S. M., Albergo, D. D., & Turner, D. H. (1983). Solvent effects on the dynamics of (dG-dC)₃. *Biopolymers*, 22(4), 1107-1131. doi:10.1002/bip.360220408

- 36) Feig, M., & Pettitt, B. M. (1999). Sodium and Chlorine Ions as Part of the DNA Solvation Shell. *Biophysical Journal*, 77(4), 1769-1781. doi:10.1016/s0006-3495(99)77023-2
- 37) Feig, M., & Pettitt, B. M. (1999). Sodium and chlorine ions as part of the DNA solvation shell. *Biophysical Journal*, 77(4), 1769-1781.
- 38) Horne, D. A., & Dervan, P. B. (1990). Recognition of mixed-sequence duplex DNA by alternate-strand triple-helix formation. *Journal of the American Chemical Society*, 112(6), 2435-2437. doi:10.1021/ja00162a063
- 39) Hare, D. R., & Reid, B. R. (1986). Three-dimensional structure of a DNA hairpin in solution: two-dimensional NMR studies and distance geometry calculations on d(CGCGTTTTTCGCG). *Biochemistry*, 25(18), 5341-5350. doi:10.1021/bi00366a053
- 40) Mizuuchi, K., Mizuuchi, M., & Gellert, M. (1982). Cruciform structures in palindromic DNA are favored by DNA supercoiling. *Journal of Molecular Biology*, 156(2), 229-243. doi:10.1016/0022-2836(82)90325-4
- 41) Gellert, M., Lipsett, M. N., & Davies, D. R. (1962). Helix Formation by Guanylic Acid. *Proceedings of the National Academy of Sciences of the United States of America*, 48(12), 2013–2018.
- 42) Phan, A. T., Modi, Y. S., & Patel, D. J. (2004). Propeller-type parallel-stranded G-quadruplexes in the human c-myc promoter. *Journal of the American Chemical Society*, 126(28), 8710.
- 43) Dai, J., Dexheimer, T. S., Chen, D., Carver, M., Ambrus, A., Jones, R. A., & Yang, D. (2006). An intramolecular G-quadruplex structure with mixed paral-

- lel/antiparallel G-strands formed in the human BCL-2 promoter region in solution. *Journal of the American Chemical Society*, 128(4), 1096.
- 44) Biffi, G., Tannahill, D., McCafferty, J., & Balasubramanian, S. (2013). Quantitative visualization of DNA G-quadruplex structures in human cells. *Nature Chemistry*, 5(3), 182-186.
- 45) Chambers, V. S., Marsico, G., Boutell, J. M., Di Antonio, M., Smith, G. P., & Balasubramanian, S. (2015). High-throughput sequencing of DNA G-quadruplex structures in the human genome. *Nature Biotechnology*, 33(8), 877-881.
- 46) Guédin, A., Gros, J., Alberti, P., & Mergny, J. L. (2010). How long is too long? Effects of loop size on G-quadruplex stability. *Nucleic Acids Research*, 38(21), 7858-7868.
- 47) Miller, M. C., Buscaglia, R., Chaires, J. B., Lane, A. N., & Trent, J. O. (2010). Hydration is a major determinant of the G-quadruplex stability and conformation of the human telomere 3' sequence of d (AG₃ (TTAG₃)₃). *Journal of the American Chemical Society*, 132(48), 17105-17107.
- 48) Lane, A. N., Chaires, J. B., Gray, R. D., & Trent, J. O. (2008). Stability and kinetics of G-quadruplex structures. *Nucleic Acids Research*, 36(17), 5482-5515.
- 49) Gu, J., Leszczynski, J., & Bansal, M. (1999). A new insight into the structure and stability of Hoogsteen hydrogen-bonded G-tetrad: an ab initio SCF study. *Chemical Physics Letters*, 311(3), 209-214.
- 50) Antonacci, C., Chaires, J. B., & Sheardy, R. D. (2007). Biophysical Characterization of the Human Telomeric Repeat (TTAGGG)₄ in Potassium Solution. *Biochemistry*. 46, 4654-4660.

- 51) Sundquist, W. I., & Klug, A. (1989). Telomeric DNA dimerizes by formation of guanine tetrads between hairpin loops. *Nature*, 342(6251), 825-829.
- 52) Laughlan, G., Murchie, A. I., Norman, D. G., Moore, M. H., Moody, P. C., Lilley, D. M., & Luisi, B. (1994). The high-resolution crystal structure of a parallel-stranded guanine tetraplex. *Science*, 520-524.
- 53) Balagurumoorthy, P., Brahmachari, S. K., Mohanty, D., Bansal, M., & Sassisekharan, V. (1992). Hairpin and Parallel Quartet Structure for Telomeric Sequences. *Nucleic Acids Research*. 20, 4061-4067.
- 54) Smargiasso, N., Rosu, F., Hsia, W., Colson, P., Baker, E. S., Bowers, M. T., ... & Gabelica, V. (2008). G-quadruplex DNA assemblies: loop length, cation identity, and multimer formation. *Journal of the American Chemical Society*, 130(31), 10208-10216.
- 55) Deng, H., & Braunlin, W. H. (1996). Kinetics of sodium ion binding to DNA quadruplexes. *Journal of Molecular Biology*, 255(3), 476-483.
- 56) Dai, T., Marotta, S. P., & Sheardy, R. D. (1995) Self-Assembly of DNA Oligomers into High Molecular Weight Species. *Biochemistry*. 34, 3655-3662.
- 57) Venczel, E. A., & Sen, D. (1993) Parallel and Antiparallel G-DNA Structures from a Complex Telomeric Sequence. *Biochemistry*. 32, 6220-6228.
- 58) Schultze, P., Hud, N. V., Smith, F. W., & Feigon, J. (1999). The effect of sodium, potassium and ammonium ions on the conformation of the dimeric quadruplex formed by the *Oxytricha nova* telomere repeat oligonucleotide d(G₄T₄G₄). *Nucleic acids research*, 27(15), 3018-3028.
- 59) Parkinson, G. N., Lee, M. P. H., & Neidle, S. (2002). Crystal Structure of Parallel Quadruplexes from Human Telomeric DNA. *Nature*. 417, 876-880.

- 60) Ambrus, A., Chen, D., Dai, J., Bialis, T., Jones, R. A., & Yang, D. (2006). Human telomeric sequence forms a hybrid-type intramolecular G-quadruplex structure with mixed parallel/antiparallel strands in potassium solution. *Nucleic Acids Research*, 34(9), 2723-2735.
- 61) Williamson, J. R. (1994) G – Quartet Structure on Telomeric DNA. *Annual Reviews of Biophysics and Biomolecular Structure*. Ed. Stroud, R. M., C. R. Cantor, and T. D. Pollard. Palo Alto: Annual Reviews, Inc.
- 62) Balagurumoorthy, P. & Brahmachari, S. K. (1994). The Structure and Stability of Human Telomeric Sequence. *Journal of Biological Chemistry*, 269, 21858-21869.
- 63) Olsen, C. M., Gmeiner, C., & Marky, L. A. (2006). Unfolding of G – Quadruplexes: Energetic, Ion and Water Contributions of G – Quartet Stacking. *Journal of Physical Chemistry B*. 110, 6962-69.
- 64) Wang, Y. & Patel, J. D. (1993) Solution Structure of the Human Telomeric Repeat d[AG₃(T₂AG₃)₃] G – Tetraplex. *Structure*. 1, 263-282.
- 65) Cang, X., Šponer, J., & Cheatham III, T. E. (2011). Explaining the varied glycosidic conformational, G-tract length and sequence preferences for anti-parallel G-quadruplexes. *Nucleic Acids Research*, 39(10), 4499-4512.
- 66) Burge, S., Parkinson, G. N., Hazel, P., Todd, A. K., & Neidle, S. (2006). Quadruplex DNA: sequence, topology and structure. *Nucleic Acids Research*, 34(19), 5402-5415.
- 67) Levy, M. Z., Allsopp, R. C., Futcher, A. B., Greider, C. W., & Harley, C. B. (1992). Telomere end-replication problem and cell aging. *Journal of Molecular Biology*, 225(4), 951-960.

- 68) Lundblad, V. (1997). The end replication problem: more than one solution. *Nature Medicine*, 3(11), 1198-1199.
- 69) Harley, C. B., Futcher, A. B., & Greider, C. W. (1990). Telomeres shorten during ageing of human fibroblasts. *Nature*, 345(6274), 458-460.
- 70) Shay, J. W., & Bacchetti, S. (1997). A survey of telomerase activity in human cancer. *European Journal of Cancer*, 33(5), 787-791.
- 71) Meyerson, M., Counter, C. M., Eaton, E. N., Ellisen, L. W., Steiner, P., Caddle, S. D., ... & Bacchetti, S. (1997). hEST2, the putative human telomerase catalytic subunit gene, is up-regulated in tumor cells and during immortalization. *Cell*, 90(4), 785-795.
- 72) Sun, D., Thompson, B., Cathers, B. E., Salazar, M., Kerwin, S. M., Trent, J. O., ... & Hurley, L. H. (1997). Inhibition of human telomerase by a G-quadruplex-interactive compound. *Journal of Medicinal Chemistry*, 40(14), 2113-2116.
- 73) Kim, M. Y., Vankayalapati, H., Shin-Ya, K., Wierzba, K., & Hurley, L. H. (2002). Telomestatin, a potent telomerase inhibitor that interacts quite specifically with the human telomeric intramolecular G-quadruplex. *Journal of the American Chemical Society*, 124(10), 2098-2099.
- 74) Zamecnik, P. C., Goodchild, J., Taguchi, Y., & Sarin, P. S. (1986). Inhibition of replication and expression of human T-cell lymphotropic virus type III in cultured cells by exogenous synthetic oligonucleotides complementary to viral RNA. *Proceedings of the National Academy of Sciences*, 83(12), 4143-4146.
- 75) Van Dongen MGJ, Geerts BF, Morgan ES, Brandt TA, De Kam ML, Romijn JA, et al. (2015) First proof of pharmacology in humans of a novel glucagon receptor antisense drug. *Journal of Clinical Pharmacology*, 55(3):298–306

- 76) Warren, M. S., Hughes, S. G., Singleton, W., Yamashita, M., & Genovese, M. C. (2015). Results of a proof of concept, double-blind, randomized trial of a second generation antisense oligonucleotide targeting high-sensitivity C-reactive protein (hs-CRP) in rheumatoid arthritis. *Arthritis Research & Therapy*, 17(1), 80.
- 77) Chi, K. N., Siu, L. L., Hirte, H., Hotte, S. J., Knox, J., Kollmansberger, C., ... & Tu, D. (2008). A phase I study of OGX-011, a 2'-methoxyethyl phosphorothioate antisense to clusterin, in combination with docetaxel in patients with advanced cancer. *Clinical Cancer Research*, 14(3), 833-839.
- 78) McErlean, E. M., McCrudden, C. M., & McCarthy, H. O. (2016). Delivery of nucleic acids for cancer gene therapy: overcoming extra-and intra-cellular barriers. *Therapeutic delivery*, 7(9), 619-637.
- 79) Yu, R. Z., Grundy, J. S., & Geary, R. S. (2013). Clinical pharmacokinetics of second generation antisense oligonucleotides. *Expert opinion on drug metabolism & toxicology*, 9(2), 169-182.
- 80) Swayze, E. E., & Bhat, B. (2007). The medicinal chemistry of oligonucleotides. *Antisense Drug Technology: Principles, Strategies, and Applications*, 2.
- 81) Wang, T., Shigdar, S., Al Shamaileh, H., Gantier, M. P., Yin, W., Xiang, D., ... & Zhang, W. (2017). Challenges and opportunities for siRNA-based cancer treatment. *Cancer Letters*, 387, 77-83.
- 82) Thi, E. P., Mire, C. E., Lee, A. C., Geisbert, J. B., Zhou, J. Z., Agans, K. N., ... & MacLachlan, I. (2015). Lipid nanoparticle siRNA treatment of Ebola-virus-Makona-infected nonhuman primates. *Nature*, 521(7552), 362-365.

- 83) Martínez, Tamara, et al. (2014) In vitro and in vivo efficacy of SYL040012, a novel siRNA compound for treatment of glaucoma. *Molecular Therapy* 22(1), 81-91.
- 84) Mannironi, C., Di Nardo, A., Fruscoloni, P., & Tocchini-Valentini, G. P. (1997). In vitro selection of dopamine RNA ligands. *Biochemistry*, 36(32), 9726-9734.
- 85) Bock, L. C., Griffin, L. C., Latham, J. A., Vermaas, E. H., & Toole, J. J. (1992). Selection of single-stranded DNA molecules that bind and inhibit human thrombin. *Nature*, 355(6360), 564-566.
- 86) Fraunfelder, F. W. (2005). Pegaptanib for wet macular degeneration. *Drugs Today*, 41(11), 703-709.
- 87) Huang, Y. F., Shangguan, D., Liu, H., Phillips, J. A., Zhang, X., Chen, Y., & Tan, W. (2009). Molecular assembly of an aptamer–drug conjugate for targeted drug delivery to tumor cells. *ChemBioChem*, 10(5), 862-868.
- 88) Bioconjugates, N. A. A New Approach for Targeting Prostate Cancer Cells Farokhzad. *Omid C*, 7668-7672.
- 89) Bock, Louis C., et al. (1992). Selection of single-stranded DNA molecules that bind and inhibit human thrombin. *Nature*, 355(6360), 564-566.
- 90) Bates, Paula J., et al. (2009). Discovery and development of the G-rich oligonucleotide AS1411 as a novel treatment for cancer. *Experimental and Molecular Pathology*, 86(3), 151-164.
- 91) Macaya, Roman F., et al. (1993). Thrombin-binding DNA aptamer forms a unimolecular quadruplex structure in solution. *Proceedings of the National Academy of Sciences*, 90(8), 3745-3749.

- 92) Li, W. X., et al. (1994), A novel nucleotide-based thrombin inhibitor inhibits clot-bound thrombin and reduces arterial platelet thrombus formation. *Blood*, 83(3), 677-682.
- 93) Bates, Paula J., et al. (1999). Antiproliferative activity of G-rich oligonucleotides correlates with protein binding. *Journal of Biological Chemistry*, 274(37), 26369-26377.
- 94) Bates, Paula J., et al. (2009). Discovery and development of the G-rich oligonucleotide AS1411 as a novel treatment for cancer. *Experimental and Molecular Pathology*, 86(3), 151-164.
- 95) White, Rebekah R., Bruce A. Sullenger, and Christopher P. Rusconi. (2000). Developing aptamers into therapeutics. *Journal of Clinical Investigation* 106(8), 929.
- 96) Rosenberg, Jonathan E., et al. (2014). A phase II trial of AS1411 (a novel nucleolin-targeted DNA aptamer) in metastatic renal cell carcinoma. *Investigational New Drugs*, 32(1), 178-187.
- 97) Rosenberg, S. A., Aebersold, P., Cornetta, K., Kasid, A., Morgan, R. A., Moen, R., ... & Merino, M. J. (1990). Gene transfer into humans—immunotherapy of patients with advanced melanoma, using tumor-infiltrating lymphocytes modified by retroviral gene transduction. *New England Journal of Medicine*, 323(9), 570-578.
- 98) Yin, H., Kanasty, R. L., Eltoukhy, A. A., Vegas, A. J., Dorkin, J. R., & Anderson, D. G. (2014). Non-viral vectors for gene-based therapy. *Nature Reviews Genetics*, 15(8), 541-555.
- 99) Wasungu, L., & Hoekstra, D. (2006). Cationic lipids, lipoplexes and intracellular delivery of genes. *Journal of Controlled Release*, 116(2), 255-264.

- 100) Yang, B., Ming, X., Cao, C., Laing, B., Yuan, A., Porter, M. A., ... & Juliano, R. L. (2015). High-throughput screening identifies small molecules that enhance the pharmacological effects of oligonucleotides. *Nucleic Acids Research*, 43(4), 1987-1996.
- 101) Lungwitz, U., Breunig, M., Blunk, T., & Göpferich, A. (2005). Polyethylenimine-based non-viral gene delivery systems. *European Journal of Pharmaceutics and Biopharmaceutics*, 60(2), 247-266.
- 102) Tinsley-Bown, A. M., Fretwell, R., Dowsett, A. B., Davis, S. L., & Farrar, G. H. (2000). Formulation of poly (D, L-lactic-co-glycolic acid) microparticles for rapid plasmid DNA delivery. *Journal of Controlled Release*, 66(2), 229-241.
- 103) Zelikin, A. N., Becker, A. L., Johnston, A. P., Wark, K. L., Turatti, F., & Caruso, F. (2007). A general approach for DNA encapsulation in degradable polymer microcapsules. *ACS Nano*, 1(1), 63-69.
- 104) Becker, A. L., Orlotti, N. I., Folini, M., Cavalieri, F., Zelikin, A. N., Johnston, A. P., ... & Caruso, F. (2011). Redox-active polymer microcapsules for the delivery of a survivin-specific siRNA in prostate cancer cells. *ACS Nano*, 5(2), 1335-1344.
- 105) Cohen, H., Levy, R. J., Gao, J., Fishbein, I., Kousaev, V., Sosnowski, S., ... & Golomb, G. (2000). Sustained delivery and expression of DNA encapsulated in polymeric nanoparticles. *Gene Therapy*, 7(22), 1896.
- 106) Iler, R. K. (1966). Multilayers of colloidal particles. *Journal of Colloid and Interface Science*, 21(6), 569-594.
- 107) Kirkland, J. J. (1965). Porous thin-layer modified glass bead supports for gas liquid chromatography. *Analytical Chemistry*, 37(12), 1458-1461.

- 108) Nicolau, Y. F. (1985). Solution deposition of thin solid compound films by a successive ionic-layer adsorption and reaction process. *Applications of Surface Science*, 22, 1061-1074.
- 110) Nicolau, Y. F., & Menard, J. C. (1988). Solution growth of ZnS, CdS and Zn_{1-x}Cd_xS thin films by the successive ionic-layer adsorption and reaction process; growth mechanism. *Journal of Crystal Growth*, 92(1-2), 128-142.
- 111) Decher, G. H. J. D., Hong, J. D., & Schmitt, J. (1992). Buildup of ultrathin multi-layer films by a self-assembly process: III. Consecutively alternating adsorption of anionic and cationic polyelectrolytes on charged surfaces. *Thin Solid Films*, 210, 831-835.
- 112) Rusling, J. F., Wasalathanthri, D. P., & Schenkman, J. B. (2014). Thin multicomponent films for functional enzyme devices and bioreactor particles. *Soft Matter*, 10(41), 8145-8156.
- 113) Kozlovskaya, V., Alexander, J. F., Wang, Y., Kunczewicz, T., Liu, X., Godin, B., & Kharlampieva, E. (2014). Internalization of red blood cell-mimicking hydrogel capsules with pH-triggered shape responses. *ACS Nano*, 8(6), 5725.
- 114) Huang, R., Li, W., Lv, X., Lei, Z., Bian, Y., Deng, H., ... & Li, X. (2015). Biomimetic LBL structured nanofibrous matrices assembled by chitosan/collagen for promoting wound healing. *Biomaterials*, 53, 58-75.
- 115) Ferreira, M., Fiorito, P. A., Oliveira, O. N., & de Torresi, S. I. C. (2004). Enzyme-mediated amperometric biosensors prepared with the Layer-by-Layer (LbL) adsorption technique. *Biosensors and Bioelectronics*, 19(12), 1611-1615.
- 116) Barsan, M. M., David, M., Florescu, M., Ţugulea, L., & Brett, C. M. (2014). A new self-assembled layer-by-layer glucose biosensor based on chitosan biopoly-

- mer entrapped enzyme with nitrogen doped graphene. *Bioelectrochemistry*, 99, 46-52.
- 117) Kim, B. S., Park, S. W., & Hammond, P. T. (2008). Hydrogen-bonding layer-by-layer-assembled biodegradable polymeric micelles as drug delivery vehicles from surfaces. *ACS Nano*, 2(2), 386-392.
- 118) Liu, F., Kozlovskaya, V., Zavgorodnya, O., Martinez-Lopez, C., Catledge, S., & Kharlampieva, E. (2014). Encapsulation of anticancer drug by hydrogen-bonded multilayers of tannic acid. *Soft Matter*, 10(46), 9237-9247.
- 119) Lvov, Y., Ariga, K., Ichinose, I., & Kunitake, T. (1995). Assembly of multicomponent protein films by means of electrostatic layer-by-layer adsorption. *Journal of the American Chemical Society*, 117(22), 6117-6123.
- 120) Kharlampieva, E., Kozlovskaya, V., & Sukhishvili, S. A. (2009). Layer-by-layer hydrogen-bonded polymer films: from fundamentals to applications. *Advanced Materials*, 21(30), 3053-3065.
- 121) Johnston, A. P., Cortez, C., Angelatos, A. S., & Caruso, F. (2006). Layer-by-layer engineered capsules and their applications. *Current Opinion in Colloid & Interface Science*, 11(4), 203-209.
- 122) Kozlovskaya, V., Kharlampieva, E., Drachuk, I., Cheng, D., & Tsukruk, V. V. (2010). Responsive microcapsule reactors based on hydrogen-bonded tannic acid layer-by-layer assemblies. *Soft Matter*, 6(15), 3596-3608.
- 123) Alexander, J. F., Kozlovskaya, V., Chen, J., Kunczewicz, T., Kharlampieva, E., & Godin, B. (2015). Cubical Shape Enhances the Interaction of Layer-by-Layer Polymeric Particles with Breast Cancer Cells. *Advanced Healthcare Materials*, 4(17), 2657-2666.

- 124) Kozlovskaya, V., Xue, B., & Kharlampieva, E. (2016). Shape-adaptable polymeric particles for controlled delivery. *Macromolecules*, 49(22), 8373-8386.
- 125) Chen, W., & McCarthy, T. J. (1997). Layer-by-layer deposition: a tool for polymer surface modification. *Macromolecules*, 30(1), 78-86.
- 126) Johnston, A. P., Cortez, C., Angelatos, A. S., & Caruso, F. (2006). Layer-by-layer engineered capsules and their applications. *Current Opinion in Colloid & Interface Science*, 11(4), 203-209.
- 127) Yu, A. I. M. I. N., Wang, Y. A. J. U. N., Barlow, E., & Caruso, F. (2005). Mesoporous Silica Particles as Templates for Preparing Enzyme-Loaded Biocompatible Microcapsules. *Advanced Materials*, 17(14), 1737-1741.
- 128) Wang, Y., Yan, Y., Cui, J., Hosta-Rigau, L., Heath, J. K., Nice, E. C., & Caruso, F. (2010). Encapsulation of Water-Insoluble Drugs in Polymer Capsules Prepared Using Mesoporous Silica Templates for Intracellular Drug Delivery. *Advanced Materials*, 22(38), 4293-4297.
- 129) Antipov, A. A., Shchukin, D., Fedutik, Y., Petrov, A. I., Sukhorukov, G. B., & Möhwald, H. (2003). Carbonate microparticles for hollow polyelectrolyte capsules fabrication. *Colloids and Surfaces A: Physicochemical and Engineering Aspects*, 224(1), 175-183.
- 130) Kozlovskaya, V., Higgins, W., Chen, J., & Kharlampieva, E. (2011). Shape switching of hollow layer-by-layer hydrogel microcontainers. *Chemical Communications*, 47(29), 8352-8354.
- 131) Yashchenok, A., Parakhonskiy, B., Donatan, S., Kohler, D., Skirtach, A., & Möhwald, H. (2013). Polyelectrolyte multilayer microcapsules templated on

- spherical, elliptical and square calcium carbonate particles. *Journal of Materials Chemistry B*, 1(9), 1223-1228.
- 132) Xue, B., Kozlovskaya, V., & Kharlampieva, E. (2017). Shaped stimuli-responsive hydrogel particles: syntheses, properties and biological responses. *Journal of Materials Chemistry B*, 5(1), 9-35.
- 133) Xie, Y. L., Wang, M. J., & Yao, S. J. (2009). Preparation and characterization of biocompatible microcapsules of sodium cellulose sulfate/chitosan by means of layer-by-layer self-assembly. *Langmuir*, 25(16), 8999-9005.
- 134) Pargaonkar, N., Lvov, Y. M., Li, N., Steenekamp, J. H., & de Villiers, M. M. (2005). Controlled release of dexamethasone from microcapsules produced by polyelectrolyte layer-by-layer nanoassembly. *Pharmaceutical Research*, 22(5), 826-835.
- 135) Zhang, X., Chen, H., & Zhang, H. (2007). Layer-by-layer assembly: from conventional to unconventional methods. *Chemical Communications*, (14), 1395-1405.
- 136) Kotov, N. A. (1999). Layer-by-layer self-assembly: the contribution of hydrophobic interactions. *Nanostructured Materials*, 12(5), 789-796.
- 137) Caruso, F., Trau, D., Möhwald, H., & Renneberg, R. (2000). Enzyme encapsulation in layer-by-layer engineered polymer multilayer capsules. *Langmuir*, 16(4), 1485-1488.
- 138) Wood, K. C., Chuang, H. F., Batten, R. D., Lynn, D. M., & Hammond, P. T. (2006). Controlling interlayer diffusion to achieve sustained, multiagent delivery from layer-by-layer thin films. *Proceedings of the National Academy of Sciences*, 103(27), 10207-10212.

- 139) Richert, L., Boulmedais, F., Lavalle, P., Mutterer, J., Ferreux, E., Decher, G., ... & Picart, C. (2004). Improvement of stability and cell adhesion properties of polyelectrolyte multilayer films by chemical cross-linking. *Biomacromolecules*, 5(2), 284-294.
- 140) Freire E. (1995) Differential Scanning Calorimetry. In: Shirley B.A. (eds) Protein Stability and Folding. *Methods in Molecular Biology*, vol 40. Humana Press
- 141) Sturtevant, J. (1987). Biochemical Applications of Differential Scanning Calorimetry. *Annual Review of Physical Chemistry*, 38(1), 463-488.
doi:10.1146/annurev.physchem.38.1.463
- 142) Woody, R. W. (1995). Circular dichroism. *Methods in Enzymology Biochemical Spectroscopy*, 246, 34-71. doi:10.1016/0076-6879(95)46006-3
- 143) Berova, N., Nakanishi, K., & Woody, R. (2000). Circular dichroism: principles and applications. New York: Wiley-VCH.
- 144) Marky, L. A., & Breslauer, K. J. (1987). Calculating thermodynamic data for transitions of any molecularity from equilibrium melting curves. *Biopolymers*, 26(9), 1601-1620. doi:10.1002/bip.360260911
- 145) Sugawara, T., Kuwajima, K., & Sugai, S. (1991). Folding of staphylococcal nuclease A studied by equilibrium and kinetic circular dichroism spectra. *Biochemistry*, 30(10), 2698-2706. doi:10.1021/bi00224a018
- 146) Zitzewitz, J. A., Bilsel, O., Luo, J., Jones, B. E., & Matthews, C. R. (1995). Probing the Folding Mechanism of a Leucine Zipper Peptide by Stopped-Flow Circular Dichroism Spectroscopy. *Biochemistry*, 34(39), 12812-12819.
doi:10.1021/bi00039a042

- 147) Gray, D. M., Wen, J., Gray, C. W., Regges, R., Regges, C., Raabe, G., & Fleischhauer, J. (2008). Measured and calculated CD spectra of G-quartets stacked with the same or opposite polarities. *Chirality*, 20(3-4), 431-440. doi:10.1002/chir.20455
- 148) Mergny, J., & Lacroix, L. (2003). Analysis of Thermal Melting Curves. *Oligonucleotides*, 13(6), 515-537. doi:10.1089/154545703322860825
- 149) Golub, G. H., & Reinsch, C. (1970). Singular value decomposition and least squares solutions. *Numerische Mathematik*, 14(5), 403-420. doi:10.1007/bf02163027
- 150) Lathauwer, L. D., Moor, B. D., & Vandewalle, J. (2000). A Multilinear Singular Value Decomposition. *SIAM Journal on Matrix Analysis and Applications*, 21(4), 1253-1278. doi:10.1137/s0895479896305696
- 151) Gray, R. D., & Chaires, J. B. (2011). Analysis of Multidimensional G-Quadruplex Melting Curves. *Current Protocols in Nucleic Acid Chemistry*, Unit17.4. <http://doi.org/10.1002/0471142700.nc1704s45>
- 152) Sukhorukov, G. B., Donath, E., Lichtenfeld, H., Knippel, E., Knippel, M., Budde, A., & Möhwald, H. (1998). Layer-by-layer self assembly of polyelectrolytes on colloidal particles. *Colloids and Surfaces A: Physicochemical and Engineering Aspects*, 137(1-3), 253-266. doi:10.1016/s0927-7757(98)00213-1
- 153) Kozlovskaya, V., Ok, S., Sousa, A., Libera, M., & Sukhishvili, S. A. (2003). Hydrogen-Bonded Polymer Capsules Formed by Layer-by-Layer Self-Assembly. *Macromolecules*, 36(23), 8590-8592. doi:10.1021/ma035084l
- 154) Riddick, T. M. (1968). Control of colloid stability through zeta potential. *Blood*, 10(1).

- 155) Hunter, R. J. (2013). *Zeta potential in colloid science: principles and applications* (Vol. 2). Academic press.
- 156) Haydon, D. A. (1961). The surface charge of cells and some other small particles as indicated by electrophoresis: I. The zeta potential-surface charge relationships. *Biochimica et Biophysica Acta*, 50(3), 450-457.
- 157) Bates, J. B. (1976). Fourier transform infrared spectroscopy. *Science*, 191(4222), 31-37.
- 158) Schrader, B. (Ed.). (2008). *Infrared and Raman Spectroscopy: Methods and Applications*. John Wiley & Sons.
- 159) Bracewell, R. N., & Bracewell, R. N. (1986). *The Fourier transform and its applications*. (Vol. 31999). New York: McGraw-Hill.
- 160) Mason, T. J., & Lorimer, J. P. (2002). Applied sonochemistry: the uses of power ultrasound in chemistry and processing.
- 161) Kremkau, F. W. (2001). *Diagnostic ultrasound: principles and instruments*. WB Saunders Company.
- 162) Ter Haar, G. (1999). Therapeutic ultrasound. *European Journal of Ultrasound*, 9(1), 3-9.
- 163) Baker, K. G., Robertson, V. J., & Duck, F. A. (2001). A review of therapeutic ultrasound: biophysical effects. *Physical therapy*, 81(7), 1351-1358.
- 164) Mitragotri, S. (2005). Healing sound: the use of ultrasound in drug delivery and other therapeutic applications. *Nature Reviews Drug Discovery*, 4(3), 255-260.